NASA Technical Memorandum 110397

An Analysis of Landing Rates and Separations at the Dallas/ Fort Worth International Airport

Mark G. Ballin and Heinz Erzberger

July 1996

NASA

National Aeronautics and
Space Administration

An Analysis of Landing Rates and Separations at the Dallas/ Fort Worth International Airport

Mark G. Ballin and Heinz Erzberger, Ames Research Center, Moffett Field, California

July 1996

Contents

Abbreviations

a/c	Aircraft
AGL	Above ground level
ASP	Arrival Sequencing Program, an operational metering system
Center	Air Route Traffic Control Center (ARTCC)
CTAS	Center-TRACON Automation System
DA	Descent Advisor; a component of CTAS
DFW	The Dallas/Fort Worth International Airport
ETA	Estimated time of arrival
ETAff	Estimated time of arrival at the meter fix (feeder fix)
FAA	Federal Aviation Administration
FAF	Final approach fix
FAST	Final Approach Spacing Tool; a component of CTAS
IFR	Instrument flight rules
IMC	Instrument meteorological conditions
mi	Statute miles
MSL	Mean sea level
nm	Nautical miles
PDF	Probability density function
rms	Root mean square
RUC	Rapid update cycle predictions of winds aloft from the National Meteorological Center
TMA	Traffic Management Advisor; a component of CTAS
TRACON	Terminal radar approach control facilities
TS	CTAS trajectory synthesis program
U_MFT	Undelayed meter fix time prediction from ASP
UTC	Universal Coordinated Time
VMC	Visual meteorological conditions
ZFW	The Fort Worth Air Route Traffic Control Center

Symbols

b	Controller separation buffer, nm
C	Maximum runway capacity, a/c/hr
i	Subscript representing i^{th} aircraft
F_A	Minimum separation fraction associated with automation
F_M	Minimum separation fraction associated with manual control
L	Aircraft landing rate over a rush period, a/c/hr
l_1	Estimate one for additional landing rate to achieve maximum runway potential, a/c/hr
l_2	Estimate two for additional landing rate to achieve maximum runway potential, a/c/hr
N	Number of aircraft that landed over a given rush period
R	Buffer reduction potential, sec
S	Aircraft longitudinal separation at the time of lead-aircraft threshold crossing, nm
S_E	Aircraft excess longitudinal separation at the time of lead-aircraft threshold crossing, nm
S_R	Aircraft required longitudinal separation at the time of lead-aircraft threshold crossing, nm
$S_{R_{avg}}$	Rush-period average required minimum separation, nm
t	Time
$T_{R_{avg}}$	Rush-period average required interarrival time, hr
V_{avg}	Average landing velocity, knots
μ_A	Excess separation time mean associated with automation such as FAST, sec
μ_M	Excess separation time mean associated with manual control, sec
ρ	Utilization fraction; equal to runway landing rate divided by its maximum capacity
σ_A	Excess separation time standard deviation associated with automation such as active FAST, sec

An Analysis of Landing Rates and Separations at the Dallas/Fort Worth International Airport

MARK G. BALLIN AND HEINZ ERZBERGER

Ames Research Center

Summary

Advanced air traffic management systems such as the Center/TRACON Automation System (CTAS) should yield a wide range of benefits, including reduced aircraft delays and controller workload. To determine the traffic-flow benefits achievable from future terminal airspace automation, live radar information was used to perform an analysis of current aircraft landing rates and separations at the Dallas/Fort Worth International Airport. Separation statistics that result when controllers balance complex control procedural constraints in order to maintain high landing rates are presented. In addition, the analysis estimates the potential for airport capacity improvements by determining the unused landing opportunities that occur during rush traffic periods. Results suggest a large potential for improving the accuracy and consistency of spacing between arrivals on final approach, and they support earlier simulation findings that improved air traffic management would increase capacity and reduce delays.

1. Introduction

Advanced air traffic management systems such as the Center/TRACON Automation System (CTAS) should yield a wide range of benefits, including reduced aircraft delays and controller workload. To determine the traffic-flow benefits achievable from future terminal airspace automation, an analysis of aircraft landing rates and separations was performed for the Dallas/Fort Worth International Airport (DFW) using live radar information. The primary goal was to obtain a reference baseline for the assessment of the CTAS as it is tested at the airport; a secondary goal was to aid in the further development of CTAS through an increased understanding of controller and pilot practices during the final approach segment of flight. This report describes the data-gathering and analysis procedure used, presents results, and makes recommendations for continued study.

1.1 The CTAS Concept

CTAS is a computer-based tool that is designed to relieve the worsening terminal-area delays caused by the continued growth of air traffic. It is intended to improve the efficiency of air traffic operations by optimizing traffic flow in terminal areas. CTAS is under development at the NASA Ames Research Center in cooperation with the Federal Aviation Administration (FAA). When complete, CTAS will consist of several integrated software tools that provide computer-generated advisories for en-route and terminal-area controllers to guide them in managing and controlling arrival traffic. CTAS will provide accurate route projections for the efficient scheduling and sequencing of aircraft as they transition from en-route to terminal airspace. In addition, it will identify potential aircraft conflicts and present options for resolving them. One of the tools, known as the Final Approach Spacing Tool (FAST), is designed to aid terminal radar approach control (TRACON) controllers. It will generate advisories to produce optimally spaced aircraft on the final approach course, thereby maximizing runway efficiency. The FAST tool will work in conjunction with the Traffic Management Advisor (TMA) tool, which performs scheduling and sequencing of arriving aircraft in airspace controlled by the Air Route Traffic Control Center (hereafter called Center) before they enter terminal airspace. Reference 1 presents a detailed overview of the CTAS design.

DFW, currently serving as a test site for CTAS, is scheduled to be the first site for field testing of the FAST component. In the testing, controllers will provide clearances to revenue flights based on the displayed advisories generated by FAST. Real-time controller-in-the-loop simulations of FAST have demonstrated its potential to increase landing rates, thereby reducing arrival delays in the Center during rush periods (ref. 2).

1.2 Study Goals

Data from actual air traffic operations must be analyzed to determine the benefits potential of new automation concepts such as CTAS. Benefits analyses that rely on theory and models in lieu of data are open to challenge.

Simulations rely on models that must be validated, so they must be used in conjunction with data collection. In addition, it is difficult to relate models based on theory to actual traffic flow. The models require simplifications of the actual air traffic environment, and often they rely on assumptions regarding traffic flow and the practices of controllers and pilots.

Data collection is also important for the design and optimization of such automation systems. A key function of CTAS is to make accurate predictions of times of arrival to the threshold. These arrival times are used to schedule and sequence aircraft. Accuracy of the predictions is dependent on many factors, several of which can be determined only through the analysis of actual data.

Arrival traffic data are also useful for understanding the practices of the controllers and pilots. This understanding can be used to optimize parameters in CTAS, such as a controller's preferred spacings on final approach. Although FAST provides spacing and sequencing only to the point of hand-off to the tower, that spacing can be done best if as much knowledge as possible about the final phases of flight is incorporated into the tool.

The primary goals of the analysis were to characterize DFW air traffic flow without automation tools, to identify some of the potential improvements of FAST and TMA in the terminal area, and to serve as a benchmark in analyzing the benefits of FAST in the future. The analysis obtained a sample of actual aircraft arrival spacings that resulted when controllers manually balanced the need to follow complex procedural constraints with the need to maintain high landing rates.

1.3 Assumptions and Scope

Previous findings based on simulation have indicated that the final approach segment is the critical point of constriction for arriving aircraft if the terminal airspace is managed effectively. Aircraft arrive at the runways in streams from several TRACON feeder gates; each of these streams may in turn be separated into two or more independent streams based on aircraft category. All streams must merge to land on three or fewer runways at DFW. If the number of arriving aircraft exceeds airport capacity, unusable time gaps between aircraft on landing can be eliminated through effective management of aircraft in the terminal airspace.

Any delays incurred by aircraft were assumed to be caused by a constriction of traffic on the final approach segments of the active runways. If it was necessary to delay aircraft, the study assumed that they were delayed in en-route (Center) airspace rather than in terminal airspace. If the assumption is made that the airport

acceptance rate was specified correctly, the buildup of Center delay in arriving aircraft indicated an arrival demand greater than the arrival capacity of the airport. If a traffic management system can achieve landings of consecutive aircraft as rapidly as is possible without violating FAA spacing minima, the study also assumed that the airport was handling arrivals at its maximum capacity. Although not investigated in this study, additional increases in landing rates may be achieved by resequencing aircraft to some optimal landing order.

The characteristics of arrival traffic flow on final approach at DFW were identified based on radar track data, recorded for a selected set of arrival rushes over a six-month period. The results are useful in obtaining an approximation of savings achievable by optimizing traffic flow in terminal airspace. Observed trends in the utilization of runways and controller practices in spacing aircraft are also useful for the design of a terminal airspace automation tool and the tuning of its internal parameters. Because the results are not comprehensive, they should not be interpreted as an accurate statistical representation of conditions or practices at DFW. Precise dollar-value estimates of the benefits of automation must be obtained through a much larger study that incorporates the impacts of surface operations, gate availability, and air-carrier banking operations as well as a more comprehensive assessment of runway utilization.

2. Approach

Results were based on empirical observation to the maximum extent possible. Traffic-flow data were collected from terminal and Center radar, from which threshold separations in time and distance were determined. Observed trends in the data were documented, and simple measures were used to characterize the potential benefits of a terminal-area air traffic automation tool. The analysis did not consider the possible limitations of existing automation tools.

The procedures used were as follows: Radar track data and additional supporting information were recorded at DFW and The Fort Worth Air Route Traffic Control Center (ZFW), as described in section 4. Using these data, landing runways and threshold crossing times were determined for each landing aircraft. (See section 5.) Estimates of optimal threshold separations were derived (section 6), and controller practices in spacing aircraft were investigated (section 7). All observations from data were followed up as much as possible through personal communication with active and former controllers at DFW. Trends in runway utilization were also observed and runway capacity was estimated (section 8). The

buildup of delays of arriving aircraft in the Center was used as the measure of the potential for airport capacity improvement. TRACON-arrival-gate crossing predictions generated by CTAS were used to quantify the delay for each aircraft; therefore, the accuracy of these predictions was evaluated (section 9).

3. Background

3.1 The Dallas/Fort Worth International Airport

Figure 1 is a plan view of the runways and airport terminals at DFW. The airport is designed to accept arrivals from the north or south. Two sets of parallel runways accept arrivals from north and south (35 R/L and 36 R/L or 17 R/L and 18 R/L), and two diagonal runways (31 R/L and 13 R/L) accept arrivals from the northwest and southeast. During north flow, some or all of Runways 31, 35, and 36 are active, and during south flow, some or all of Runways 13, 17, and 18 are active. The gate area is located between the two sets of north/south runways.

The parallel north/south sets each have two runways that are separated by approximately 1000 ft. The inboard runways are normally used for departing aircraft, and the outboard runways for arrivals. Because of their proximity, Runways 18R and 18L (36L and 36R) are dependent:

when both are used for arrivals under instrument conditions, longitudinal separation between aircraft must be maintained by the controller as if the two approach courses were a single course. Runways 17R and 17L (35L and 35R) are similarly dependent.

Figure 2 is a schematic of the approaches at DFW. The outer marker and final approach fix (FAF) locations, approximately five nautical miles (nm) from the runway thresholds, are coincident at DFW. All approaches follow direct line-of-sight paths from the FAF to the threshold, except for a special noise-abatement approach that is often used for Runway 31R during visual conditions. Under the stadium visual approach, aircraft are directed over Texas Stadium and are then required to make a left turn to acquire the runway approximately two nautical miles (nm) from the threshold.

3.2 Separation Regulations

During the approach and landing phases of flight, the FAA mandates that an aircraft following another aircraft must be longitudinally separated by a specified minimum distance to mitigate the danger of wake turbulence caused by the lead aircraft. The rules are based on the weight classification of the aircraft. Small aircraft are classified as those that have a maximum certified takeoff weight
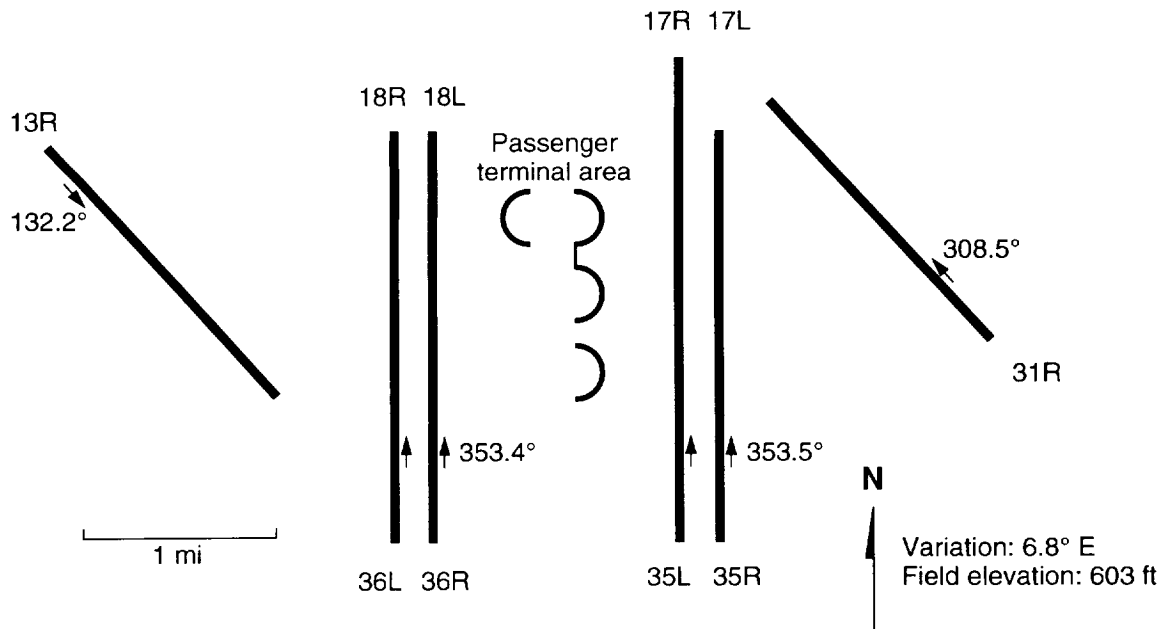
Figure 1. Simplified schematic of The Dallas/Fort Worth International Airport.
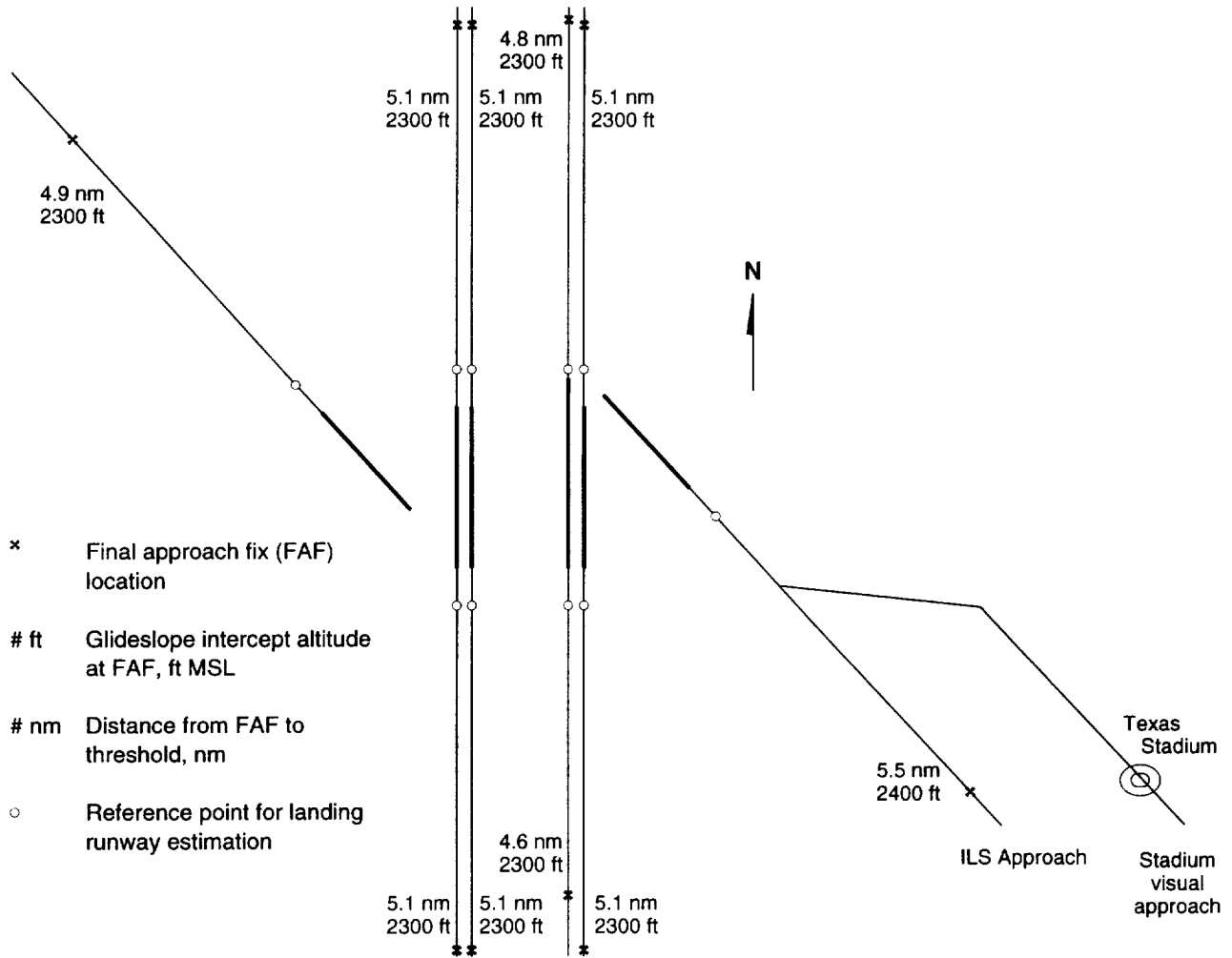
Figure 2. Approaches at the Dallas/Fort Worth International Airport.

less than or equal to 12,500 lbm; large aircraft are heavier than 12,500 lbm but no heavier than 300,000 lbm; and heavy aircraft have maximum certified takeoff weights greater than 300,000 lbm. The Boeing 757 (B757) aircraft, though classified as large, has been given a special set of separation criteria because increased wake turbulence has been attributed to this aircraft (ref. 3).

Table 1 shows the FAA approach and landing separation minima for each combination of lead/trail aircraft weight classifications and the B757. Controller clearances must comply with the separation minima up to the time that the lead aircraft crosses the runway threshold. Under dry runway conditions, DFW utilizes reduced separation criteria, as specified in reference 3: the 3-nm aircraft separation minima are reduced to 2.5 nm, as shown in table 2.

Table 1. Minimum required in-trail landing separations

(leading aircraft down, trailing aircraft across)

Minimum required separation, nm	Heavy	Large	Small	B757
Heavy	4	5	6	5
Large	3	3	4	3
Small	3	3	3	3
B757	4	4	5	4

4

Table 2. Minimum required in-trail landing separations at DFW under dry runway conditions

(leading aircraft down, trailing aircraft across)

Minimum required separation, nm	Heavy	Large	Small	B757
Heavy	4	5	6	5
Large	2.5	2.5	4	2.5
Small	2.5	2.5	2.5	2.5
B757	4	4	5	4

Although the captain assumes ultimate responsibility for the safety of his aircraft, the air traffic controller is responsible for maintaining separation between aircraft operating on instrument flight rules (IFR) flight plans (such as commercial air carriers). However, a pilot can accept responsibility for separation between his aircraft and another aircraft that he can see. In this situation, the pilot is responsible for maintaining the amount of separation that he deems safe. The transfer of responsibility requires direct communication between the controller and the pilot.

Pilots are often requested to accept responsibility for visual separation under visual meteorological conditions (VMC), which typically corresponds to a ceiling greater than or equal to 500 ft above the minimum vectoring altitude and visibility greater than or equal to 3 statute miles (mi). (See ref. 3.) The minimum vectoring altitude at DFW varies between 2000 and 2200 ft above mean sea level (MSL). Therefore, at DFW, the minimum ceiling for VMC is approximately 2000 ft above ground level (AGL).

Lower ceilings or visibility correspond to instrument meteorological conditions (IMC). Under IMC, the pilot conducts an instrument approach using either a precision or a nonprecision procedure; precision approaches use equipment to provide vertical and lateral course guidance, whereas nonprecision approaches provide only lateral guidance. Under these conditions, the air traffic controller is responsible for providing clearances to the pilot to maintain separation with the leading aircraft, although the pilot may accept responsibility if he has visual contact.

For each final approach course, an approach gate is used to vector aircraft for instrument final approaches. At DFW, the approach gates are located on the approach courses approximately 2 nm outside the FAF. Under IMC, aircraft are required to intercept the final approach course at least 2 nm beyond the approach gate. Pilots may request a closer intercept to expedite a landing, but not

inside the FAF. Under DFW local procedures, aircraft may intercept the approach course inside the approach gate for weather conditions with a ceiling greater than or equal to 3000 ft AGL and visibility greater than or equal to 5 mi.

Under instrument conditions, the simultaneous use of the parallel runways at DFW (17 and 18 or 35 and 36) requires coordination. Under "simultaneous approaches" operation, the runways can be used independently; i.e., once established on their final approach courses, aircraft on one course do not impact clearances to the aircraft on the other course. Another operating mode, referred to as "staggered approaches," requires 2-nm separations between aircraft that are on different final approach courses, resulting in a staggered pattern of landings. Staggered approaches do not have the requirement that all aircraft must intercept the approach path at or before passing the approach gate. Although simultaneous approaches enable greater runway utilization than staggered approaches, they require two additional controllers for monitoring.

A more detailed description of FAA separation regulations for radar arrivals may be obtained from the FAA air traffic control handbook (ref. 3).

4. Data Recording

Recordings of live traffic flow at DFW were made over a 6-month period during the winter of 1994–95. Radar track data were supplied using a direct feed from the ZFW radar and the DFW ASR-9 terminal radar. Center and terminal radar recordings were made simultaneously to identify arrival rush periods in terminal airspace based on delay buildup in the Center, and to provide Center delays of each aircraft to augment the landing separation analysis. The combined recordings, which started up to 30 minutes prior to crossing the meter gate and continued until the TRACON radar track dropped out near the runway threshold, provided position histories of each arriving aircraft.

4.1 Dataset

A dataset suitable for analysis was extracted from the complete set by eliminating recordings containing incomplete information and recordings that contained unusual situations. Recordings with winds greater than 15 knots were also eliminated because the analysis tools were not developed to account for the separation time expansion that occurs under such conditions. The resulting usable rush-period dataset was made up of 30 individual rush periods, with each period containing

landings to all active runways. At least two runways were active for all recordings.

For each recording, the following additional information was gathered to support the analysis: 1) flight rules in effect, 2) airport visibility, 3) airport ceiling, 4) runway conditions, 5) wind bearing and velocity at the airport, 6) approach type in effect (simultaneous or staggered), 7) the aircraft acceptance rate, and 8) special conditions or restrictions in effect.

4.2 Rush-Period Identification

Rushes must be accommodated in the scheduling of controller staff work time because they significantly impact controller workloads. A schedule of rush periods at DFW that was current at the time of the data recording is shown in figure 3. For the analysis, starting and ending times of each rush were determined by selecting large contiguous periods for which landing demand appeared to exceed airport capacity. These periods corresponded to a buildup of meter fix crossing delays in the Center. To ensure that any observed arrival gaps were not caused by the need to allow other aircraft to depart, the recordings were examined to verify that the landing runways and any runways dependent on them were exclusively committed to arriving aircraft.

Figure 4 illustrates Center arrival delays through a plan-view representation of radar tracks for arriving aircraft. The concentric dotted circles represent constant-radius distances from the airport, in nm. All metering of traffic into terminal airspace is performed with respect to the four arrival meter gates, which are equally spaced approximately about the 40-nm radius. They can be seen in the figure as the four points of convergence of aircraft tracks. The recording corresponds to a severe rush period, so many arriving aircraft were required to wait in a holding pattern before crossing the meter gate.

Center delay buildup was identified by using the Center recordings as input to CTAS, which estimated undelayed times of arrival at the meter fix points (ETAff) up to 30 minutes ahead of time. The ETAff values are computed by the CTAS TMA using information such as the aircraft type, its flight plan, and its position, ground speed, and altitude. Weather is also normally used by the TMA to compute ETAff values, but weather information was not available for the recordings of this study. In computing these values, TMA assumes that undelayed direct routing is used between the measuring point and the meter fix. For each aircraft, the ETAff value was subtracted from the actual meter fix crossing time to obtain an estimate of delay incurred by each aircraft in the Center.

Figure 5 illustrates these estimates of rush-period delay buildup over time. Delay values for each aircraft, in seconds, were plotted as a function of actual meter fix crossing time. The ETAff values used in computing these delays correspond to the meter fix crossing time of each aircraft, predicted at the time when it was expected to cross the meter fix 19 minutes later. These ETAff values are referred to herein as the 19-minute estimates, or $ETAff_{19}$. The figure shows three distinct rush periods separated by periods of low delay. The first rush period corresponds to times of 20:00 to 20:50 Universal Coordinated Time (UTC), which corresponds to 14:00 to 14:50 in DFW local time. Figure 3 shows that this rush corresponds to an expected arrival rush from the west and northeast meter gates. Since there is a 15- to 20-minute difference between meter fix crossing times and threshold crossing times, the rush periods identified for the analysis were adjusted based on this terminal airspace flight time.

5. Interarrival Distance and Time Measurement

A NASA Ames Research Center analysis code called AN (ref. 4) was modified to provide estimates of the landing runway and threshold crossing time for each aircraft. The aircraft landing order for each runway was then determined and threshold interarrival spacings and times were estimated.

The AN program was augmented with a function that identified all aircraft radar tracks in a terminal radar recording that corresponded to the final approach segment. It then determined the landing runway and threshold crossing time for each track. Radar tracks of aircraft on final approach normally do not extend to the threshold, so the existing radar data were used to extrapolate aircraft flightpaths to the most likely runway. All aircraft that were on the final approach course were treated as landing aircraft since they occupied a landing slot.

The landing runway estimation logic identified a landing runway for each aircraft from the full set of runway candidates. The algorithm eliminated all implausible candidates, and it then selected the most likely runway from the remaining candidates. It used knowledge about landing procedures to the extent possible, but it also relied on several tuning parameters that were set through trial and error. The logic is described in appendix A.

The recorded data showed that, as opportunities permitted, some arriving aircraft were reassigned to inboard runways, which were normally reserved for departures. This reassignment was often made less than 20 seconds before crossing the threshold. To allow

FEL - controller operating position (Feeder East Low)
MOP - Departure gate
BUJ - Northeast meter gate (Blueridge)
SCY - Southeast meter gate (Scurry)

WEST	DFW Local Time	EAST

Arrival rush coming from all four corners; about half are props. FEL is beneficial to flow. ⟹ 0640 0650 ⟹ Eastbound rush: 35 to 40 a/c; bulk goes through Lake Gate; lasts approx. 40 minutes.

0800 ⟹ East and west rush; almost an even split; lasts 40 minutes.

0800 ⟸ Arrival rush starts from east and ends from west; lasts approx. 1 hour.

East and west departure rush; almost an even split; lasts approx. 50 minutes. ⟸ 0920

0930 ⟸ Arrival rush from east; almost an even split between BUJ and SCY; lasts approx. 40 minutes.

1030 ⟸ Arrival rush from east; mostly Delta jets; lasts approx. 30 to 35 minutes.

1050 ⟹ Minor west departure push; several north and south are included; lasts approx. 30 minutes.

Major arrival rush from the west; several props are included; lasts approx. 45 to 50 minutes. ⟹ 1130

West departure push through MOP gate; several north and south departures; lasts 30 minutes. ⟸ 1140

1250 ⟹ Major east and north departure push; lasts 45 to 50 minutes.

Arrival rush from the west with some traffic at BUJ; lasts 25 to 30 minutes. ⟹ 1300

1400 ⟸ Arrival rush from east; lasts approx. 50 minutes; FEL is beneficial to flow.

1420 ⟹ East departure push; half go through the Lake sector; lasts approx. 25 minutes.

Arrival rush from the west and BUJ; lasts approx. 50 minutes. ⟹ 1530

West departure push; lasts approx. 30 minutes. ⟸ 1550

1700 ⟹ East departure push; half go through the Lake sector; lasts approx. 50 minutes.

1700 ⟸ Arrival rush from east; lasts approx. 50 minutes; FEL is beneficial to flow.

Major arrival rush from the west and BUJ; lasts approx. 55 minutes. ⟹ 1830

Westbound departure push; MOP gets bulk of traffic; lasts 50 minutes. ⟸ 1830

2000 ⟹ East departure push; Lake gets most of traffic; several north departures; lasts approx. 1 hour.

West departure push over MOP; several north and south departures in push; lasts approx. 30 minutes. ⟸ 2010 2150 ⟸ Arrival rush from east; numerous freighters arrive in the rush; lasts approx. 50 minutes.
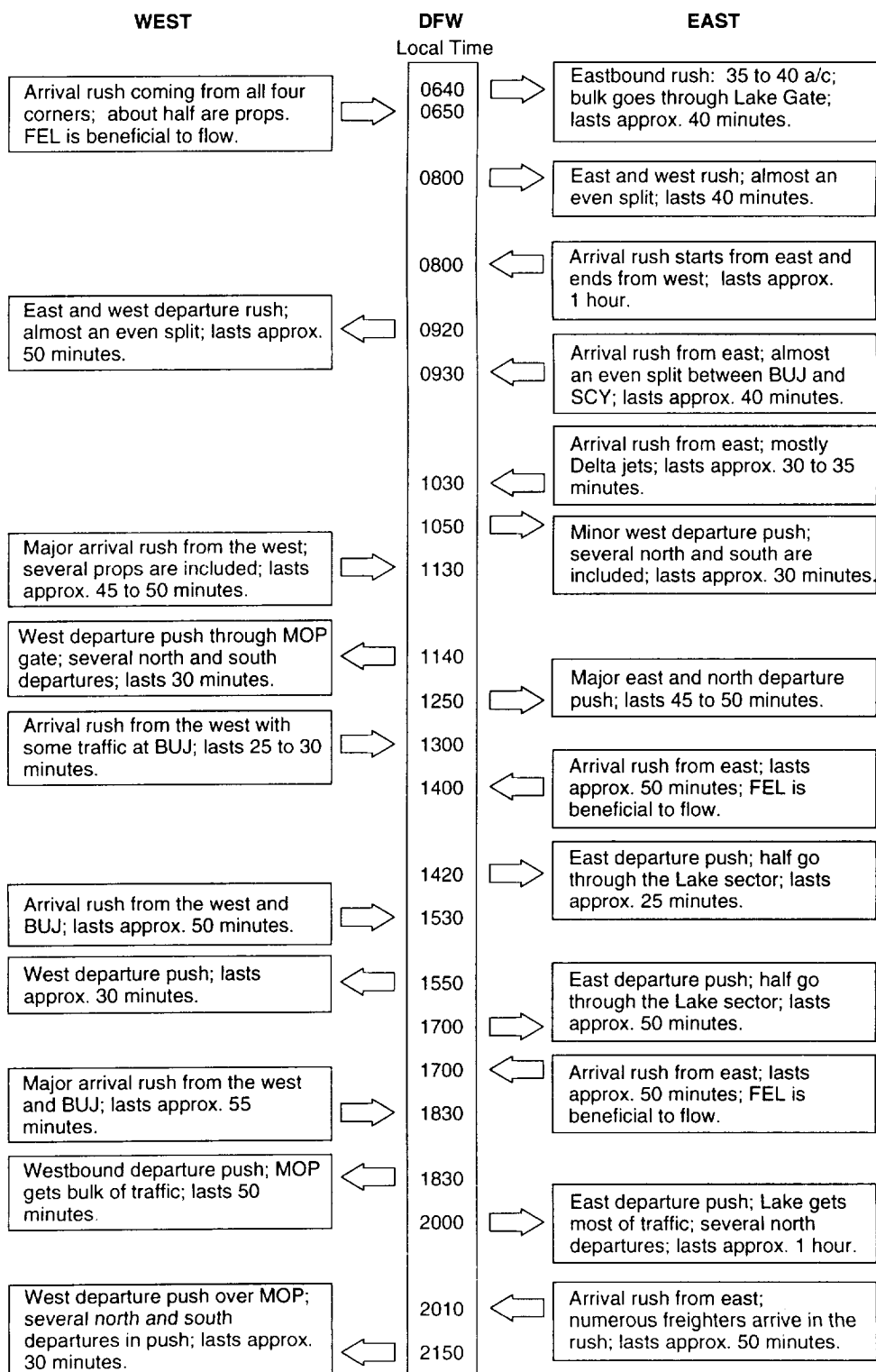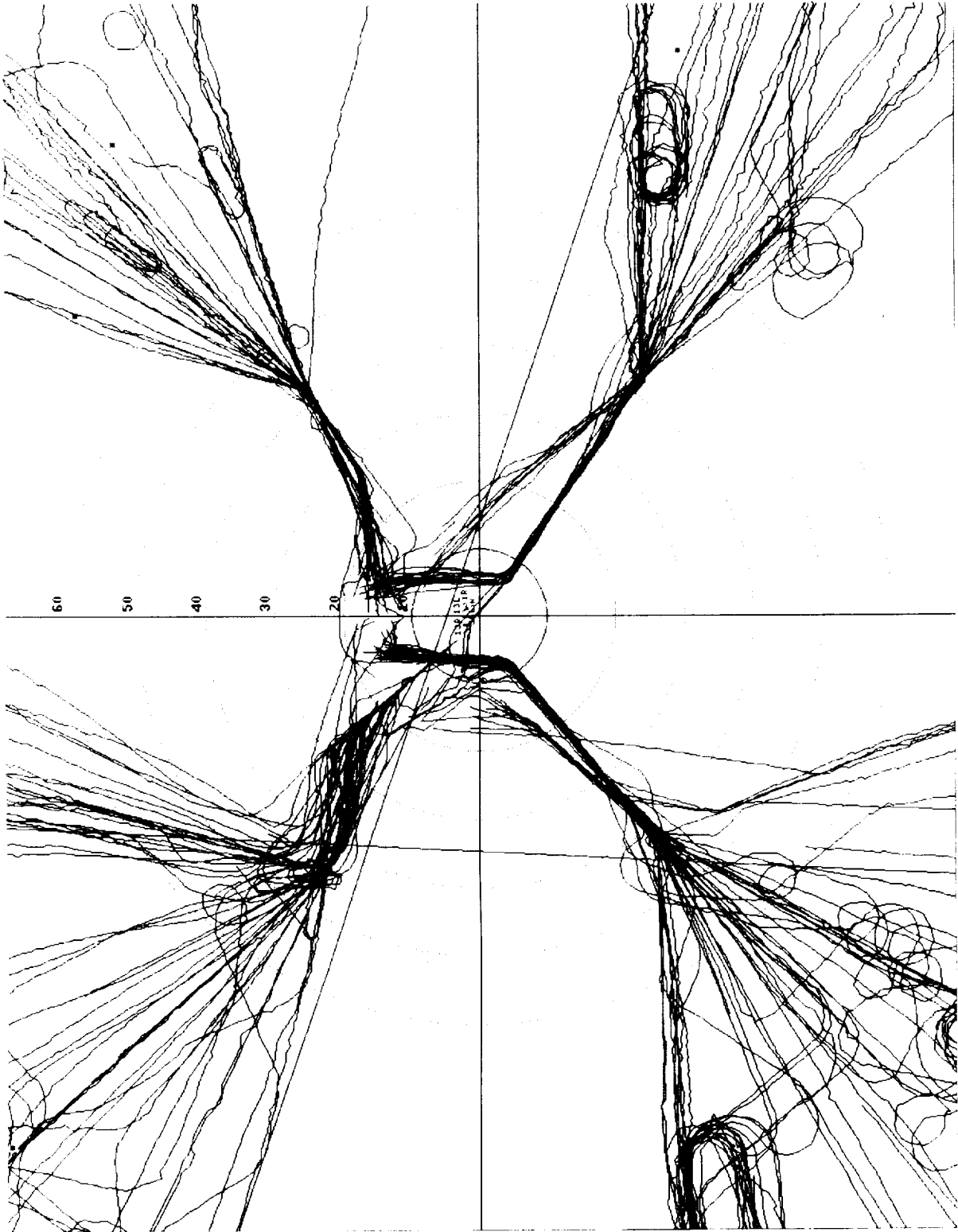
Figure 3. DFW rush-period schedule.

Figure 4. Radar tracks of arriving aircraft in the ZFW Center and the DFW TRACON.

60
50
40
30
20

(Overcrossing Time – ETA_FF) vs. Overcrossing Time. Number associated with point is the Gate #, 0 = No Gate assigned
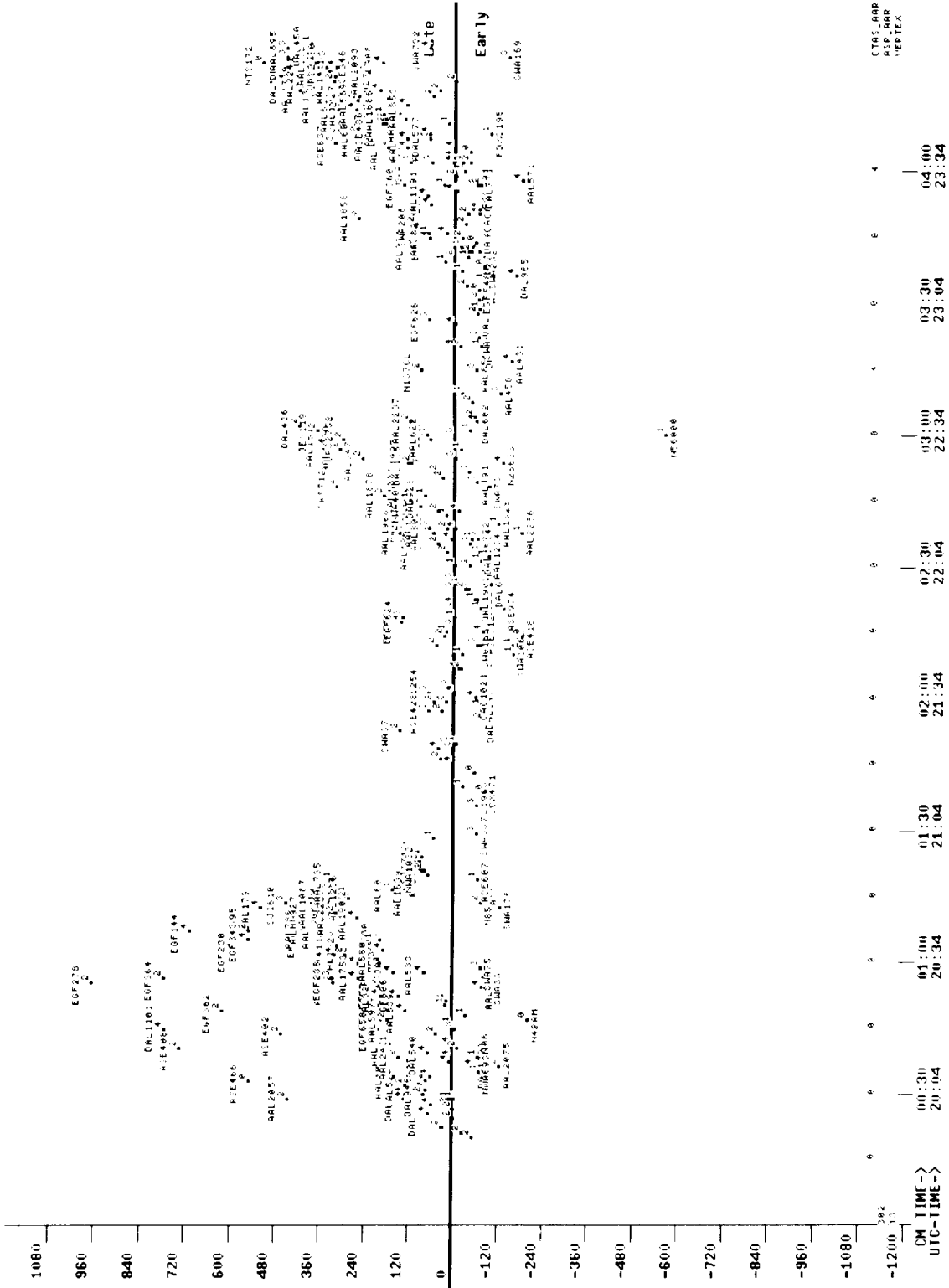
Number of AC = 318

Figure 5. Rush-period delay buildup over time.

9

exclusion of the reassignment from the analysis, a reference point for measurement of the landing runway was established. (See fig. 6.) The position of this no-reassign point was adjustable along the final approach course from the threshold to the beginning of the common approach path. A position of 0.5 nm before the threshold was established by determining the closest point on the approach prior to the point that most aircraft started their heading change for the inboard runway, or started a climb-out if executing a missed approach.

To estimate the threshold crossing time, the algorithm interpolated between the two radar hits closest to the no-reassign point to obtain a time of closest approach. The aircraft ground speed was then used to extrapolate to the threshold. A comparison with tower observations showed the threshold crossing times to be accurate to within about 10 seconds.

Very few wrong estimates of aircraft landing runways could be tolerated. Each incorrect estimate that an aircraft did *not* land on a particular runway resulted in an incorrect unused slot in the arrival stream, a possibly incorrect lead/trail class combination, and an incorrect assessment of landing rate. Incorrect estimates that aircraft *did* land on a particular runway resulted in increased counts of negative excess separations. A validation was performed to ensure that these errors were small. Landing runways and threshold crossing times were recorded for 1135 aircraft by an observer located in the DFW tower. The validation was performed under visual approach conditions. The landing estimation errors were found to be low after a zero-phase-shift Butterworth-characteristic filter was added to attenuate noise in the radar data.

An average error rate of 0.9 percent was seen in the landing runway estimations. Data feed and radar dropout errors caused additional errors, resulting in a total error rate of 2.3 percent for the full validation sample. This rate was deemed acceptable for the analysis. Aircraft landing on Runway 31R sometimes used the stadium visual approach, which caused the landing runway function to fail. Therefore, Runway 31R was excluded from the analysis when this approach was being used. Other errors were caused by very large separations between leading and trailing aircraft, which invalidated the function's line-of-sight separation distance approximation. Because these cases were rare, they were not removed from the analysis.

6. Optimal Spacings Estimation

To predict a time of threshold crossing, an automation program must use a representative model of expected aircraft trajectories during the final approach segment. In CTAS, trajectories are generated by a process called the trajectory synthesizer (TS). The TS relies on a knowledge base consisting of aircraft performance models, aircraft physical characteristics such as weight, and pilot procedures for instrument and visual final approaches. The trajectories can be used to determine representative approach profiles, defined herein as the distance to the threshold as a function of time to threshold crossing. In this study, the profiles were investigated and modified to represent the observed trajectories more accurately. The modified approach profiles were then used as a basis for estimating optimal spacings between aircraft on the final approach segments.
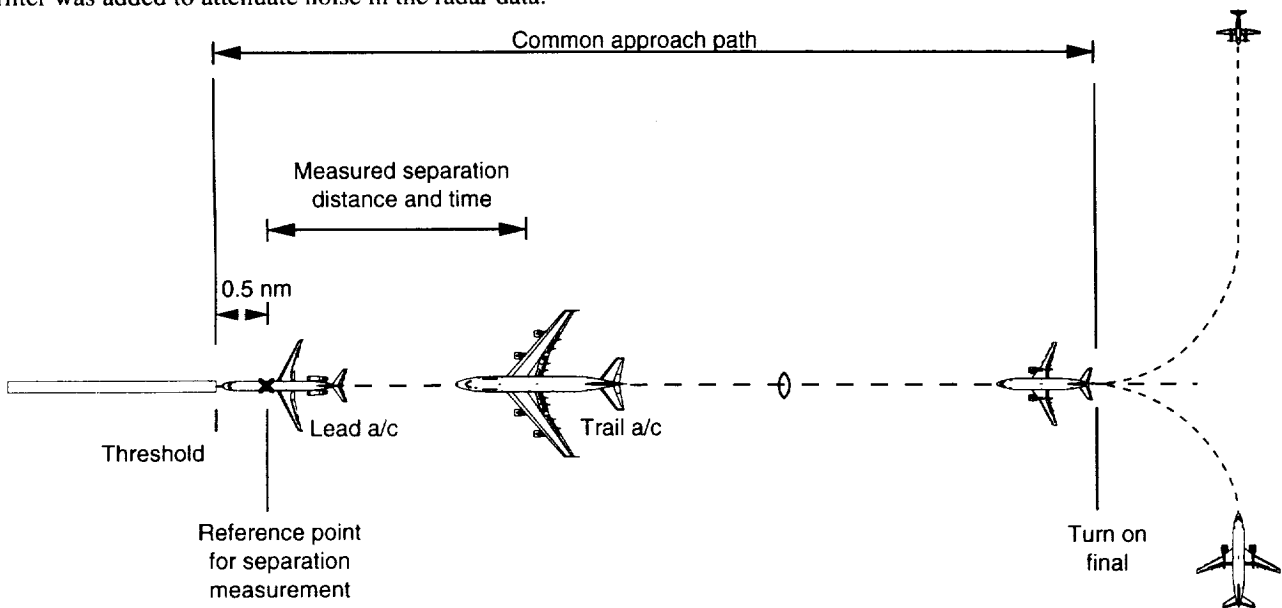

Figure 6. Threshold spacing measurements for landing sequences.

6.1 CTAS Aircraft Approach Profiles

The pilot procedures components of the TS final approach trajectories were based on formal training courses of the U.S. Air Force, United Airlines, and America West Airlines (ref. 5). All approaches were categorized as being one of two types: VMC, corresponding to probable visual approaches; and IMC, for probable weather-minimum instrument approaches. For VMC, the TS is designed to hold a constant speed to the FAF. At the FAF, the aircraft begins to decelerate to its final approach speed, which it typically captures about two nm later. Under weather-minimum conditions, pilots are trained to reduce high workload during the final portion of the approach by making all speed adjustments and configuration changes early. Therefore, for IMC, the TS initiates a deceleration to final approach speed two to three nm before the FAF, and acquires the final approach speed at the FAF.

Without records of voice communication between the pilot and the radar controller, it is impossible to determine whether data for a given aircraft correspond to a visual or a weather-minimum instrument approach. As explained in section 3.2, during a visual approach, a pilot may choose not to follow the FAA separation minima if he feels it is safe to have less separation. Crosswind conditions and his altitude relative to the lead aircraft will impact the pilot's separation decisions. Pilots often try to hold maximum speed as long as possible, and, depending on experience with the aircraft, will decelerate and capture final approach speed as late as one mile before the threshold (ref. 5). In addition, the aircraft landing weight can play a significant role in the pilot's speed decisions.

6.2 Required Separations Model

Minimum separation constraints are most critical for the final approach flight segment, when all aircraft share a common approach path and the danger from wake turbulence is highest (fig. 6). Under VMC, the common path is typically about six nm long at DFW; under IMC, final-approach-course intercept requirements result in a common approach path that is approximately nine nm long. A slow leading aircraft may be overtaken by a faster trailing aircraft, so the aircraft must be spaced so that they will not violate the minimum requirements at the threshold. A fast leading aircraft will pull away from a slower trailing aircraft, so minimum separation occurs before crossing the threshold.

A model was developed to convert required minimum separations that apply over the entire common path to actual required minima at the threshold. The model was also used to estimate the corresponding required threshold

interarrival times. This "required separations model" is dependent on the length of the common approach path and the final approach trajectories of the leading and trailing aircraft. A simple model based on constant speeds during the entire final approach segment is not acceptable, since aircraft typically slow to a landing speed near the FAF, as explained in section 6.1. The threshold separation was defined as the separation when the leading aircraft crosses the threshold, determined such that no separation constraint was violated along the entire common path. The common path separation was defined similarly for the point when the trailing aircraft crosses the start of the common path. Using an iterative loop, an automated function compared representative approach profiles of leading and trailing aircraft from the start of the common path to the threshold, and adjusted the spacings between the profiles so that the separation constraint was not violated along the path. Figure 7 illustrates the threshold and common-path distance and time separations as defined for the study. The figure shows an example for which the minimum required separation occurred between the common-path start and the threshold.

The required-separations model categorized all aircraft types into six classes in order to distinguish among aircraft that have different required minimum separations or significantly different landing speeds. The speed/weight classes were 1) heavy aircraft, 2) large jets, 3) large turboprops, 4) small turboprops, 5) small props, and 6) B757s. Large props were categorized as large turboprops and small jets were categorized as small turboprops for the study.

Profiles for the speed/weight classes and the two approach conditions were generated by the TS for use in the study. (See appendix B.1 for profiles of five of the analyzed classes.) The profiles were generated for conditions of zero winds at the runway and a head wind that increased with altitude by 0.001 knot/ft. Typical aircraft types and landing weights were used for each speed/weight class. The appendix also shows profiles based on analysis of data, as discussed in the following sections.

Outputs of the model are in the form of 6 × 6 separation tables, shown in appendix B.2 for several cases to be discussed. For each case, the common path length, approach conditions, and source of the profiles are given. The leading aircraft are determined by the rows of each matrix, and trailing aircraft by the columns. In addition to the separations, the point of minimum separation for the lead aircraft is provided, as well as the time for the trailing aircraft to travel from the common-path start to the threshold.
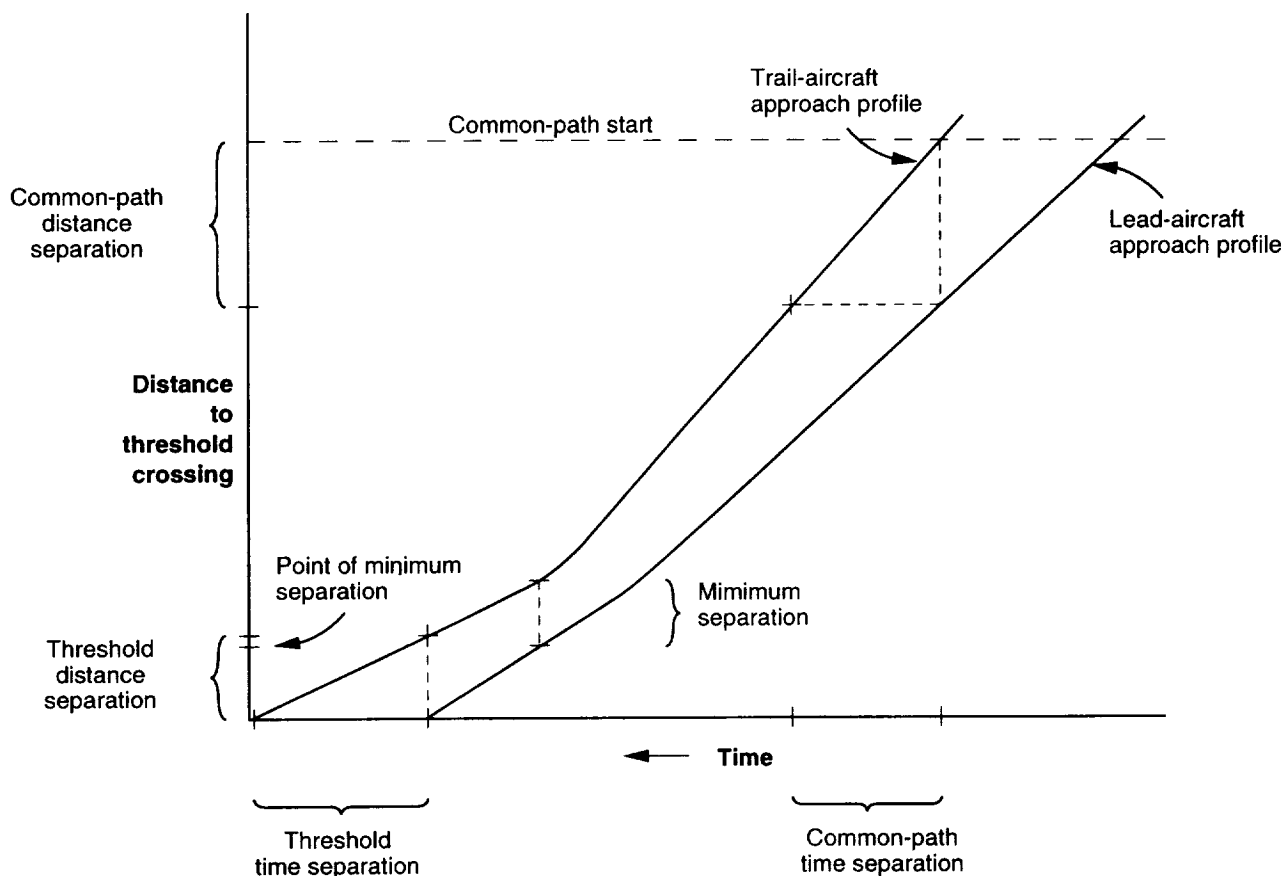
Figure 7. Definitions of required separations at the threshold and the beginning of the common path.

6.3 Comparison of Data and CTAS Profiles

By comparing the measured threshold time separations of each lead/trail pair with the corresponding distance separations, approach profiles near the threshold can be estimated. Figure 8 is a plot of the distance and time separations for all lead/trail pairs inside the FAF. Because each data point corresponds to the time that the lead aircraft crosses the threshold, the measurements correspond to the times and distances to the threshold for the trailing aircraft.

The approach speeds observed exhibit a wide variation, and correlation with a linear fit was low. (See fig. 8.) The residuals from the linear fit have a nearly normal distribution, with a standard deviation of about 13 seconds. The figure highlights the fact that differences in wind speed, company procedures, aircraft landing weight, and/or pilot technique may need to be modeled to predict approach profiles with high accuracy.

To compare the profiles used by CTAS with the observed results, the data were separated into a VMC set corresponding to probable visual approaches and an IMC set

containing probable instrument approaches. The IMC set consisted of recordings with weather conditions for a ceiling less than 1000 ft AGL and visibility less than 3 mi. These low values usually corresponded to conditions of rain and/or fog.

For the VMC cases, data and TS-generated approach profiles agreed well for all except one of the five evaluated aircraft speed/weight classes. Figure 9 compares the TS large-jet VMC profile with actual distance/time separation data for all VMC cases having large jets in trail. In the figure, a linear fit of the data between 0 and 3 nm was used to approximate the average final approach speed. For this case, the observed data show good agreement with the TS-generated approach profile. The high variance in the data suggests that providing automated advisories for spacings that are accurate to within a few seconds requires the modeling of additional parameters. Some of the variance results from the fact that, under VMC, aircraft are not required to follow the final approach course through the approach gate.

12
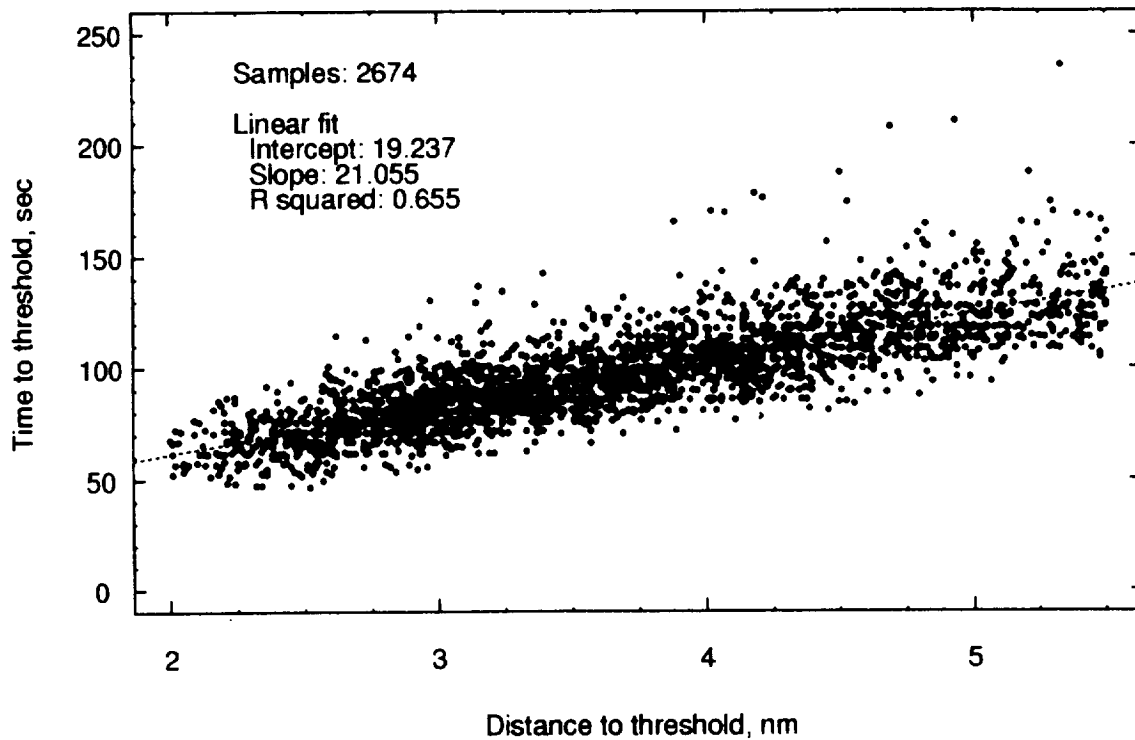
Figure 8. Distance and time separation comparisons for all recorded separation combinations inside the FAF.

Large turboprops had the poorest data agreement with the current TS-generated profiles. As seen in figure 10, the TS profiles tend to underestimate the final approach speed by approximately 17 knots. Threshold landing times obtained from the required separations model tended to overestimate required time spacings by 20 to 25 seconds for all cases with large turboprops in trail. Clearly, the TS must be modified to more accurately reflect the live data results for large turboprops.

Less overall agreement was found for the IMC comparisons, although the small number of data samples made conclusions difficult. Contrary to expectations, variation in the data was found to be of the same order of magnitude as that of the VMC data. Figure 11 is an example of a data and TS comparison for large jets in trail under IMC. A linear fit of the data between 0 and 5 nm to the threshold was used to approximate the final approach speed. As seen in the figure, the data predict a speed that is lower than the TS prediction by approximately 10 knots, a difference that is within the range of wind conditions encountered in the data. Among the speed/weight classes, the large turboprops and B757 comparisons showed the poorest agreement. Table 3 summarizes the comparison of TS-generated approach profiles with DFW data; small props were not included in the table because of their small sample size.

6.4 Model Modifications

Improved estimates of IMC and VMC approach profiles were developed by using the data. Linear fits of the data were combined with assumptions about speeds beyond the FAF and knowledge of pilot procedures. The required separations model was then modified to use these improved profile estimates to obtain optimal time separations for the aircraft lead/trail pair combinations. The results are shown in tables 4 and 5. Note that the observed results show lower differences in speed between many of the speed/weight class types than predicted by the TS profiles. Therefore, problems of widening separation gaps or overtaking aircraft were found to be smaller than anticipated.

Table 6 contains standard and maximum deviations in the flight times from the FAF to the threshold. The variability of results for the heavy, small-turboprop, and B757 VMC cases is low enough to be accounted for largely by winds. The 15-knot wind variability in the data would account for a 12- to 25-second difference between minimum and maximum values. In contrast, the large-jet class, which has aircraft types with a wide range of weights and final approach speeds, has very large variability. A comprehensive error-source analysis is needed to determine the causes of flying time differences on the

13
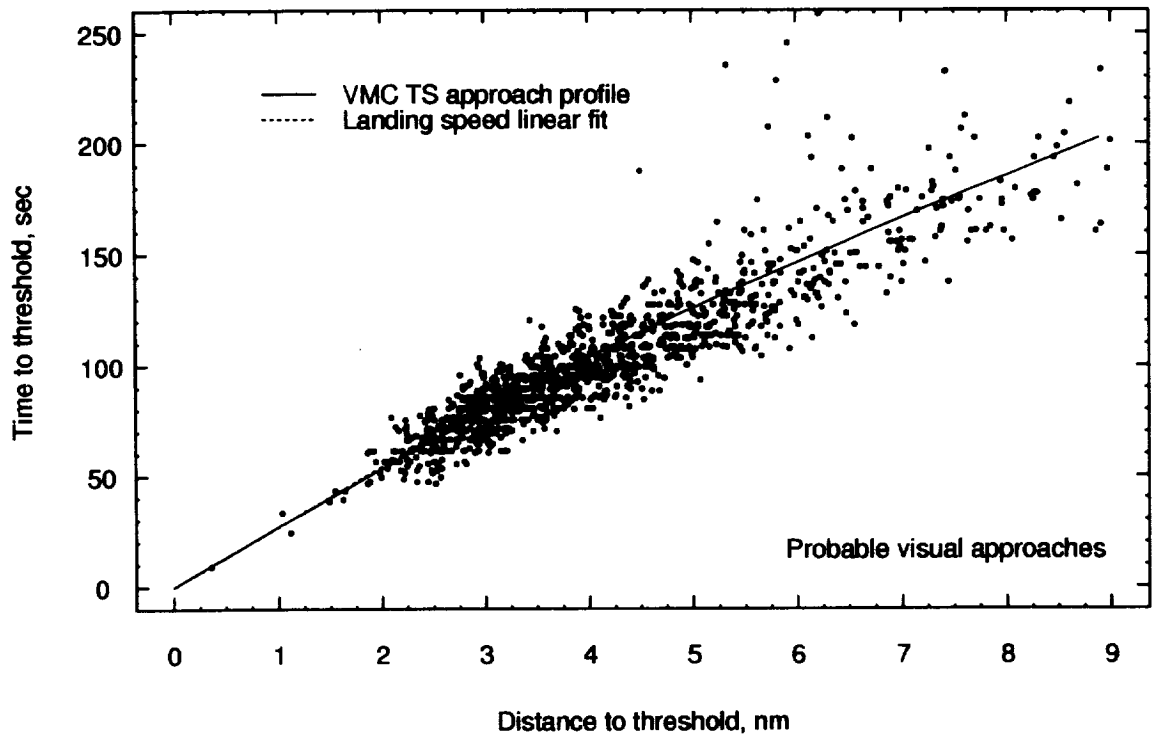
Figure 9. Distance and time separation comparisons for all VMC cases with large jets in trail.
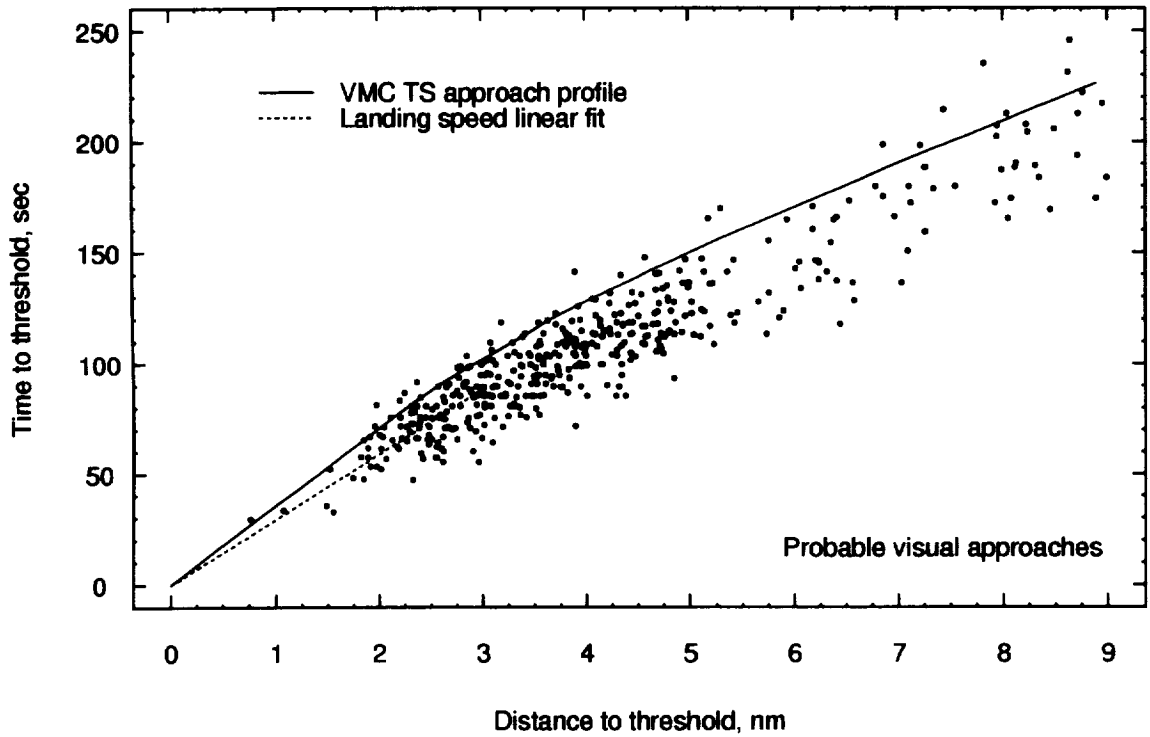
Figure 10. Distance and time separation comparisons for all VMC cases with large turboprops in trail.

250

IMC TS approach profile
.... Landing speed linear fit

200

Time to threshold, sec

150

100

50

Probable instrument approaches

0

0   1   2   3   4   5   6   7   8   9

Distance to threshold, nm
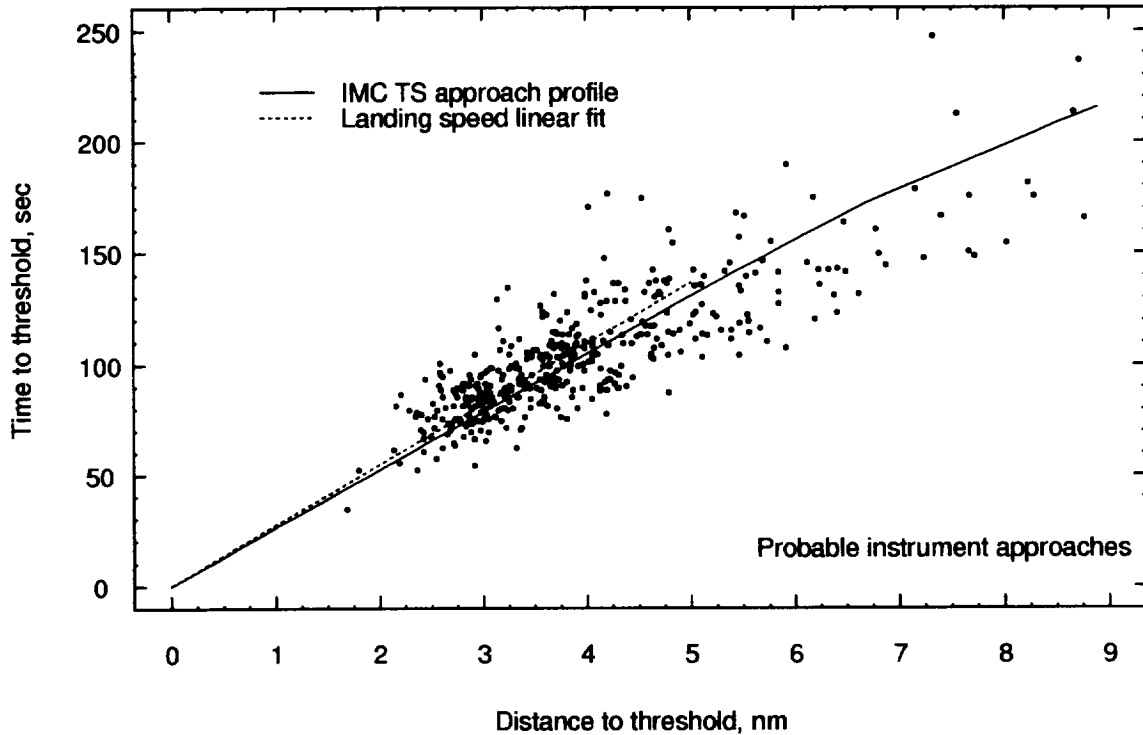
Figure 11. Distance and time separation comparisons for all IMC cases with large jets in trail.

Table 3. Summary comparison of TS approach profiles with DFW data

Aircraft speed/weight class and conditions	Final approach ground speed, knots			Time to threshold at 5 nm, sec		
	TS profile	Data linear fit	Data – TS	TS profile	Data linear fit	Data – TS
Heavy, VMC	153	136	–17	116	127	11
Large jet, VMC	133	133	0	127	127	0
Large turboprop, VMC	100	121	21	150	128	–22
Small turboprop, VMC	108	116	8	145	138	–7
B757, VMC	146	128	–18	120	131	11
Heavy, IMC	150	134	–16	117	134	17
Large jet, IMC	138	127	–11	130	142	12
Large turboprop, IMC	104	123	19	174	146	–28
Small turboprop, IMC	105	122	17	163	147	–16
B757, IMC	146	123	–23	121	146	25

Table 4. VMC separation time estimates[a]

(leading aircraft down, trailing aircraft across)

	Separations, seconds	Heavy	Large jet	Large turboprop	Small turboprop	B757
Heavy	Common path	103	125	126	157	129
	Threshold	103	125	128	157	130
Large jet	Common path	66	66	67	108	66
	Threshold	67	66	76	115	72
Large turboprop	Common path	76	76	75	114	75
	Threshold	67	66	75	115	71
Small turboprop	Common path	78	78	78	78	78
	Threshold	67	66	75	78	71
B757	Common path	106	106	107	136	108
	Threshold	103	103	109	138	108

[a]Based on observed data approach profiles and assuming a common approach path length of 6 nm.

final approach segment. The level of modeling accuracy needed by an automation tool to provide the appropriate level of benefit should also be investigated.

7. Separations Analysis

Threshold separations associated with arrival rushes were analyzed statistically to document and understand current threshold spacing under high-demand arrival conditions. All records associated with weather conditions that required aircraft to follow the final approach course through the approach gate were included. Small props were not analyzed because the low frequency of small-prop landings at DFW resulted in a small sample size.

7.1 Statistical Characteristics

Figure 12 is a histogram of aircraft separation distances for all lead/trail combinations with 2.5-nm required minimum separations. A probability density function with a smoothing window equal to the distance between the first and third quartiles is also shown. The density function and histogram were each determined directly from the data samples. The vertical dashed line represents the minimum required separation. The distribution is asymmetric, with a maximum point corresponding to approximately 3.2 nm and a tail extending to the right. The tail is caused by arrival gaps, which occurred because landing aircraft were not in position to follow a leading aircraft at the required minimum distance. Separations in 7.5 percent of the cases were smaller than the required

minimum; figure 13 shows the corresponding time separations.

The figures are representative of almost all the separation distributions observed. Vandevenne and Lippert developed a simple parametric model that characterizes landing separation distributions (ref. 6); it has two components: "busy periods," or intervals when aircraft are available for landing at the maximum runway capacity, and "idle periods," for all other times. Busy periods represent a situation in which there is no lost runway capacity caused by a lack of aircraft in position, so all separation differences from the FAA minima are caused by the limits of accuracy achievable by the controller and pilot. They are represented by a normal distribution. For idle periods, controller/pilot accuracy effects are combined with the effects of gaps, which are the excess separations that cannot be closed by a trailing aircraft. These idle periods are represented by the convolution of a normal distribution and a Poisson distribution of the arrival gaps. The probability density function (PDF) that describes rush-period separations is equal to the busy-period PDF multiplied by the runway utilization fraction, ρ, plus the idle-period PDF multiplied by $1 - \rho$. The distribution characteristics resulting from the model of reference 6 agree well with those of the recorded data.

In another study, several controller spacing aids were evaluated using simulations of final approach traffic during rush periods (ref. 7). The subjects were responsible for all the major tasks of approach controllers, including spacing, sequencing, and issuing vectors. The simulations were conducted for instrument conditions. Frequency

Table 5. IMC separation time estimates[a]

(leading aircraft down, trailing aircraft across)

Separations, seconds		Heavy	Large jet	Large turboprop	Small turboprop	B757
Heavy	Common path	107	137	140	171	138
	Threshold	107	142	149	177	146
Large jet	Common path	74	71	62	115	69
	Threshold	67	71	76	120	75
Large turboprop	Common path	81	77	74	117	76
	Threshold	67	71	74	117	73
Small turboprop	Common path	81	77	75	74	76
	Threshold	67	71	74	74	73
B757	Common path	116	116	117	146	116
	Threshold	107	113	109	147	116

[a]Based on observed data approach profiles and assuming a common approach path length of 9 nm.

Table 6. Deviations in times of flight from the FAF to the threshold

Aircraft speed/weight class	Standard deviation, sec		Max value – min value, sec	
	VMC cases	IMC cases	VMC cases	IMC cases
Heavy	9	22	36	45
Large jet	20	20	142	86
Large turboprop	18	21	61	63
Small turboprop	13	Insufficient data	27	Insufficient data
B757	12	Insufficient data	43	26
Combined data	19	22	156	95

distributions of excess time and distance separations were found to be symmetrical, and the authors presented their results using measures of standard deviation. These results tend to support the busy-period component of the reference 6 model.

The parametric model of reference 6 was used in that study as a basis for a maximum likelihood estimation of runway utilization and controller/pilot accuracy. However, the model is a simplified representation of actual traffic flow; it uses only one required minimum separation value and one controller buffer value for all arrival traffic. Therefore, the model was deemed unacceptable for analyzing DFW traffic. Instead, an assumption was made that the Poisson distribution associated with gaps does not significantly impact the observed distributions in the range of separations from

the minimum to the distribution maximum; i.e., gaps associated with missed slots are assumed not to significantly affect the left side of the distribution. The impact of the gaps was removed as much as possible by assuming that the left side of the distribution is equal to the left side of a symmetrical distribution that represents traffic flow with no gaps.

Since the maximum point of the distribution is to the right of the required minimum separation, controllers may have been (intentionally or unintentionally) adding extra separation buffers to account for spacing imprecision. In the discussion that follows, the distribution maximum point was used as a measure of this aim point and as the mean of a symmetrical distribution that would represent traffic flow with no gaps.

Figure 12. Distribution of distance separations for all cases wtih 2.5-nm required minimum separations.
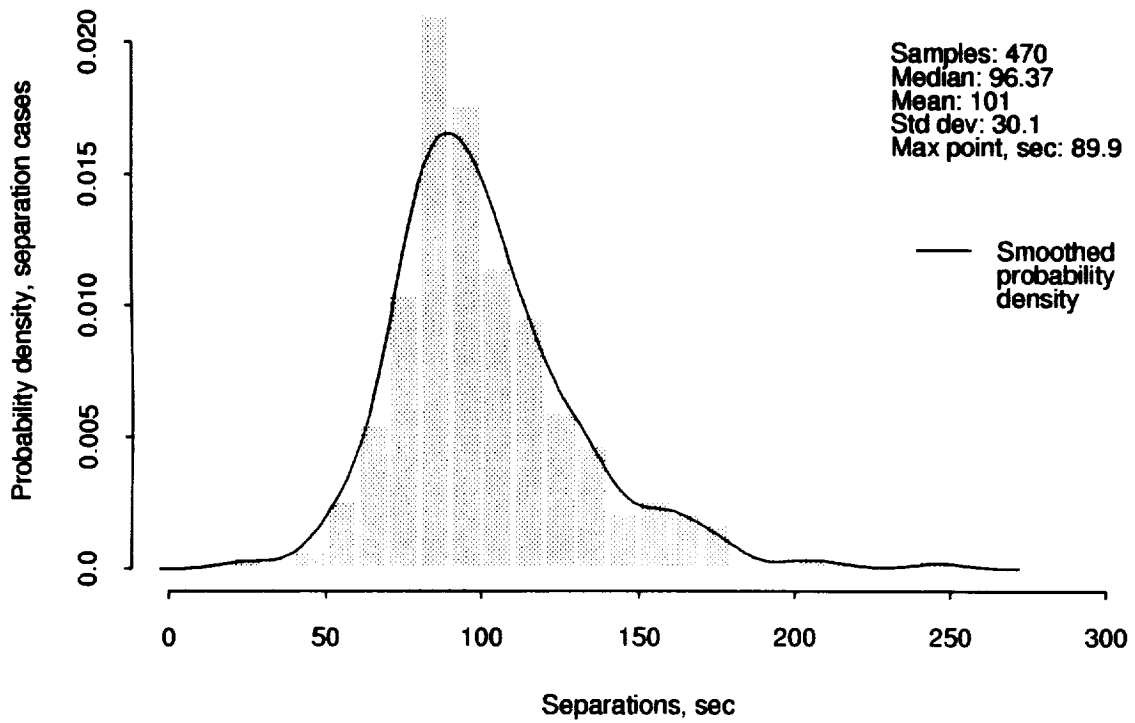
Figure 13. Distribution of time separations for all cases with 2.5-nm required minimum separations.

18
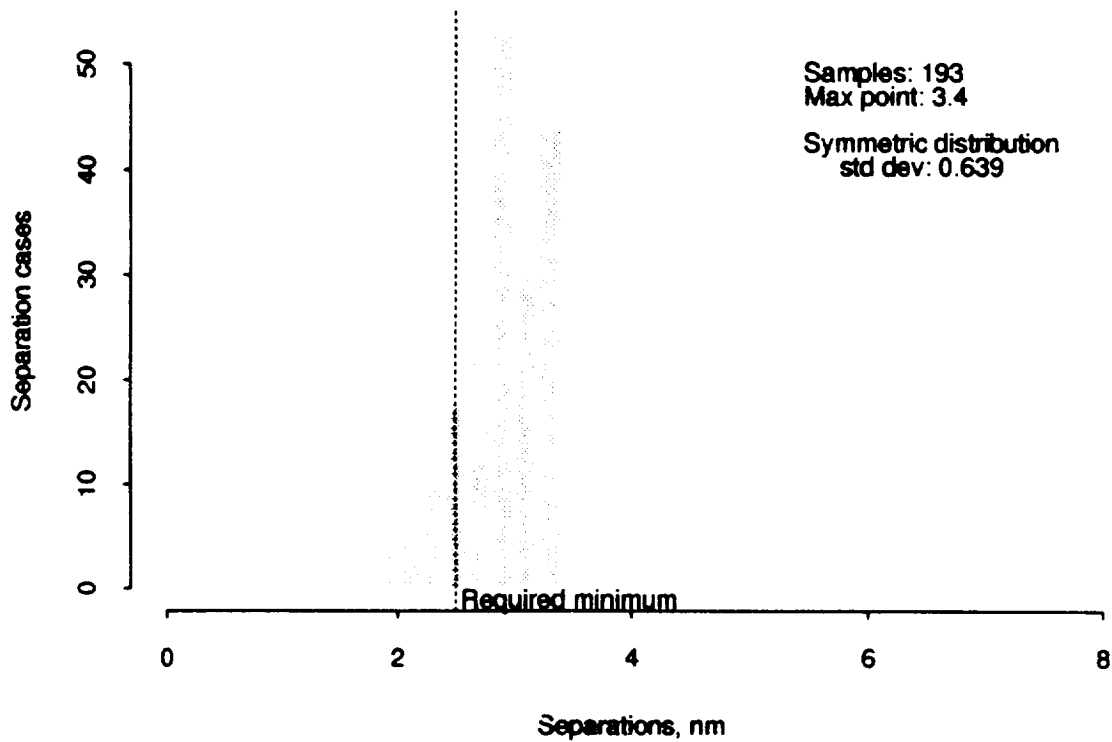
Figure 14. Filtered separation distance distribution for all cases with 2.5-nm required minimum separations.

With these assumptions, the controller/pilot spacings accuracy was obtained by filtering out all data points that have spacings greater than the distribution maximum, and then obtaining the root mean square (rms) deviation of the samples with respect to the maximum point. Figure 14 shows this filtered separation distance half-distribution for the 2.5-nm required separations case. The standard deviation was found to be approximately 0.6 nm. Note that, since the maximum point was based on the smoothed density function, it does not necessarily agree with the maximum population class shown by the histogram.

The full symmetric distribution that would occur for cases with no gaps was obtained by adding the left side half-distribution to its mirror image. For this distribution, nine percent of the cases had smaller separations than the required instrument approach minimum. This metric is referred to as the minimum separation fraction, F_M, in the discussion that follows.

The time separations for the samples of figure 14 are shown in figure 15. To obtain an approximation of the dispersion of time separations, a symmetric distribution maximum point, defined as the time separation that corresponds to the distance maximum of figure 14, was determined by fitting data to relate distance spacings to time spacings. The fitted model was used to determine the

time separation that corresponds to the distance maximum. Once obtained, the maximum time point was used as the mean value in the standard deviation computation. For the 2.5-nm required separations case of the figure, the standard deviation is about 20 seconds.

Figure 16 shows the distance separation distributions for all lead/trail combinations with 3-nm required minimum separations, which usually resulted from separation restrictions caused by wet runways or fog. A comparison with figure 12 shows the distributions to be almost identical, indicating that controllers do not distinguish between 2.5-nm and 3-nm separations. Controllers appear to be aiming for separations slightly over 3 nm for both cases.

Figure 17 presents the distributions for five-nm required minimum separations. The small number of samples makes conclusions difficult, but the spacing precision appears to be quite low. The distribution also appears to have a significant left tail, with some separations actually lower than three nm. No excess buffer is evident from the distribution. A controller suggested that the low separations seen in this case may have resulted from trailing turboprops, which are able to land well past the runway marker. By landing long on visual approaches, turboprops are able to stay above the leading-aircraft flightpath, thereby avoiding its wake. However, examination of the
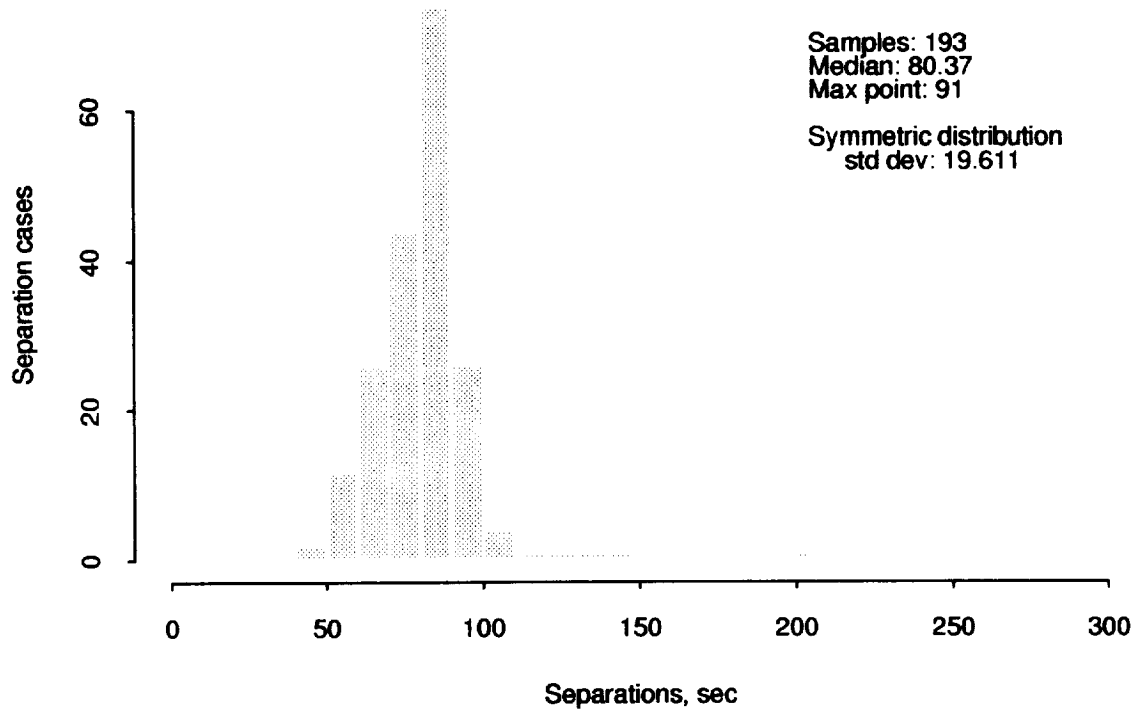
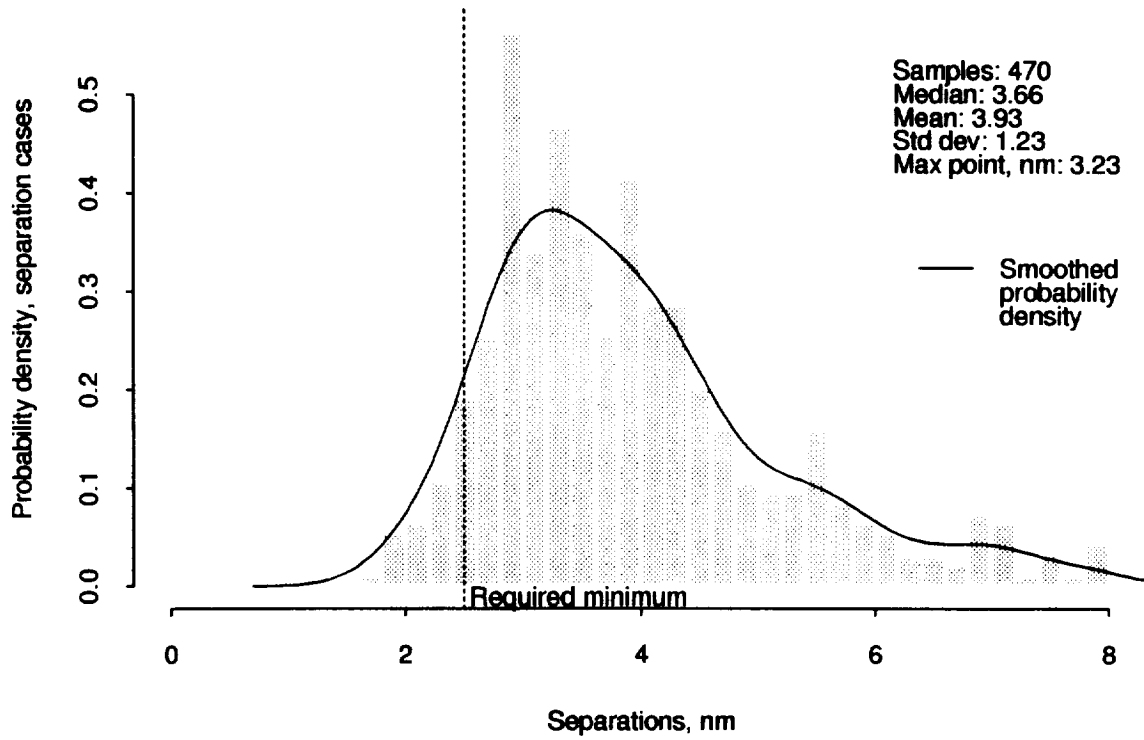Figure 15. Filtered separation time distribution for all cases with 2.5-nm required minimum separations.
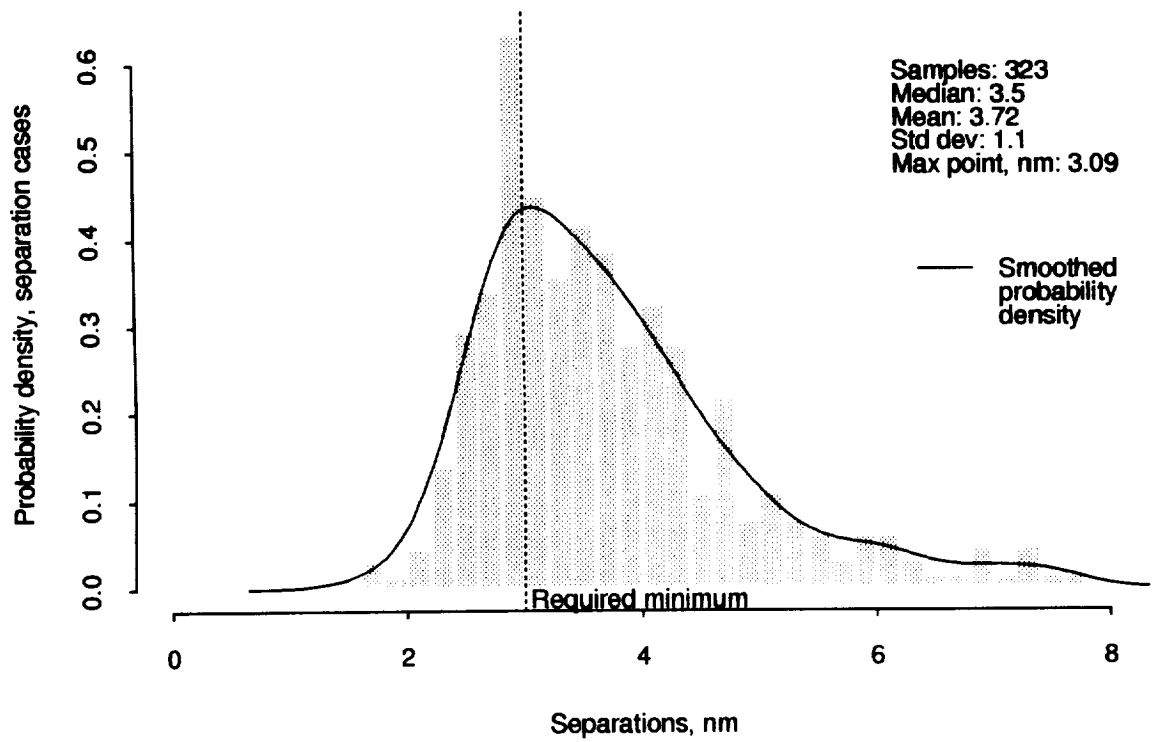
Figure 16. Distribution of distance separations for all cases with 3-nm required minimum separations.

20
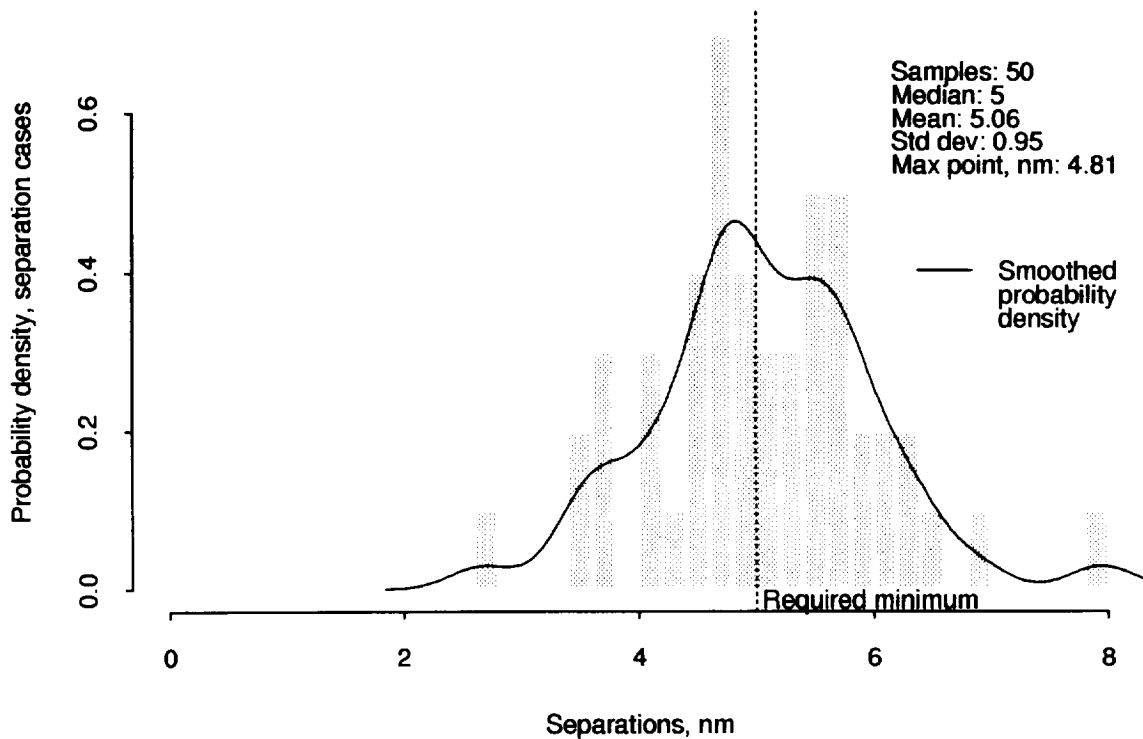
Figure 17. Distribution of distance separations for all cases with 5-nm required minimum separations.

data showed no such correlation between turboprops and the low separations.

Table 7 compares results of the rush-period analysis, broken out by minimum required separation, and results of the simulations of reference 7 are also shown. The live data results tend to support the earlier simulation findings: for manually controlled traffic, standard deviations of interarrival time separation distributions are approximately 19 to 20 seconds for an arrival mix made up mostly of 2.5-nm required separations. The table also shows that both spacing precision and controller buffers tend to decrease with increasing required minimum separations. The results were found not to correlate with weight class or separation restrictions; perhaps some controllers were aiming for one average separation distance that was adequate for most cases.

7.2 Controller Target Separations

Final approach target separations at the threshold used by the controllers were estimated by using results presented in previous sections and observations of individual lead/trail speed/weight class combinations; they are summarized in table 8. Although TRACON controllers are probably most concerned with achieving good separations at the point of handoff to the tower, the

threshold separations presented are believed to be good approximations of the controller target separations. The analysis of section 6.3 showed low incidences of significant separation changes between the FAF and the threshold.

These distance separations were used in conjunction with the required separations model to estimate controller target time separations. The results are shown in tables 9 and 10 for the VMC and IMC cases. The estimates can be used as a reference baseline for future assessments of spacing improvements due to automation. It may be appropriate for an automated spacing tool to schedule threshold arrivals based on these target times instead of times based on required minimum spacings.

7.3 Buffer Reduction Potential

The controller target separations were also used to develop a simple method for estimating the potential for an automated spacing tool to reduce spacings, thereby increasing arrival capacity. As previously explained, the target separations were assumed to include the minimum required separation and a buffer. Because lower separation variance is anticipated when using an automated tool, some reduction of the buffer can be achieved without changing the minimum separation fraction. The amount

21

Table 7. Rush-period arrival spacing precision

Minimum required separation, nm	Samples	Max point, excess nm	Symmetric separation std dev, nm	Symmetric separation std dev, sec	Minimum separation fraction, F_M
2.5	470	0.7	0.64	19.6	0.09
3.0	323	0.1	0.53	19.6	0.38
4.0	112	0.4	0.86	25.5	0.33
5.0	50	-0.2	0.83	38.2	0.56
Simulation, ref. 7[a]	514	0.31 (mean)	0.65	19.49	N/A

[a]Lumped subject data interarrival error for 170-knot manual pattern procedure. Arrival traffic weight class mix was made up of 87.5-percent large and 12.5-percent heavy, resulting in minimum required separations as follows: 87.5 percent—2.5 nm; 1.5 percent—4 nm; 11 percent—5 nm.

Table 8. Estimated controller target threshold crossing separations[a] in nm

(leading aircraft down, trailing aircraft across)

Aircraft speed/weight class	Heavy	Large jet	Large turboprop	Small turboprop	B757
Heavy	4.2	5.2	5.6	6.2	5.2
Large jet	3.2	3.2	3.6	4.2	3.1
Large turboprop	3.1	3.1	3.2	4.2	3.1
Small turboprop	3.1	3.1	3.1	3.1	3.1
B757	4.2	4.2	4.2	5.2	4.2

[a]For conditions having a ceiling less than 3000 ft AGL or visibility less than 5 mi.

Table 9. VMC controller target separation time estimates, based on live data approach trajectories and assuming a common approach path length of 6 nm

(leading aircraft down, trailing aircraft across)

	Separations, seconds	Heavy	Large jet	Large turboprop	Small turboprop	B757
Heavy	Common path	108	130	139	161	133
	Threshold	108	130	140	161	134
Large jet	Common path	84	85	95	114	83
	Threshold	85	85	101	120	87
Large turboprop	Common path	89	89	94	118	91
	Threshold	82	82	94	120	87
Small turboprop	Common path	91	91	94	95	93
	Threshold	82	82	82	95	87
B757	Common path	110	110	111	140	112
	Threshold	108	108	113	141	112

of reduction can be calculated if a value of standard deviation associated with the automated system, σ_A, is specified. The resulting reduced buffer size can then be used as input to a Monte Carlo simulation of the automation tool to determine the overall benefits achievable.

The buffer reduction potential, R, determined as a function of σ_A, is illustrated in figure 18. Using a fitted function, the time separation associated with the required minimum separation was estimated; then a symmetric distribution estimate of the time separation data was made to obtain the distribution mean, μ_M, and the minimum separation fraction, F_M. A normal distribution that had an identical minimum separation fraction, F_A, was used to represent the distribution achievable through automation. It was obtained by calculating the fractile associated with F_A for a normal distribution with a standard deviation equal to σ_A and a mean equal to zero. The mean, μ_A, was then determined by subtracting the obtained fractile value from the required minimum time separation. The buffer reduction potential was equal to $\mu_M - \mu_A$.

Given the assumption of normal distributions, the buffer reduction potential was a linear function σ_A. Table 11 shows the resulting buffer reduction slopes for the four required separation cases. For the 2.5-nm cases, each second of reduction in standard deviation results in a buffer compression of about 1 sec. If a value of σ_A of 10 sec can be achieved through automation, a buffer reduction of approximately 7.5 sec can be obtained, which corresponds to a 7- to 9-percent time reduction between landing aircraft.

This estimate of buffer reduction potential is strongly dependent on the minimum separation fraction and the size of the excess buffer observed in the data. For example, the excess buffer is slightly negative for the

Table 10. IMC controller target separation time estimates, based on live data approach trajectories and assuming a common approach path length of 9 nm

(leading aircraft down, trailing aircraft across)

	Separations, seconds	Heavy	Large jet	Large turboprop	Small turboprop	B757
Heavy	Common path	112	141	157	177	143
	Threshold	112	146	165	183	150
Large jet	Common path	93	91	102	121	88
	Threshold	86	91	107	125	92
Large turboprop	Common path	95	93	94	123	92
	Threshold	83	88	94	123	91
Small turboprop	Common path	95	93	91	91	92
	Threshold	83	88	91	91	91
B757	Common path	121	122	123	152	122
	Threshold	112	119	123	153	122

Table 11. Buffer reduction potential, assuming the observed minimum separation fraction is maintained by an automated system

Minimum required separation, nm	Reduction slope, sec R per sec σ_A	R, sec for $\sigma_A = 10$ sec
2.5	-1.00	7.5
3.0	-0.25	1.5
4.0	-0.25	4.5
5.0	2.00	0

23
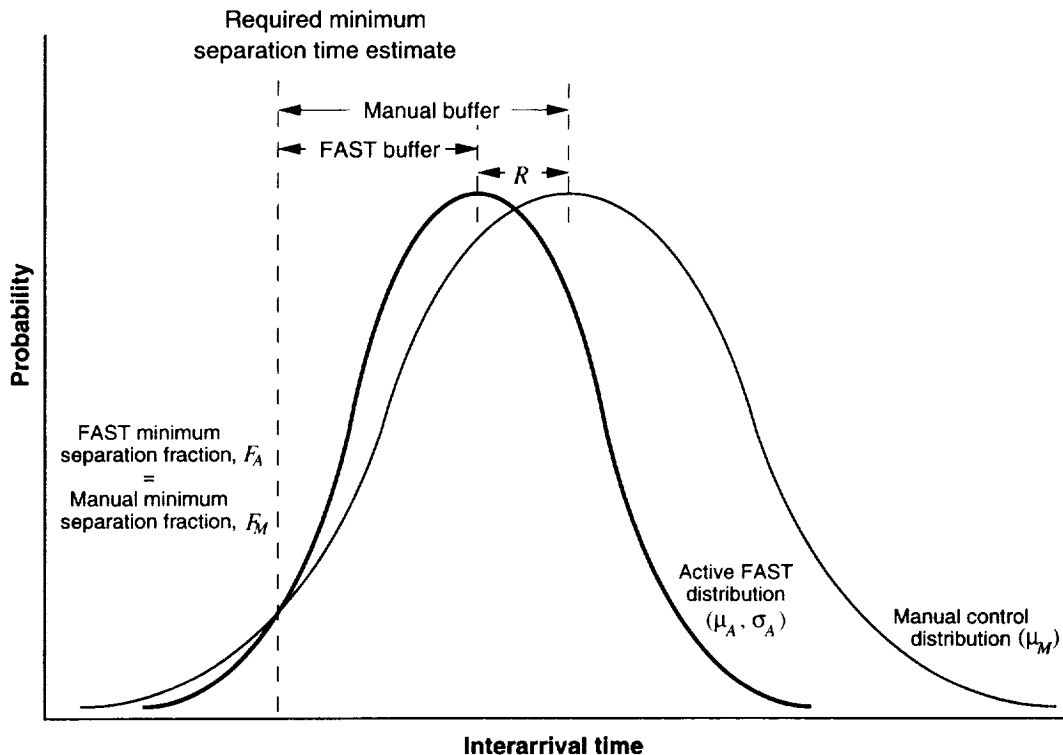
Figure 18. Method for estimating the potential of active FAST to reduce the controller buffer.

five-nm minimum required separations case, resulting in no potential for buffer reduction, as seen in table 11. The results may not be representative because of the small sample size for the five-nm case, but they indicate that the improvement possible for this case is small at best, using the buffer reduction performance metric as defined. Further study is needed to identify and develop performance metrics that capture the full value of more accurate spacing.

8. Runway Utilization and Capacity

An analysis of runway utilization and capacity was performed for all runways that were active during each of the 30 recorded rush periods. Spacings of individual aircraft pairs and the relationship of these spacings to each other were examined to identify usage trends. For each aircraft pair, interarrival distance and time separations were compared with the required threshold minima, which were computed using the required separations model.

8.1 Threshold Spacing Plots

A graphical representation of landing spacing as a function of time was developed to facilitate the analysis.

An example of the graphic, referred to herein as a "threshold interarrival spacing plot," is shown in figure 19. Overall runway utilization can also be seen, and aircraft landing order and type mixes can be determined from the plot. Excess separations are represented as vertical bars attached to a horizontal zero line that corresponds to the minimum required separation at the runway threshold. Positive excess values represent cases when additional runway landing rate could have been obtained by closing up spacings between aircraft. Negative values may or may not constitute separation violations, depending on whether or not the pilot has assumed responsibility for a visual approach. Information relating to the landing aircraft is displayed at the apex of each bar, and all separations information refers to spacing of the aircraft with respect to a leading aircraft. The bold numbers display minimum required separations; they are based on the required separations model with modified final approach profiles, as described in section 6.4. The aircraft type and call sign are also displayed for each bar.

Some simple computations were performed for each runway rush period to obtain approximations of runway utilization and capacity. They were intended to provide conservative estimates, except for some special situations as noted. An aircraft landing rate, L, was determined over the interval defined by the first leading aircraft and the

24

Figure 19. Threshold interarrival spacing plot showing typical runway utilization during rush periods.

25

last trailing aircraft, and results were adjusted to represent aircraft per hour:

$$L = \frac{N-1}{t_N - t_1} \quad \text{(a/c/hr)}$$

where N is the number of aircraft that landed over the rush period and t is the time. The average required minimum separation $(S_{R_{avg}})$ that included a controller separation buffer b was also determined. The buffer was used to keep all capacity estimates conservative.

$$S_{r_{avg}} = \frac{1}{N-1} \sum_{i=2}^{N} \left(S_{r_i} + b \right) \quad \text{(nm)}$$

An approximation was also made of the number of additional aircraft that could have landed per hour. The positive and negative excess separations were totaled to obtain a net excess for the rush period, which was adjusted to units of aircraft per hour. This result was divided by the average required minimum separation and limited to values greater than or equal to zero:

$$l_1 = \max \left[0, \frac{1}{S_{R_{avg}}(t_N - t_1)} \sum_{i=2}^{N} S_{E_i} \right] \quad \text{(a/c/hr)}$$

where excess separation (S_E) was defined as the actual longitudinal separation minus the required separation for each in-trail aircraft.

$$S_E = S - S_R \quad \text{(nm)}$$

A more commonly used alternative estimate of additional runway capacity was obtained by calculating the maximum capacity with no excess separations and subtracting the actual landing rate from it:

$$l_2 = \max[0, C - L] \quad \text{(a/c/hr)}$$

The maximum capacity was found by inverting the time separation corresponding to the average required minimum separation:

$$C = \frac{1}{T_{R_{avg}}} \quad \text{(hr)}$$

where $T_{R_{avg}}$ represents the average required interarrival time for the rush period, including the buffer. $T_{R_{avg}}$ was a function of the average required minimum separation and the average landing velocity,

$$T_{R_{avg}} = \frac{S_{R_{avg}}}{V_{avg}} \quad \text{(hr)}$$

where V_{avg} was empirically determined from the analysis of landing speeds to be 125.8 knots for IMC and 128.6 knots for VMC.

The estimate displayed on the threshold spacing plots, l_1, yields a higher result than the alternative, l_2. Assuming that negative excess separations seen in the data are acceptable, the l_1 estimate may be a better representation of the maximum potential of each runway.

Inputs to the analysis included meteorological conditions and known separation restrictions. A no-reassign point of 0.5 nm was used for all cases. Common approach path lengths were assumed to be 6 nm for VMC approaches and 9 nm for IMC approaches, and the controller spacing buffer, b, was set equal to 0.25 nm. Note that decreasing the controller buffer increased the estimates of runway capacity and additional aircraft possible to land.

Although the inboard parallel runways are normally used for departures, arriving aircraft are directed to land on the inboard runways in some cases. Because the closely spaced north/south parallel runways are dependent, they were combined into one effective runway for the analysis. Hence, Runways 17R and 17L were combined into Runway 17, 18R and 18L were combined into 18, 35R and 35L were combined into 35, and 36R and 36L were combined into 36.

8.2 Threshold Interarrival Time Plots

Using the interarrival times obtained from the required separations model, a similar time history plot was generated for time separations. An example that corresponds to the rush period of figure 19 is shown in figure 20. The vertical bars represent excess separation in seconds. In these "threshold interarrival time plots," any positive Center delay incurred by an aircraft is indicated in seconds by the small number at the apex followed by "CD," and excess threshold time is indicated similarly with "ET." For the positive excess times, the bold portion of each vertical bar represents the portion of excess separation that could have been removed because the aircraft was delayed in the Center. In the figure, all aircraft that were delayed had Center delays larger than the excess time separations, so their corresponding vertical bars are entirely bold. If the Center delay was less than the excess time for an aircraft, its vertical bar was bold over the portion corresponding to the amount of the excess time that could have been reduced. As would be expected, the majority of aircraft landing during the rush periods were delayed in the Center.

The Center delay values associated with the bold vertical bars were summed to obtain a value of potential Center delay reduction. This estimate assumed that aircraft were

Excess separation, sec

All separation cases evaluated
Airport runway(s) evaluated: 18R/18L
All aircraft types evaluated
No-reassign point: 0.50 nm before threshold

Approach conditions: IMC
Separation restrictions: 3 nm
Extra separation buffer: 0.25 nm

Total number of cases: 29
Number of a/c landed: 30
Sum of excess separations: 48.12 nm
  Sum of positive excess seps: 50.38 nm
  Sum of negative excess seps: 2.25 nm
Analysis time period: 00:57
  Analysis start time: 00:40
  Analysis finish time: 01:37
Time between first and last a/c: 00:55:29
Avg required min sep w/buffer: 3.61 nm, 103 sec
Landing rate (a/c per hr): 32.4
Additional a/c per hr possible: 14
Potential Center delay reduction: 499 sec/hr
Total Center delay: 9952 sec/hr

250 225 200 175 150 125 100 75 50 25 0 −25 −50 −75 −100 −125

CM TIME—>
UTC-TIME—>

00:50 / 16:40   01:00 / 16:50   01:10 / 17:00   01:20 / 17:10   01:30 / 17:20

Figure 20. Threshold interarrival time plot showing typical runway utilization during rush periods.

27

delayed because of the lack of runway availability, and that no additional delays were incurred in terminal airspace. The estimate was adjusted to units of seconds of Center delay per rush hour, and is shown in the figure. Vertical bars corresponding to negative values are not considered in the computation; these aircraft could not land at an earlier time without reducing separations further below the required minima.

Although the delay reduction calculation is approximate, it may be a conservative estimate of the actual potential for reducing delays. If two or more aircraft with positive excess times and Center delays are in sequence, further delay reduction could be obtained by rescheduling the lead aircraft to land earlier, thereby increasing the excess time and delay reduction potential of the trailing aircraft. To obtain an approximation of the upper bound of delay reduction potential, the total of all positive delays incurred in the Center for all displayed aircraft is also provided in the figure. This value is also adjusted to show seconds of delay per hour of rush period.

8.3 Plot Analysis Examples

Figure 19 corresponds to a rush period referred to as the "Noon Balloon" by DFW personnel; it lasted approximately 1 hour, with an arrival type mix resulting in an average required minimum separation (with buffer) of about 3.6 nm. The landing rate during this period was about 32 aircraft per hour, and an additional 14 aircraft could have landed with no increase in negative excess separations. These values are typical of results seen for the north/south runways during IMC.

The correlation between this threshold interarrival spacing plot and the interarrival time plot of figure 20 is good: similar trends are observed in both plots, an indication that the approach profiles extracted from the data are representative of flight times to the threshold for the various aircraft types. An exception is aircraft LSS1262, which has a lower excess time separation than would be expected from the distance plot. This aircraft, a large turboprop, had a much higher speed than was predicted by the required separations model. Although further refinement of the required separations model may be needed, the results shown are greatly improved over initial results that were based on the original TS-generated approach profiles.

Another example of the correlation between the two types of plots is seen in figures 21 and 22. The general trends are in excellent agreement. Note that the excess times seen in figure 22 are slightly larger than they should be to match the excess distance spacings. This discrepancy can be seen in the figures by comparing plots for aircraft with

very small excess distance separations, such as DAL1029. The required separations model appears to overestimate the interarrival times by approximately 10 seconds for this case. The opposite trend can be seen in figures 19 and 20. The variability of winds on final approach may account for the differences observed.

8.4 Observed Trends

Several characteristics were observed in the threshold interarrival plots for individual runways:

8.4.1 Controller differences– In many cases, the large variations seen in the results may be attributable to variations in controller capability. Figures 19 and 20 are good representations of typical IMC arrival separations in the observed data, and the performance measures shown are representative of the overall results for IMC. Large excess separations are observed, even during Center delay buildup, and a few small negative excess separations occur. Figures 23 and 24 represent a different "Noon Balloon" rush with very similar meteorological conditions. In the latter rush, very accurate separations are maintained between aircraft; the landing rate is high, and the number of additional aircraft possible to land is very small. Because of the high runway utilization, the potential for Center delay reduction has been lowered by 35 percent. If the recorded dataset is considered a basis for judgment, the latter rush represents excellent runway utilization by manual control.

Both recordings were made under IMC, with 3-nm separation restrictions and wet runways. Both sets of results are shown for Runway 18. The latter rush occurred during two-runway arrivals operations, whereas the former rush occurred during normal three-runway operations. For both rushes, there was significant delay buildup in the Center. The large differences in the two sets of results can possibly be attributed to differences between the TRACON radar controllers. If so, a possible measure of the effectiveness of automation is the reduction of these differences.

8.4.2 Impact of meteorological conditions– As explained in section 6.1, meteorological conditions on approach impact the practices of pilots and procedures followed by pilots and controllers. Some of these differences in the procedures can be seen by comparing radar tracks of rush periods for conditions better than 3000-ft ceiling/5-mi visibility with those under poorer conditions. Figure 25 is an example of north-flow arrivals during poor conditions. The airport ceiling was reported to be 1000 ft AGL with 5-mi visibility, and there was no precipitation. Most of the aircraft tracks are seen to be

28

Excess
separation,
nm

All separation cases evaluated
Airport runway(s) evaluated: 35R
All aircraft types evaluated
No-reassign point: 0.50 nm before threshold

Approach conditions: VMC
Separation restrictions: None
Extra separation buffer: 0.25 nm

Total number of cases:	19
Number of a/c landed:	20
Sum of excess separations:	13.71 nm
Sum of positive excess seps:	16.34 nm
Sum of negative excess seps:	2.62 nm
Analysis time period:	00:34
Analysis start time:	03:15
Analysis finish time:	03:49
Time between first and last a/c:	00:32:14
Avg required min sep w/buffer:	3.16 nm, 88 sec
Landing rate (a/c per hr):	37.2
Additional a/c per hr possible:	8

10.0
9.0
8.0
7.0
6.0
5.0
4.0
3.0
2.0
1.0
0.0
-1.0
-2.0
-3.0
-4.0
-5.0

CM TIME->
UTC-TIME->

03:25   03:35   03:45
20:39   20:49   20:59

DAL941
MD88
2.5

AAL1772
FK10

AAL49
B767
2.5

5.0 DAL540
DAL110 B737
MD88
2.5

DAL845
B727
2.5

AAL2225
MD8
2.5

DAL1935
MD88
2.5

DAL946
B727
2.5

DAL1727
B727
2.5

DAL1029
B737
2.5

AAL71
B767
2.5

FAL50 EGF364
MD8
5.0   2.6
EGF364
SF34

ASE952
E120
2.5

DAL661
B767
2.5

AAL2057
B727
5.0

2.6
EGF114
SF34

AAL2293
FK10
2.5

AAL491
B757
2.5

Figure 21. Threshold interarrival spacing plot for the time/distance correlation example.

29

30

Figure 22. Threshold interarrival time plot for the time/distance correlation example.

All separation cases evaluated
Airport runway(s) evaluated: 35R
All aircraft types evaluated
No-reassign point: 0.50 nm before threshold

Approach conditions: VMC
Separation restrictions: None
Extra separation buffer: 0.25 nm

Total number of cases:	19
Number of a/c landed:	20
Sum of excess separations:	13.71 nm
Sum of positive excess seps:	16.34 nm
Sum of negative excess seps:	2.62 nm
Analysis time period:	00:34
Analysis start time:	03:15
Analysis finish time:	03:49
Time between first and last a/c:	00:32:14
Avg required min sep w/buffer:	3.16 nm, 88 sec
Landing rate (a/c per hr):	37.2
Additional a/c per hr possible:	8
Potential Center delay reduction:	398 sec/hr
Total Center delay:	2417 sec/hr

Excess separation, sec

250 225 200 175 150 125 100 75 50 25 0 -25 -50 -75 -100 -125

CM TIME->
UTC-TIME->

03:25 / 20:39   03:35 / 20:49   03:45 / 20:59

Figure 23. Threshold interarrival spacing plot for a high-runway-utilization period.

All separation cases evaluated
Airport runway(s) evaluated: 18R/18L
All aircraft types evaluated
No-reassign point: 0.50 nm before threshold

Approach conditions: IMC
Separation restrictions: 3 nm
Extra separation buffer: 0.25 nm

Total number of cases:	46
Number of a/c landed:	47
Sum of excess separations:	12.89 nm
Sum of positive excess seps:	18.01 nm
Sum of negative excess seps:	5.12 nm
Analysis time period:	01:20
Analysis start time:	01:10
Analysis finish time:	02:30
Time between first and last a/c:	01:16:03
Avg required min sep w/buffer:	3.51 nm, 100 sec
Landing rate (a/c per hr):	37.1
Additional a/c per hr possible:	2

All separation cases evaluated
Airport runway(s) evaluated: 18R/18L
All aircraft types evaluated
No-reassign point: 0.50 nm before threshold

Approach conditions: IMC
Separation restrictions: 3 nm
Extra separation buffer: 0.25 nm

|	
Total number of cases:	46
Number of a/c landed:	47
Sum of excess separations:	12.89 nm
Sum of positive excess seps:	18.01 nm
Sum of negative excess seps:	5.12 nm
Analysis time period:	01:20
Analysis start time:	01:10
Analysis finish time:	02:30
Time between first and last a/c:	01:16:03
Avg required min sep w/buffer:	3.51 nm, 100 sec
Landing rate (a/c per hr):	37.1
Additional a/c per hr possible:	2
Potential Center delay reduction:	324 sec/hr
Total Center delay:	21481 sec/hr
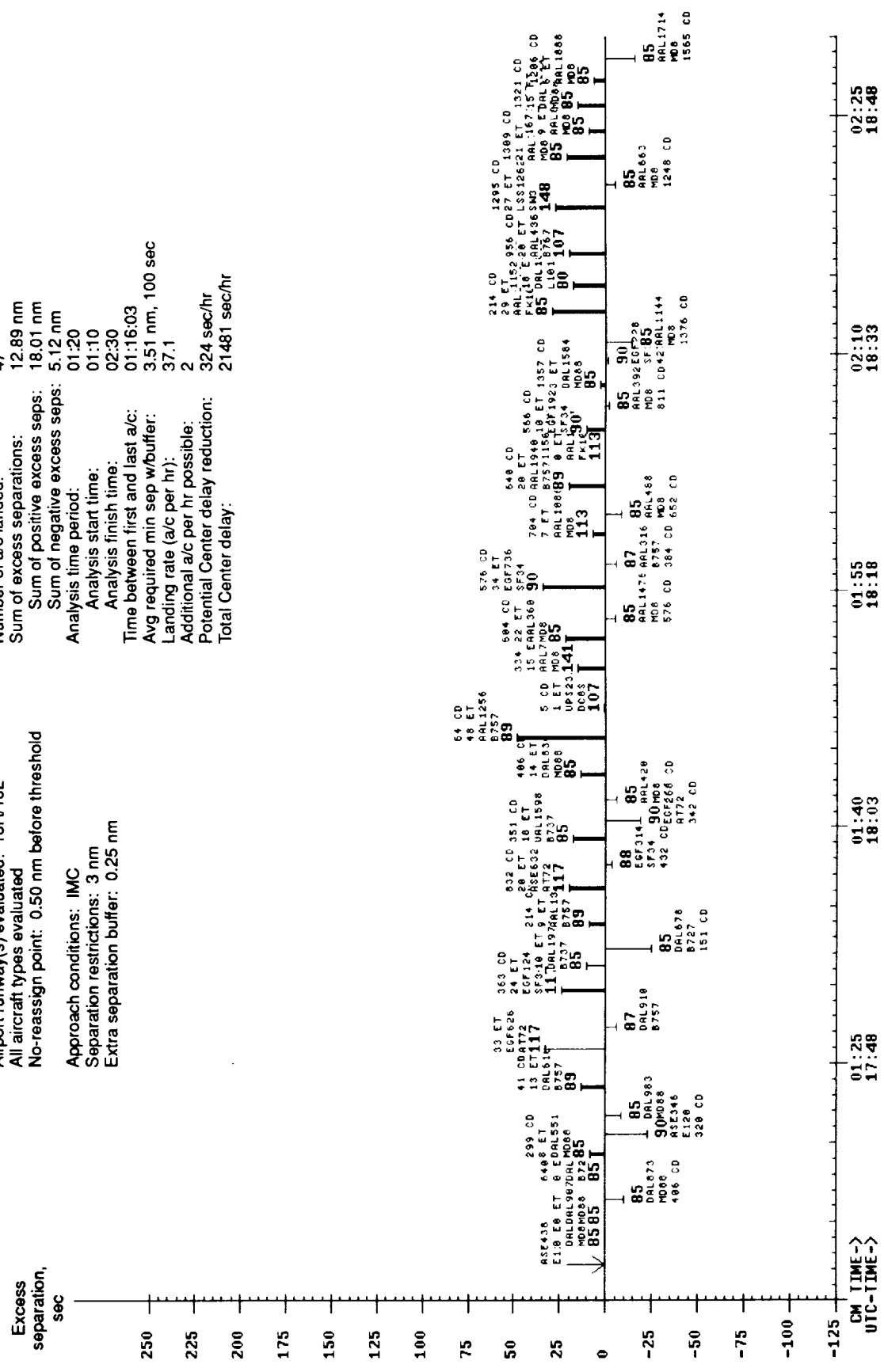
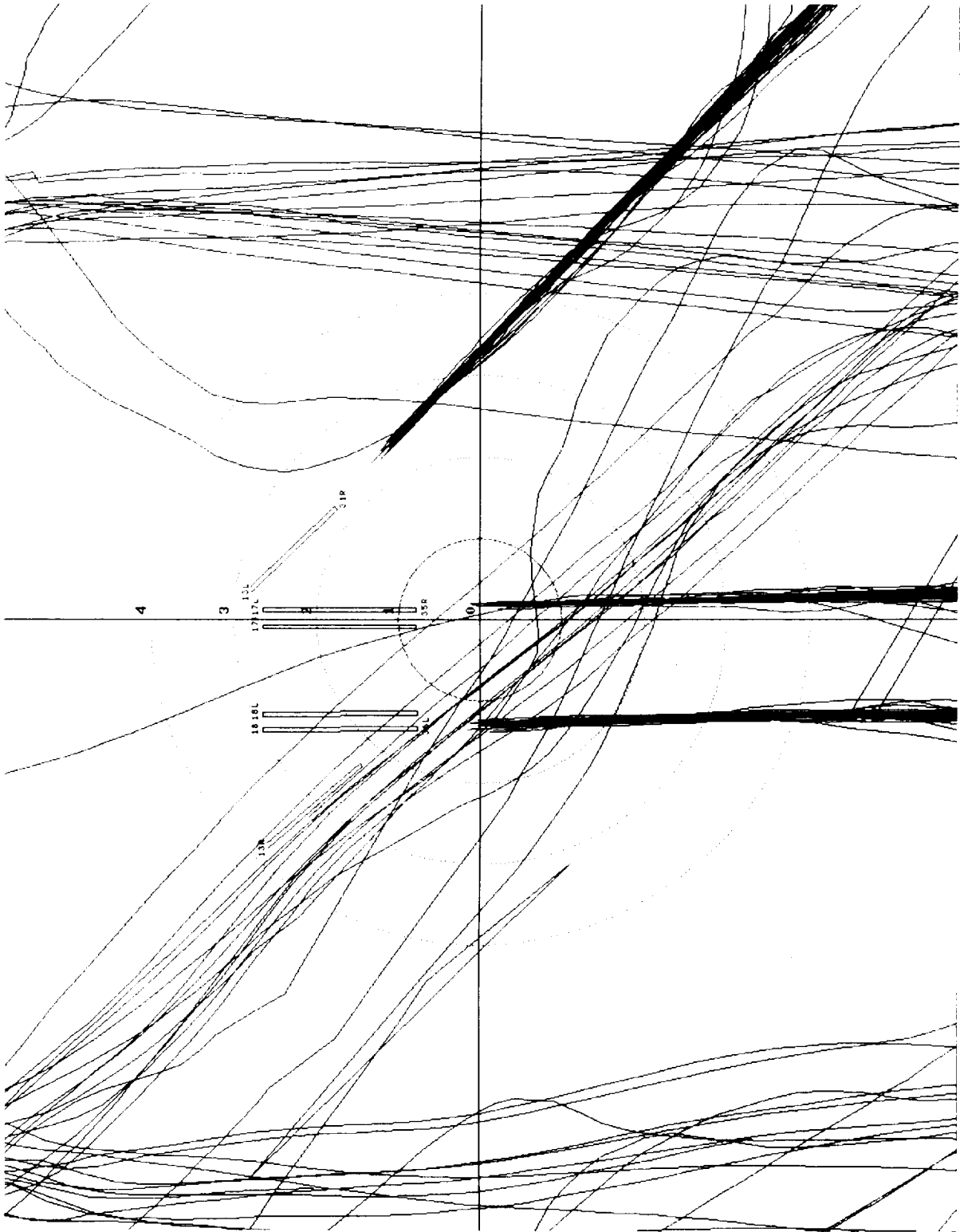Figure 24. Threshold interarrival time plot for a high-runway-utilization period.

Figure 25. Example of radar tracks during IMC.

straight and lined up with the landing runways; they are tightly grouped laterally as they approach the runway thresholds, and no aircraft are reassigned to the inboard north/south runways. Figure 26 shows a similar rush period that occurred during good weather conditions; there was no ceiling, and the visibility was 15 mi. Some aircraft are seen to turn on to the final approach course as late as 4 nm from the threshold. For Runway 31R, the stadium visual approach was in effect for some aircraft. The tracks also display much larger deviations from the runway centerline near the runway threshold, and some aircraft were directed to land on the inboard north/south runways.

Figures 27 and 28 show the threshold interarrival spacing and time plots that correspond to the poor conditions of figure 25. Aircraft are approximately evenly spaced, with only a few slightly negative excess separations. The landing rate is lower than 40 aircraft per hour. Figures 29 and 30 correspond to the good-weather case. Aircraft are less evenly spaced, and there are more negative excess separations. The number of additional aircraft that could be landed is smaller, and the landing rate is more than 40 aircraft per hour. The use of inboard runways for arrivals, the efficient utilization of runways by turbo-props, and the spacing discretion of pilots flying during visual conditions all contribute to the higher arrival rates observed in good weather.

8.4.3 Lengths of rush periods– Rush-period lengths varied from a low of 15 minutes to a high of almost 2 hours. The median value of the dataset was 50 minutes. Figure 31 is an example of an unusually long rush period, lasting 111 minutes. Two runways were in operation, with a ceiling of 300 ft AGL and 1.5-mi visibility. This rush probably corresponded to a delayed arrival rush from the east combined with a rush from the west at 18:30 CST. Controller practices and runway utilization seem fairly consistent over the duration of the rush period. The potential Center delay reduction of 761 sec/hr is very large, as would be expected under such poor conditions.

8.4.4 Observed controller practices– Figure 32 shows an example of low runway utilization, which existed even though aircraft were experiencing large delays in the Center. The runway shown is 31R, a diagonal runway for north-flow traffic. The diagonal runways were observed to be underutilized frequently, especially during VMC. The controllers may have tried to accommodate the air carriers, who may prefer the north/south runways at DFW. Surface operations required from a diagonal runway are usually greater, and there are time delays associated with crossing the north/south runways to get to the passenger terminals. The low utilization of the

diagonals was found to be independent of the direction of the arrival rush.

Figure 33 shows an example of extremely high runway utilization. The rate of 48 aircraft per hour resulted from the large number of negative excess separations. It should be noted that, even under these conditions, there was potential for reducing Center delay and for landing additional aircraft.

Another characteristic that was consistently observed in the data can be seen in figures 27 and 28. Aircraft that follow B757s tend to cross the threshold with negative excess separations more frequently than for other types. An example is flight AAL201, which has a negative excess separation of about 0.8 nm. This trend highlights the complexity and difficulty of the controller's task in achieving different required spacings for the various combinations of aircraft weight classes.

8.5 Combined Data Analysis

All the rush-period recordings were combined so that approximations of utilization and capacity could be made for each runway and the airport. Table 12 summarizes the number of rush periods used for each runway in the combined dataset. As can be seen, IMC rush periods were difficult to obtain, especially for the diagonal runways. These numbers should be kept in mind when interpreting the combined results.

Table 12. Runway rush periods

Landing runway	Number of rush periods	
	IMC	VMC
13R	2	6
17	6	6
18	6	6
31R	1	6
35	3	15
36	3	15
Total	21	54

8.5.1 Runway landing rates– The combined dataset landing rates for each runway are shown in table 13; landing rates were found to be greater under VMC than under IMC. This trend probably resulted from the pilot discretion issues discussed in section 3.2. Landing rates were also observed to be lower for the diagonal runways
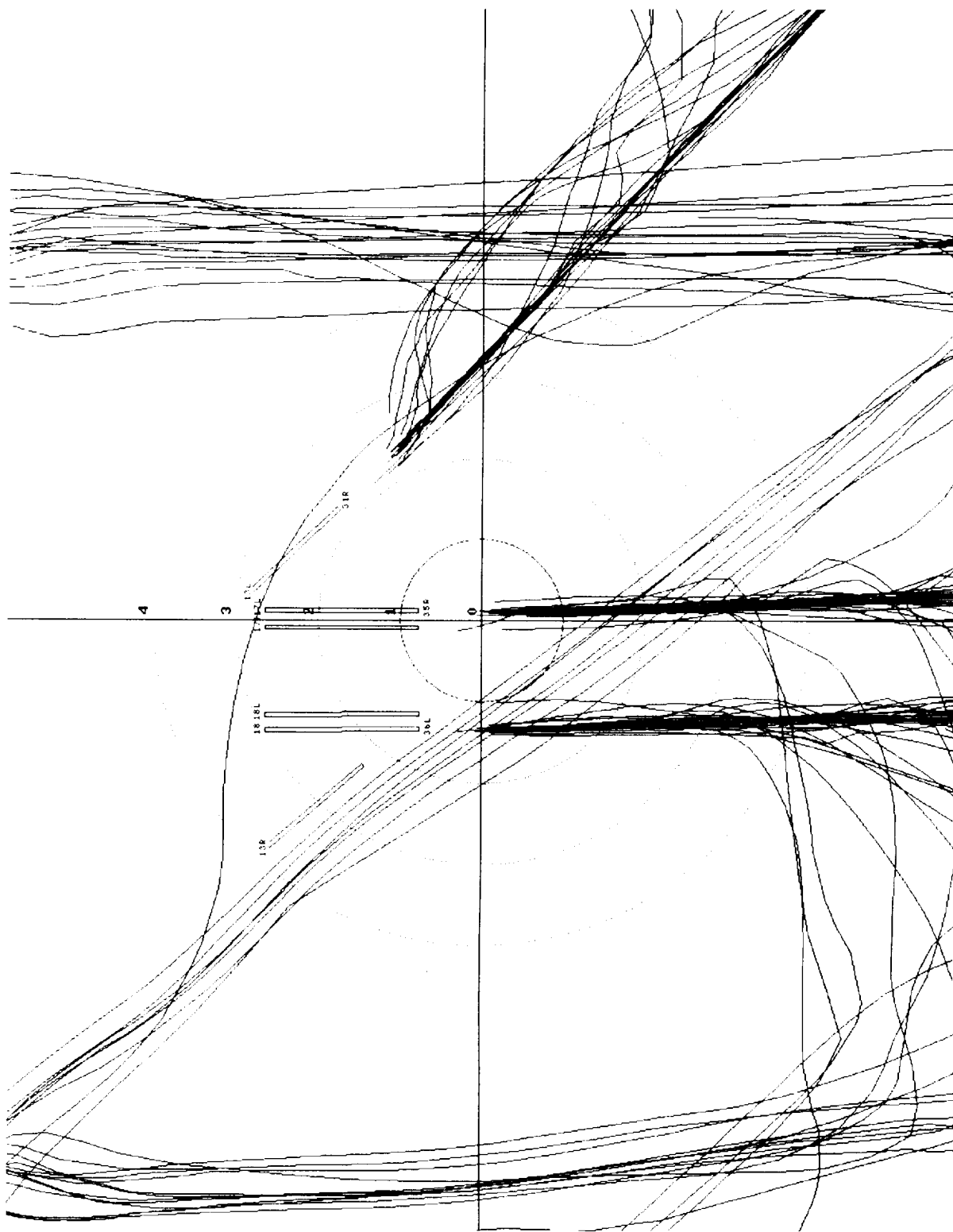
Figure 26. Example of radar tracks during VMC.

Excess separation, nm

All separation cases evaluated
Airport runway(s) evaluated: 35R
All aircraft types evaluated
No-reassign point: 0.50 nm before threshold

Approach conditions: VMC
Separation restrictions: None
Extra separation buffer: 0.25 nm

Total number of cases:	18
Number of a/c landed:	19
Sum of excess separations:	10.75 nm
Sum of positive excess seps:	12.61 nm
Sum of negative excess seps:	1.86 nm
Analysis time period:	
Analysis start time:	00:30
Analysis finish time:	00:55
Time between first and last a/c:	01:25
Avg required min sep w/buffer:	00:29:10
Landing rate (a/c per hr):	2.98 nm, 83 sec
Additional a/c per hr possible:	39.1
	7

10.0
9.0
8.0
7.0
6.0
5.0
4.0
3.0
2.0
1.0
0.0
-1.0
-2.0
-3.0
-4.0
-5.0

CM TIME—>
UTC-TIME—>

01:00 / 16:45
01:05 / 16:50
01:10 / 16:55
01:15 / 17:00
01:20 / 17:05
01:25 / 17:10

AAL85 B757
AAL584 B727 2.5
AAL1079 FK10 2.5
4.0 AAL291 MD8
AAL392 MD8 2.5
AAL1428 MD8 2.5
AAL1581 MD11 2.5
5.0 USA1217 MD8
AAL1527 B727 2.5
AAL736 MD8 2.5
EGF504 SF34 2.6
2.5 AAL1643 MD8
2.5 AAL1845 FK10
AAL420 MD8 2.5
AAL1888 MD8 2.5
AAL824 MD8 2.5
2.5 AAL1616 FK10
AAL1714 MD8 2.5
UPS2277 DC08 2.5

Figure 27. Spacing characteristics during an IMC rush period.

Excess
separation,
sec

All separation cases evaluated
Airport runway(s) evaluated: 35R
All aircraft types evaluated
No-reassign point: 0.50 nm before threshold

Approach conditions: VMC
Separation restrictions: None
Extra separation buffer: 0.25 nm

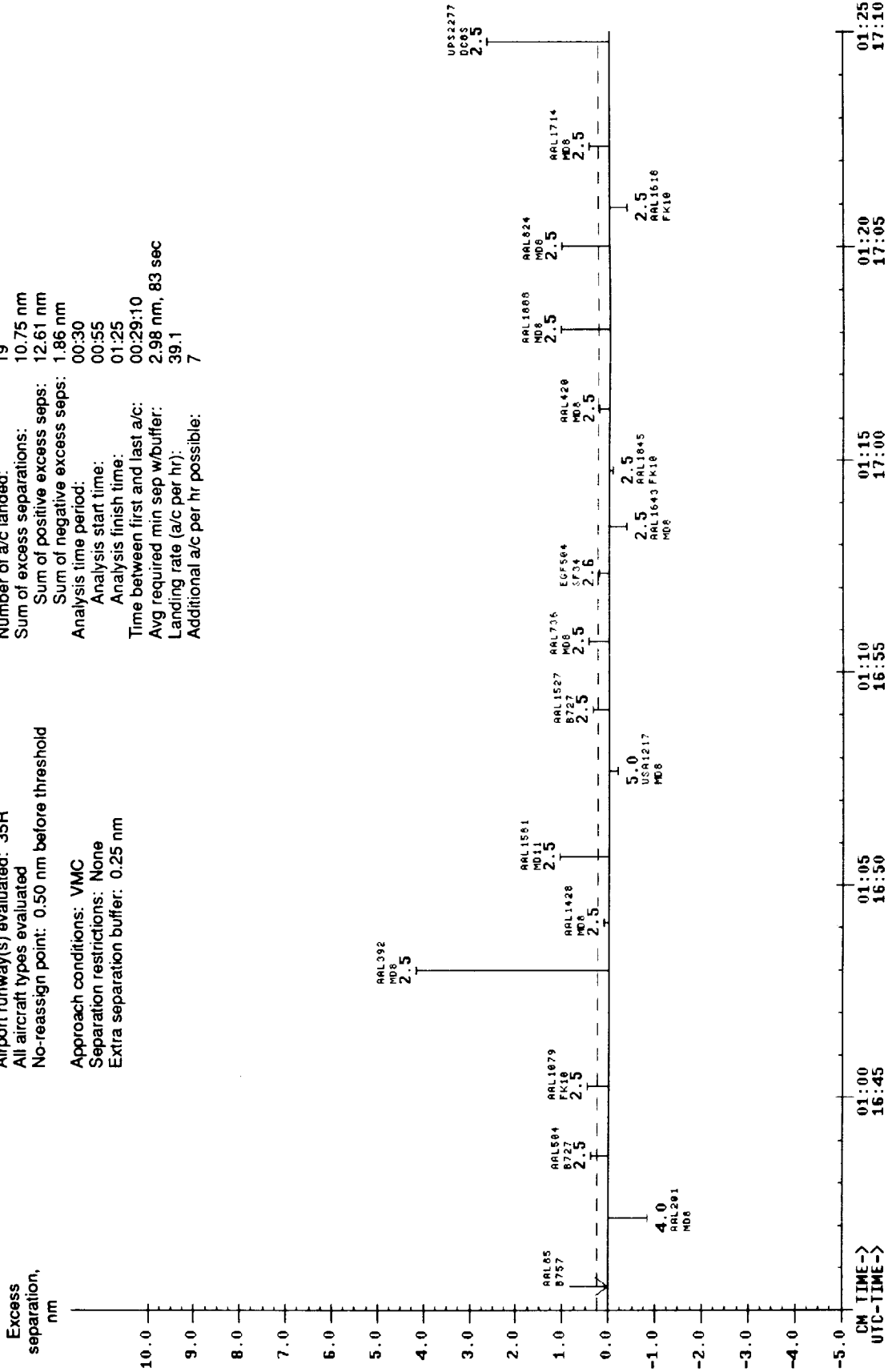| Total number of cases: | 18 |
Number of a/c landed:	19
Sum of excess separations:	10.75 nm
Sum of positive excess seps:	12.61 nm
Sum of negative excess seps:	1.86 nm
Analysis time period:	
Analysis start time:	00:30
Analysis finish time:	00:55
	01:25
Time between first and last a/c:	00:29:10
Avg required min sep w/buffer:	2.98 nm, 83 sec
Landing rate (a/c per hr):	39.1
Additional a/c per hr possible:	7
Potential Center delay reduction:	401 sec/hr
Total Center delay:	5159 sec/hr

Figure 28. Interarrival time characteristics during an IMC rush period.

37

EXCESS SEPARATION, nm

All separation cases evaluated
Airport runway(s) evaluated: 36L
All aircraft types evaluated
No-reassign point: 0.50 nm before threshold

Approach conditions: VMC
Separation restrictions: None
Extra separation buffer: 0.25 nm

Total number of cases:	35
Number of a/c landed:	36
Sum of excess separations:	14.48 nm
Sum of positive excess seps:	21.51 nm
Sum of negative excess seps:	7.03 nm
Analysis time period:	00:55
Analysis start time:	00:30
Analysis finish time:	01:25
Time between first and last a/c:	00:51:09
Avg required min sep w/buffer:	3.11 nm, 87 sec
Landing rate (a/c per hr):	42.2
Additional a/c per hr possible:	5

Y-axis (EXCESS SEPARATION, nm): 10.0, 9.0, 8.0, 7.0, 6.0, 5.0, 4.0, 3.0, 2.0, 1.0, 0.0, -1.0, -2.0, -3.0, -4.0, -5.0

X-axis:
CM TIME-> : 00:40, 00:50, 01:00, 01:10, 01:20
UTC-TIME-> : 22:02, 22:12, 22:22, 22:32, 22:42

Figure 29. Spacing characteristics during a VMC rush period.

Excess separation, sec

All separation cases evaluated
Airport runway(s) evaluated: 36L
All aircraft types evaluated
No-reassign point: 0.50 nm before threshold

Approach conditions: VMC
Separation restrictions: None
Extra separation buffer: 0.25 nm

Total number of cases: 35
Number of a/c landed: 36
Sum of excess separations: 14.48 nm
  Sum of positive excess seps: 21.51 nm
  Sum of negative excess seps: 7.03 nm
Analysis time period:
  Analysis start time: 00:55
  Analysis finish time: 00:30
Time between first and last a/c: 01:25
Avg required min sep w/buffer: 00:51:09
Landing rate (a/c per hr): 3.11 nm, 87 sec
Additional a/c per hr possible: 42.2
Potential Center delay reduction: 5
Total Center delay: 228 sec/hr
2640 sec/hr

CM TIME ->
UTC-TIME ->

00:40   00:50   01:00   01:10   01:20
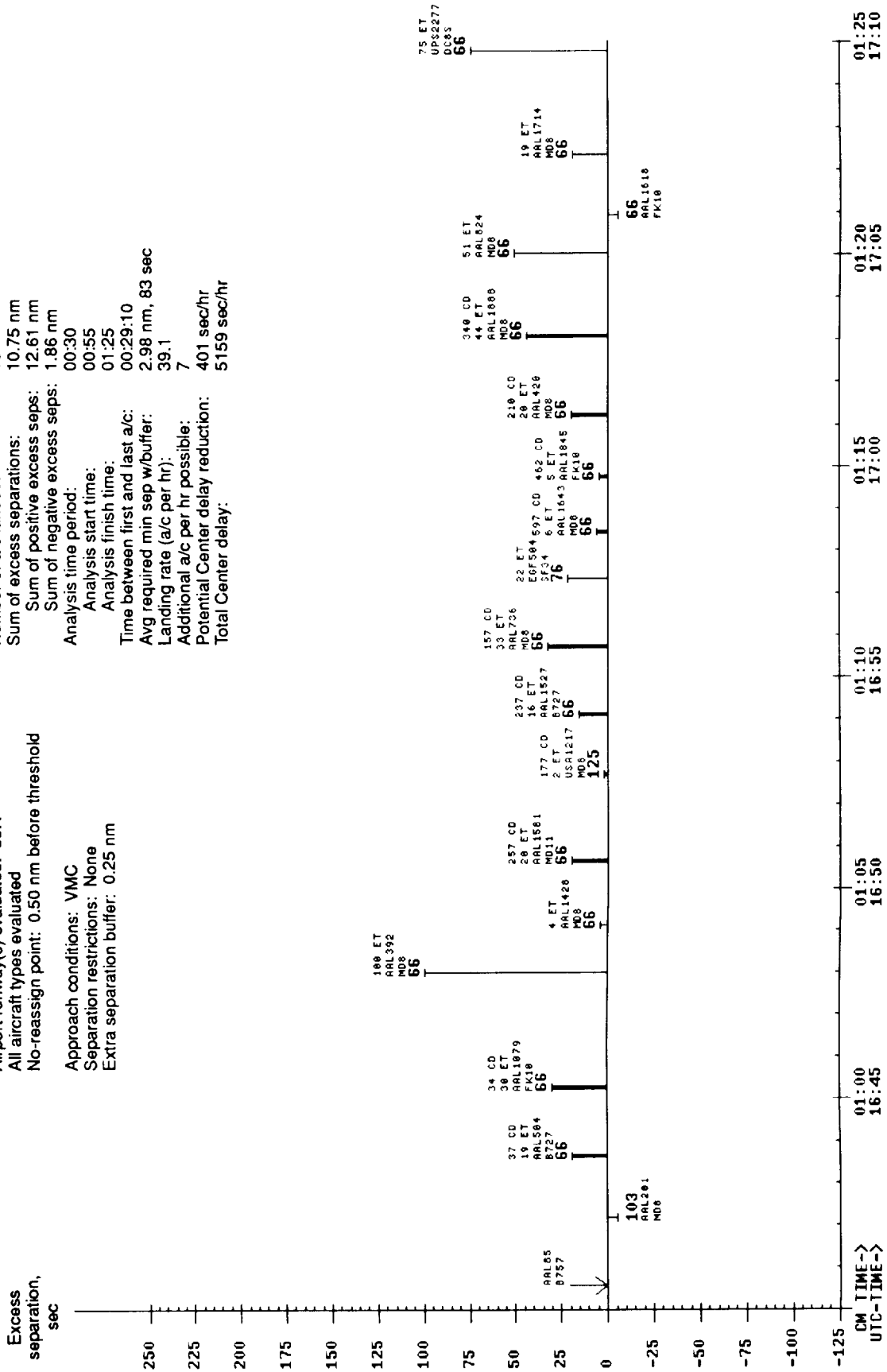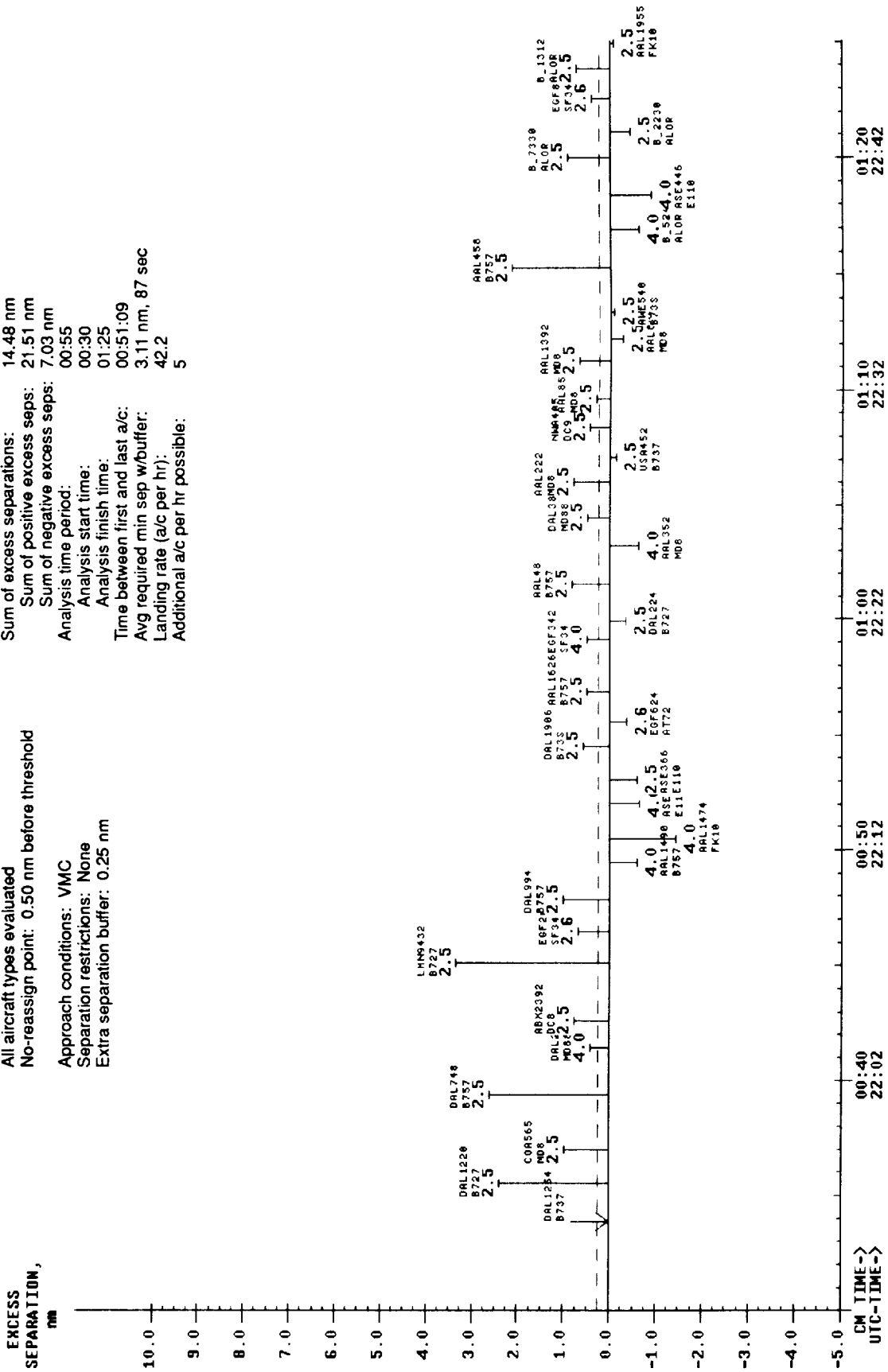22:02   22:12   22:22   22:32   22:42

Figure 30. Interarrival time characteristics during a VMC rush period.

39

All separation cases evaluated
Airport runway(s) evaluated: 35R
All aircraft types evaluated
No-reassign point: 0.50 nm before threshold

Approach conditions: IMC
Separation restrictions: None
Extra separation buffer: 0.25 nm

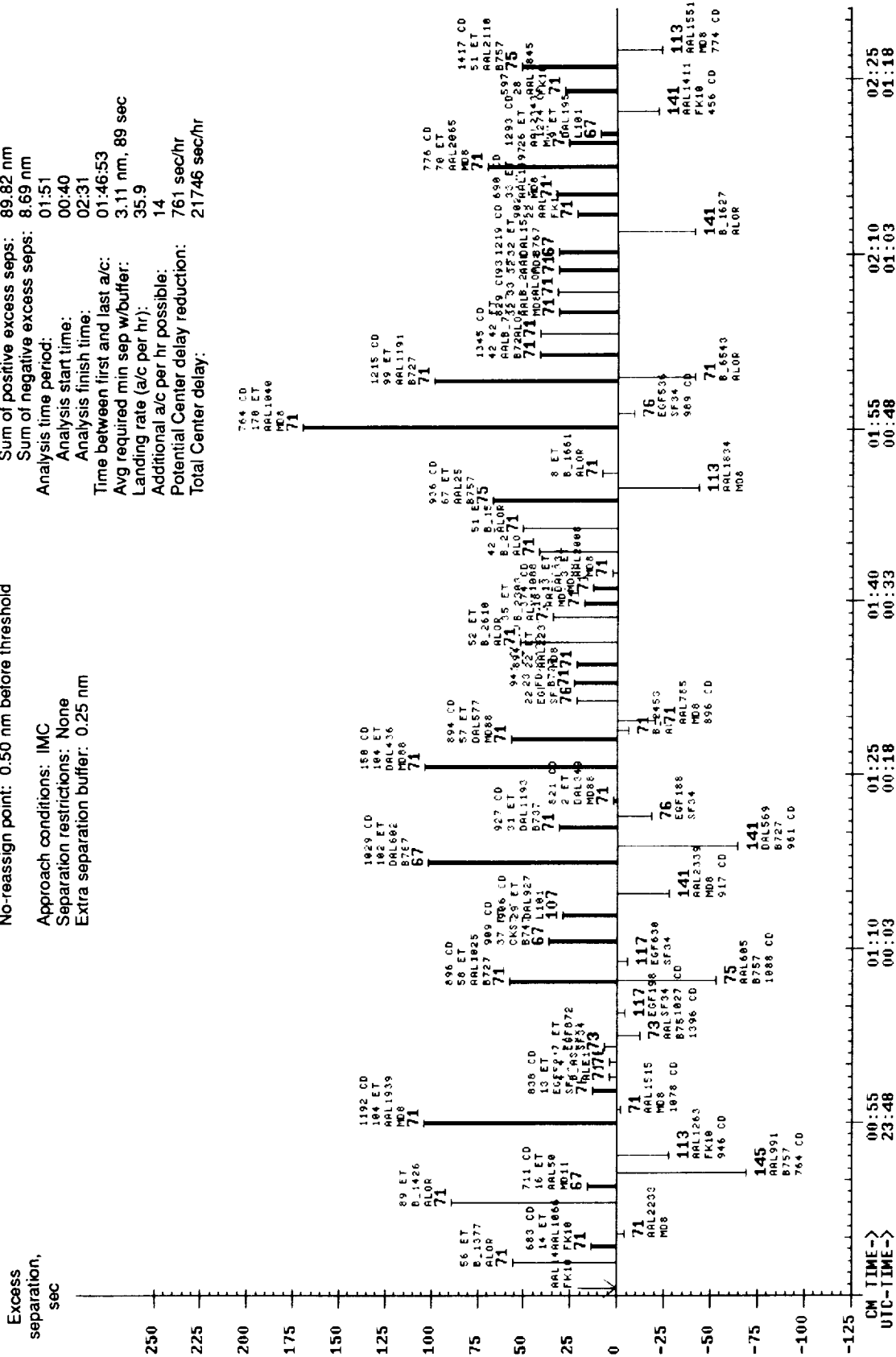|	
Total number of cases:	63
Number of a/c landed:	64
Sum of excess separations:	81.12 nm
Sum of positive excess seps:	89.82 nm
Sum of negative excess seps:	8.69 nm
Analysis time period:	01:51
Analysis start time:	00:40
Analysis finish time:	02:31
Time between first and last a/c:	01:46:53
Avg required min sep w/buffer:	3.11 nm, 89 sec
Landing rate (a/c per hr):	35.9
Additional a/c per hr possible:	14
Potential Center delay reduction:	761 sec/hr
Total Center delay:	21746 sec/hr

Excess
separation,
sec

Figure 31. Example of a long rush period.

All separation cases evaluated
Airport runway(s) evaluated: 31R
All aircraft types evaluated
No-reassign point: 0.50 nm before threshold

Approach conditions: VMC
Separation restrictions: None
Extra separation buffer: 0.25 nm

Total number of cases:	22
Number of a/c landed:	23
Sum of excess separations:	
Sum of positive excess seps:	66.63 nm
Sum of negative excess seps:	68.73 nm
	2.10 nm
Analysis time period:	00:54
Analysis start time:	00:13
Analysis finish time:	01:07
Time between first and last a/c:	00:52:06
Avg required min sep w/buffer:	3.42 nm, 96 sec
Landing rate (a/c per hr):	26.5
Additional a/c per hr possible:	22
Potential Center delay reduction:	905 sec/hr
Total Center delay:	5425 sec/hr

Excess
separation,
sec

250
225
200
175
150
125
100
75
50
25
0
-25
-50
-75
-100
-125

CM TIME->
UTC-TIME->

00:23   00:33   00:43   00:53   01:03
23:45   23:55   00:05   00:15   00:25

Figure 32. Example of low runway utilization.

41

Excess
separation,
sec

All separation cases evaluated
Airport runway(s) evaluated: 18R/18L
All aircraft types evaluated
No-reassign point: 0.50 nm before threshold

Approach conditions: VMC
Separation restrictions: None
Extra separation buffer: 0.25 nm

Total number of cases:	13
Number of a/c landed:	14
Sum of excess separations:	2.89 nm
Sum of positive excess seps:	8.04 nm
Sum of negative excess seps:	5.15 nm
Analysis time period:	00:20
Analysis start time:	00:35
Analysis finish time:	00:55
Time between first and last a/c:	00:17:29
Avg required min sep w/buffer:	2.95 nm, 83 sec
Landing rate (a/c per hr):	48.0
Additional a/c per hr possible:	3
Potential Center delay reduction:	199 sec/hr
Total Center delay:	2292 sec/hr

250
225
200
175
150
125
100
75
50
25
0
-25
-50
-75
-100
-125

CM TIME->   00:40   00:45   00:50   00:55
UTC-TIME->   17:47   17:52   17:57   18:02

AAL606
DC10

256 CD
35 ET
AAL345
FK10
125

14 ET
AAL1538
B727
66

66
DAL634
MD80

9 ET
DAL298
B727
66

66
AAL1460
FK10
94 CD

80 ET
AAL570
FK10
66

66
AAL6
MD8

76
LSS1262
SW3
21 CD

28 ET
AAL1752
B727
66

211 CD
23 ET
AAL2034
MD8
66

66
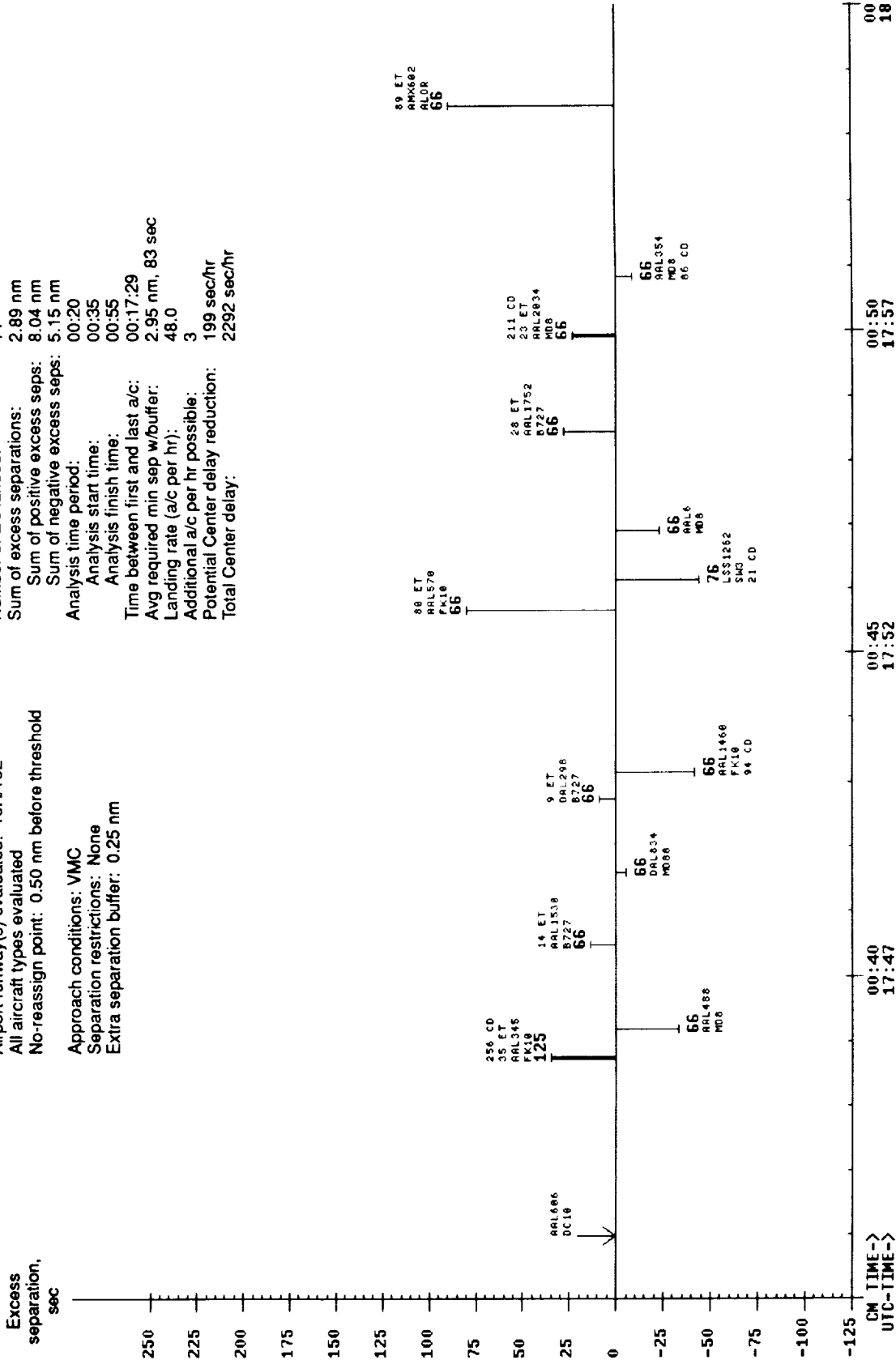AAL354
MD8
86 CD

89 ET
AMX602
ALOR
66

66
AAL488
MD8

Figure 33. Example of high runway utilization.

42

Table 13. Runway landing rates during rush periods

Condition	Landing rates, a/c/hr	Landing runway					
		13R	17	18	31R	35	36
IMC	Mean	30.4	35.4	31.7	16.3	33.1	34.1
	Minimum	27.5	32.2	23.8	16.3	26.8	32.8
	Maximum	33.3	40.7	37.1	16.3	36.5	35.4
VMC	Mean	30.9	40.7	35.9	31.5	37.7	37.9
	Minimum	20.8	31.3	25.0	23.3	27.3	29.2
	Maximum	35.0	46.5	48.0	38.6	47.0	42.2

Table 14. Potential runway capacity increases

Condition	Capacity increase, I_1	Landing runway			
		17	18	35	36
IMC	Mean, a/c/hr	7.7	9.2	18.7	16.3
	Min, a/c/hr	3	2	14	12
	Max, a/c/hr	13	14	24	19
	Percent increase	21.7	28.9	56.4	47.8
VMC	Mean, a/c/hr	12.3	15.2	13.5	10.3
	Min, a/c/hr	4	3	7	2
	Max, a/c/hr	23	22	32	27
	Percent increase	30.3	42.3	35.7	27.1

under VMC. Arrival loads were more similar among the active runways under IMC, although there were insufficient data to draw conclusions about Runway 31R. The results also showed that there were wide ranges of runway utilization during rush periods, with landing rates as low as 16 aircraft/hour and as high as 48 aircraft/hour.

8.5.2 Potential runway capacity increases– Table 14 summarizes capacity increases possible, based on the I_1 measure described in section 8.1. Because the diagonal runways were often not operated at capacity, they were not included in the table. Average increases ranged between 8 and 19 aircraft/hour for IMC, and between 10 and 15 aircraft/hour for VMC. Some potential increases were possible for all recorded rushes. The VMC potential increase values were unexpected; they resulted from the assumption that negative excess separations seen in the data are acceptable. The low spacing consistency under VMC caused many excess separations, thereby resulting in large potential increases. Table 15 summarizes the

Table 15. Potential maximum runway capacities (all conditions)

Landing runway	Maximum capacity, a/c/hr (I_1 method)	Zero-excess maximum capacity, a/c/hr (I_2 method)
13R	50.3	39.9
17	48.0	40.3
18	46.0	39.1
31R	60.5	41.2
35	51.3	41.9
36	48.5	40.8

potential maximum capacities for all meteorological conditions. Given the arrival mix at DFW, the results indicate that the potential maximum landing rates are

approximately 50 aircraft/hour for each runway, using the additional aircraft estimate. The table also shows the maximum capacities achievable, based on no positive or negative excesses. The two methods produce results that differ by about 10 aircraft/runway-hour.

8.5.3 Airport results– Table 16 summarizes the speed/weight class breakdown of DFW arrivals. The combined rush-period set was found to consist of approximately 60 percent large jets and 20 percent large turboprops; heavies and B757s make up most of the remainder. Unknown types, which resulted from a lack of flight-plan information for those aircraft, occurred because of known problems in the live data feeds, recording software that had not completed development, and some occasional poor recording practices. None of these problems was related to aircraft type, so the unknowns should have had the same speed/weight class mix as the complete set.

Table 17 presents combined averages of several measures used to characterize DFW arrival traffic. The required minimum separations were found to average 3.15 nm for the entire dataset. The IMC portion of the set had average values that were slightly higher. Since table 16 shows the arrival speed/weight class mixes to be very similar for both conditions, these differences are probably attributable to special separation restrictions that were applied for poor approach conditions. Airport landing rates are seen to average about 75 aircraft/hour under IMC and over 90 aircraft/hour under VMC, but VMC potential increases were larger because of low utilization of the diagonal runways.

A maximum airport capacity of over 130 aircraft/hour may be achievable, assuming that the observed negative excess separations are acceptable. The potential Center delay reduction averaged 1100 to 1400 sec/hr. The VMC reduction potential was higher than the IMC potential, again because of the low utilization of the diagonal runways under VMC. The total Center delay incurred by aircraft in the dataset averaged about 14,000 sec/hr of airport operation for VMC. For IMC, the total Center delay was about 28,000 sec/hr, probably because several severe storm fronts were captured in the data recordings. How much of this delay can be reduced through automation is not clear.

The potential for airport landing capacity increase was also computed for each rush period using the additional aircraft estimate (l_i). Although the small size of the dataset makes conclusions difficult, results ranged from a 5-percent increase to an almost 95-percent increase in capacity, with a median value of 36 percent. Using the zero-excess alternative measure, a 15-percent capacity improvement potential was found. In addition, a median value of 1200 sec of Center delay per airport rush hour could have been reduced. Using a direct-operating-cost estimate of $41 per aircraft per min (ref. 8), this translates to a cost savings of about $3.3 million per year at DFW, assuming that no other factors prevent the airport from handling the increased landing capacity.

These throughput and delay reduction estimates may be conservative, assuming that the observed negative excess separations are acceptable. As explained in section 8.2, the measures used did not account for delay reduction by adjusting the aircraft landing times. A back-of-the-envelope adjustment of the runway and period shown in figure 20 resulted in an increase in Center delay reduction potential from 499 sec/hr to 1196 sec/hr.

Table 16. Speed/weight class mix of DFW arrivals

Speed/weight class	All rush-period arrivals	IMC rush-period arrivals	VMC rush-period arrivals	All arrivals
Heavy	96	38	58	185
Large jet	1108	356	752	1855
Large turboprop	333	131	202	713
Small turboprop	56	13	43	123
Small prop	3	1	2	4
B757	164	55	109	271
Unknown	149	45	104	428
Total	1909	639	1270	3579

Table 17. Airport combined averages

Averages	Conditions	Airport (all runways)	North/south runways only
Required minimum separation, nm[a]	IMC	3.34	3.32
	VMC	3.08	3.08
Landing rate, a/c/hr	IMC	75.6	67.1
	VMC	93.7^b	75.9
Potential increase, percent (l_1 method)	IMC	39.2	34.1
	VMC	42.3	32.7
Maximum capacity, a/c/hr (l_1 method)	IMC	105.4	90.0
	VMC	133.4^b	100.7
Potential Center delay reduction, sec/hr	IMC	1127.0	994.0
	VMC	1403.0^b	1023.0
Total Center delay, sec/hr	IMC	27887.0	26224.0
	VMC	14177.0	11548.0

[a]Values include 0.25 nm additional separation buffer.

[b]For some cases, Runway 31R could not be analyzed because the stadium visual approach was used. No compensating adjustment was made to the results shown.

A manual adjustment of 7 runway rush recordings yielded Center delay reductions from 1.2 to 2.4 times the unadjusted values, with an average of 1.8. Additional delay reduction can be expected through optimal runway assignment and by resequencing aircraft to some optimal landing order. Therefore, the computed potentials shown in table 17 should be interpreted as approximate lower-bound estimates of the improvements obtainable by using a spacing, sequencing, and runway assignment tool.

9. Arrival-Gate-Crossing Accuracy

The computed TMA ETAff values were evaluated. As described in section 4.2, ETAff values at 19 and 30 minutes to the meter fix (ETAff$_{19}$ and ETAff$_{30}$) were computed. Equivalent predictions from the Arrival Sequencing Program (ASP), a computer program that is currently used for traffic metering, were also assessed and compared to the TMA values.

TMA ETAff prediction errors arise from several sources: The arrival times are computed from a predicted trajectory that is based on a direct routing to the meter fix. The prediction assumes that a default descent profile will be followed, based on the aircraft type and its flight state. En-route controllers may cause the aircraft to cross the meter fix later than anticipated by routing it along its flight-plan path, which is often not direct, or by

intentionally delaying the aircraft. These types of actions cause the ETAff predictions to be earlier than the actual meter fix crossing time, resulting in positive delays. En-route controllers may also cause the aircraft crossing time to be different from the TMA prediction on the direct route by choosing a cruise speed or a descent profile other than that assumed by the TMA. These controller actions, as well as winds-aloft errors and aircraft trajectory modeling errors, reduce the ETAff prediction accuracy.

The analysis assumed that a controller cleared an aircraft to fly directly to the meter fix whenever he could have done so without exceeding the terminal airspace acceptance rate. This acceptance rate was also assumed to be an accurate representation of TRACON arrivals capacity. Therefore, if there was no error in the ETAff predictions, all observed delay represented actual delay.

The set of Center data recordings used for the runway analysis consisted of over 4400 aircraft separation pairs, recorded over a 6-month period for a large range of weather conditions. No weather information was recorded, so no winds were used by the CTAS TMA in making the estimated-time-of-arrival (ETA) predictions. Although no recordings were excluded from the dataset, the data should not be interpreted as a comprehensive representation of DFW conditions. The recordings were

often made during periods that would be beneficial for arrival spacings analysis, so the results may be biased toward instrument weather conditions.

Figure 34 shows the probability density of the $ETAff_{19}$ delays for the dataset. The distribution was assumed to consist of the convolution of a normal distribution component that represents ETAff prediction accuracy and some other distribution caused by delays. To estimate prediction accuracy, it was necessary to remove the effects-of-the-delays component. An approximation of $ETAff_{19}$ prediction accuracy was made by constructing a symmetrical distribution based on the left side of the observed distribution; the location of the distribution maximum corresponded to an approximate predictor bias. In the figure, the 19-min TMA predictions are seen to

have a very low bias of 15 sec and a standard deviation of 103 sec. Since no weather information was used, the low bias may indicate that the average wind velocity for the complete sample was close to zero, although it may instead indicate that the bias caused by no weather predictions is canceled by other biases in the TMA models.

The undelayed meter fix time prediction (U_MFT_{19}) distribution from the ASP is compared with the $ETAff_{19}$ distribution in figure 35. The ASP distribution was found to predict crossing time with a bias of 76 sec and a standard deviation of 125 sec. The figure indicates that the ASP may be less accurate in predicting crossing times. Both predictors were impacted similarly by the presence of delays.
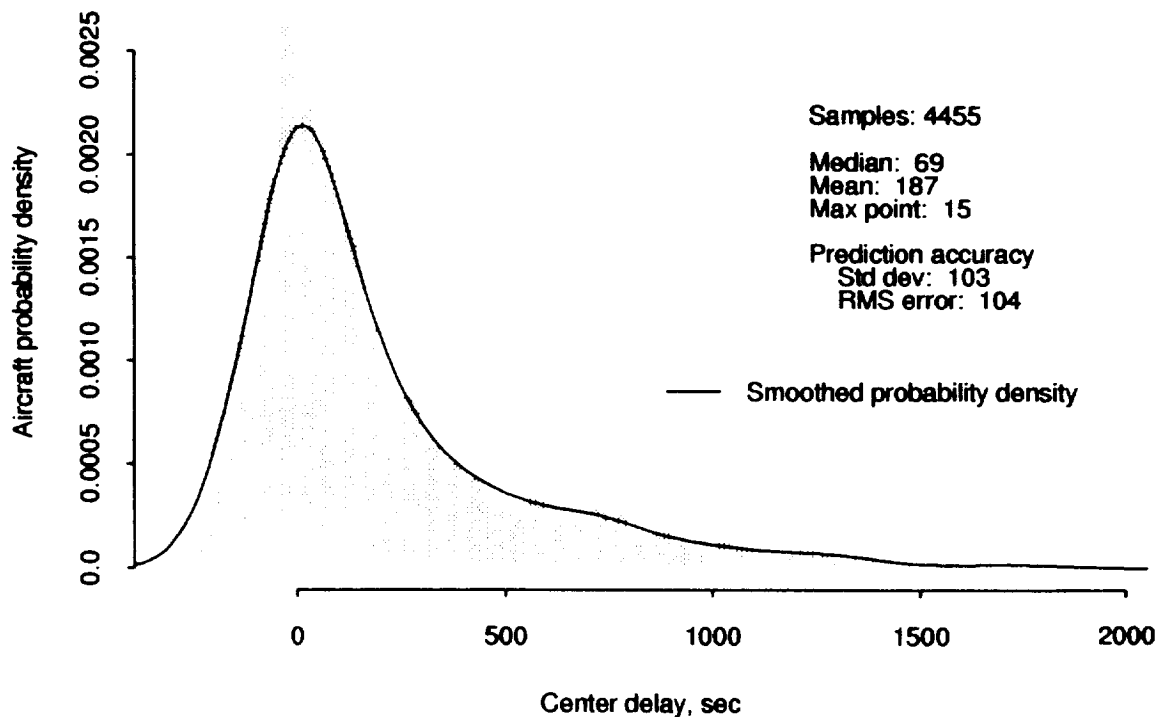

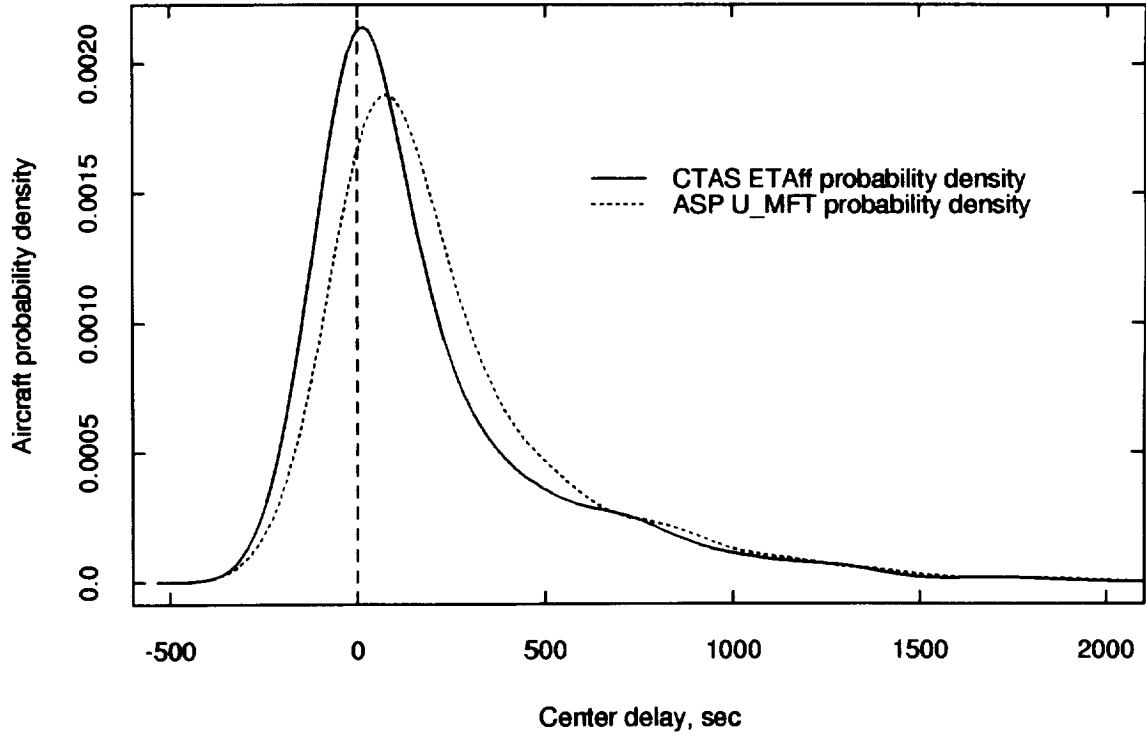Figure 34. Distribution of CTAS 19-min ETA predictions.

46

Figure 35. Comparison of CTAS and ASP 19-min ETA predictions.

Table 18. Meter fix crossing prediction analysis results

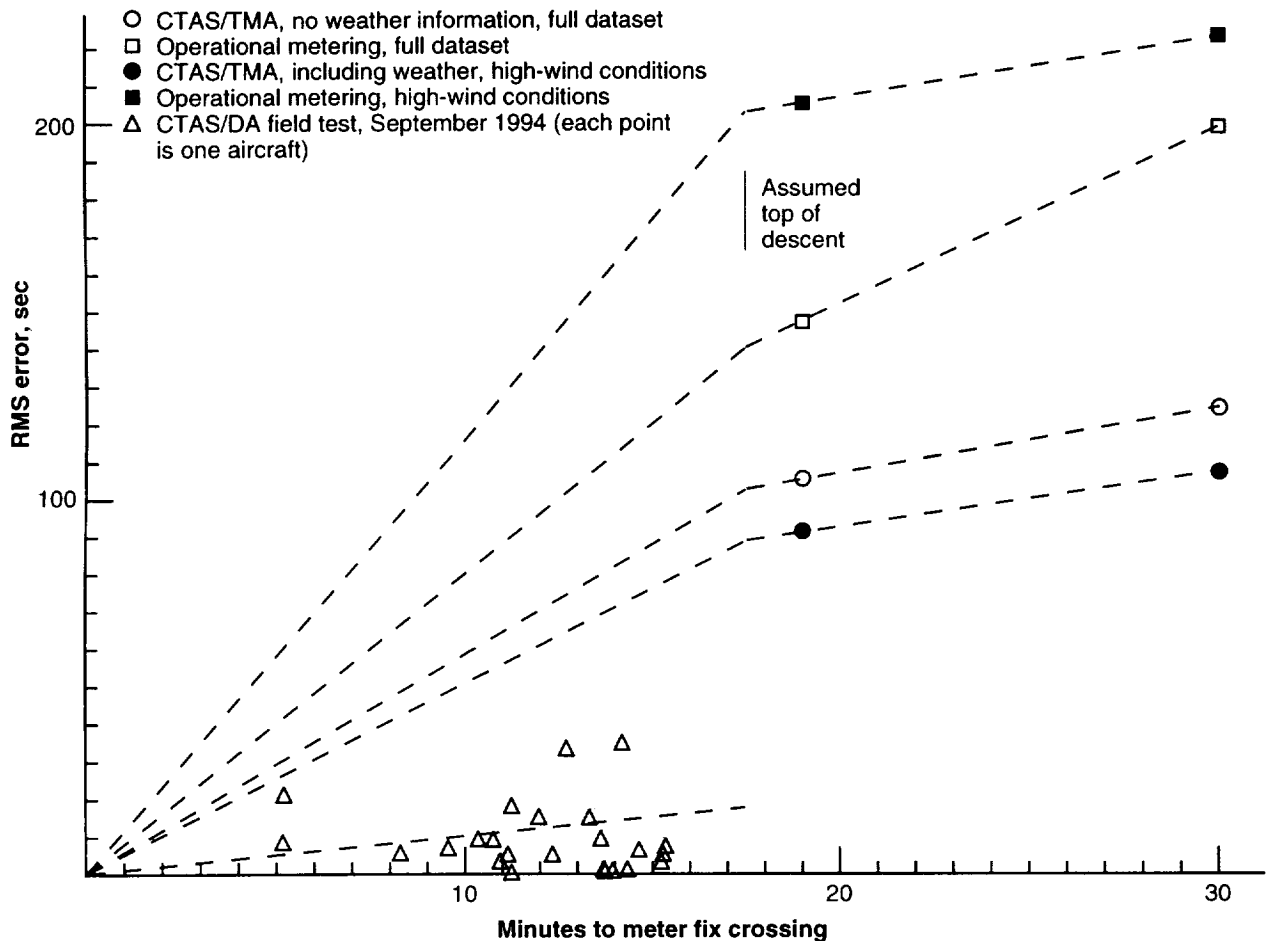| Dataset	Minutes to meter fix	Symmetric distribution mean, sec		Symmetric distribution std dev, sec	
		TMA	ASP	TMA	ASP
All data	19	15	76	103	125
	30	1	119	124	157
Jets only	19	27	84	109	121
	30	3	131	129	151
Turboprops only	19	−13	48	90	126
	30	−3	60	117	148

Figure 36. Estimated accuracy of CTAS and ASP meter fix crossing predictions.

Table 18 summarizes bias and standard-deviation approximations for the 19- and 30-min ETAff predictions; results are also broken out separately for jets and turboprops. For the full dataset, the CTAS TMA prediction biases were much smaller than the equivalent ASP biases. Standard deviations of the TMA predictors were also slightly smaller. The ASP predictions of the mean were found to degrade with increased time to meter fix crossing, whereas there was no observable degradation in the TMA mean. The turboprop predictions appeared to be slightly better than the jets predictions for both TMA and ASP.

Further insight is obtained from a plot of the rms error of the two predictions, as shown in figure 36. The data corresponded to the cruise portion of flight, since the top of descent is usually between 15 and 19 min to the meter fix. Errors of the TMA predictions were smaller than those of the ASP predictions, and errors of both predictions were found to decrease from the 30-min estimates to the 19-min estimates.

One recording was also made for which the TMA predictions used rapid-update-cycle (RUC) predictions of winds aloft from the National Meteorological Center. It was made during high-wind conditions. Also shown on the plot are rms errors of the 19- and 30-min predictions from these data; they were about 15 percent lower than the TMA errors from the full dataset. The ASP prediction errors from these data are also shown; they were found to be higher than those of the full dataset.

Although zero prediction error would be expected at zero min to crossing, linear extrapolations of the data do not intersect zero error at zero time. The descent portion of flight may have been the source of most of the prediction error. Estimates of error as a function of prediction time, shown by dashed lines, are represented in the plot as having two distinct slopes corresponding to the cruise and descent portions of flight.

Some initial results of a recent CTAS Descent Advisor (DA) field test are also shown. Conducted using revenue flights in September 1994, this test is described in

reference 9. The field test results show the rms errors resulting from giving pilots a descent clearance based on a CTAS four-dimensional descent profile. The TMA/DA errors were found to be significantly smaller than those of all other predictions. Extrapolation to the 19-min point indicates a potential fivefold improvement over the TMA-only predictions without weather data inputs. In addition, some of the aircraft used in the field test were equipped with a flight-management system, and for many of these aircraft, errors were too small to measure using Center radar data.

10. Discussion

10.1 Results Summary

Major findings are summarized as follows:

- A large range of runway utilization occurred during rush periods at DFW, with landing rates as low as 16 and as high as 48 aircraft per runway-hour. The diagonal runways were often underutilized, suggesting that large improvements in capacity can be achieved through greater use of those runways.

- Observed trends in the results indicate that the controller has a difficult task in achieving different spacings for the many combinations of aircraft speeds and weight classes: 1) nearly identical separation distributions for situations with 2.5-nm minimum required separations and those with 3-nm separations under restrictions; 2) large numbers of negative excess separations and small target buffers for the higher required minimum separation cases; and 3) a very high incidence of negative excess separations for aircraft following B757s.

- Widely differing performance results were observed for similar conditions, even during periods of delay buildup in the Center. Although these variations may indicate a large range in controller performance, they may also be indicative of the random process that characterizes aircraft arrivals.

- A large potential existed to reduce the controller separation buffer through increased spacing precision, especially for lead/trail combinations having smaller required minimum separations.

- Differences between approach profiles across speed/weight classes were greater for the TS-generated profiles than for profiles derived from observation. Therefore, the impacts of gap widening or closing between the point of final approach course intercept and the threshold were smaller than anticipated.

10.2 Recommendations for Further Work

The study highlighted the need for continued analysis efforts to establish a more comprehensive reference baseline and to support CTAS development. Suggested areas for concentration are given in the following paragraphs.

10.2.1 Suggested CTAS development–

- The sum of the minimum required separation and a controller buffer results in a controller target separation that should be added to the FAST spacing logic. The presented results should be used as initial estimates of these target separations.

- Simulations of FAST should be performed to estimate the level of spacing precision achievable. This information can be used to establish the achievable level of reduction of the controller separation buffer.

- Large differences are evident in the speeds of aircraft on the final approach segment, even within the speed/weight classes defined by the study. This variability is not entirely accounted for by winds, so further investigation of pilot practices, aircraft types, and landing weights may be necessary to develop the understanding needed to predict threshold crossing times with high accuracy.

- Agreement between the TS-generated approach profiles and observed results for the six aircraft speed/weight classes varies from poor to fair. Modification to the TS is needed to enable better CTAS predictions of threshold crossing times, especially for the large turboprops class. The profiles developed from observation should be used as a starting point.

- Since diagonal runways appear to be underutilized at DFW, application of a runway-allocation parameter to an automation tool that would balance the preferences of the carriers with the need to minimize arrival delays may be beneficial. One possible implementation is to determine a value of acceptable delay to be incurred through the direct elicitation of air carrier preferences. For example, an air carrier may consider a two-minute delay a break-even point for landing on a north/south runway; if the delay savings achievable by using a diagonal runway is greater than two minutes for a given aircraft, that aircraft would be directed to land on a diagonal runway.

- To obtain the maximum benefit from terminal-area automation tools, an effort may need to be devoted to reducing the variability of aircraft flying times on the final approach segment. This effort may require a greater sophistication in modeling of aircraft types, their flight state, and/or pilot procedures. If this

variability is shown to be caused by pilot procedures, the importance of pilots' maintaining an agreed-upon final-approach speed should be examined.

10.2.2 Refined analysis–

- A more extensive dataset should be collected to increase confidence in the results of this study. RUC weather recordings should be made simultaneously. In addition, it would be highly beneficial to record which aircraft are following visual separation procedures, and the time of transfer of responsibility for separation from the controller to the pilot. If dollar-value benefits need to be determined, the dataset should represent a comprehensive and representative range of conditions at DFW.

- The maximum runway capacity is strongly dependent on the acceptability of the negative excess separations observed. Further work is necessary to develop a better measure of this maximum capacity, which is probably affected by factors that were not examined in this study.

- The required separations model should be expanded to include the impact of winds.

- The rescheduling of adjacent landing aircraft that are delayed in the Center should be automated to achieve a more accurate estimate of potential Center delay reduction.

- The analysis tools should be expanded to account for departing aircraft on dependent runways.

- The accuracy of CTAS ETAs at the meter fix should be established after including RUC weather in the data recordings.

10.3 Conclusions

The analysis results indicate that there is a large potential for utilizing runways more effectively through improved management of aircraft in terminal airspace. They support earlier simulation findings that CTAS can increase airport capacity and reduce delays. Although the analysis is not comprehensive, the results indicate that the benefits will probably be measured in terms of millions of dollars in direct-operating-cost savings per year for traffic flying into DFW.

11. References

1. Erzberger, H.; Davis, T. J.; and Green, S. M.: Design of Center-TRACON Automation System. AGARD-CP-538, paper no. 11, presented at the AGARD Guidance and Control Symposium on Machine Intelligence in Air Traffic Management, Berlin, Germany, May 11–14, 1993.

2. Davis, T. J.; Erzberger, H.; Green, S. M.; and Nedell, W.: Design and Evaluation of an Air Traffic Control Final Approach Spacing Tool. Journal of Guidance, Control, and Dynamics, vol. 14, no. 4, July–Aug. 1991, pp. 848–854.

3. FAA Order 7110.65J, Air Traffic Control. (Air Traffic Control Handbook), Federal Aviation Administration, Sept. 1993.

4. Neuman, F.; Erzberger, H.; and Schueller, M. S.: CTAS Data Analysis Program. NASA TM-108842, Oct. 1994.

5. Personal communication with David McCracken, Sterling Federal Systems, Inc., Feb. through Apr. 1995.

6. Vandevenne, H. F.; and Lippert, M. A.: Using Maximum Likelihood Estimation to Determine Statistical Model Parameters for Landing Time Separations. Technical Memorandum 41L-0400, MIT Lincoln Laboratory, Apr. 1992.

7. Credeur, L.; Capron, W. R.; Lohr, G. W.; Crawford, D. J.; Tang, D. A.; and Rodgers, W. G., Jr.: Final-Approach Spacing Aids (FASA) Evaluation for Terminal-Area, Time-Based Air Traffic Control. NASA TP-3399, Dec. 1993

8. Hunter, G.: Estimating CTAS Benefits Nationwide. Presented to the CTAS Benefits Analysis Technical Information Meeting, NASA Ames Research Center, July 13, 1995.

9. Green, S. M.; Vivona, R. A.; and Sanford, B.: Descent Advisor Preliminary Field Test. AIAA Paper 3368, Proceedings of the 1995 AIAA Conference on Guidance, Navigation, and Control, Baltimore, Md., Aug. 1995.

Appendix A – Runway Selection Logic

The runway selection logic identifies the landing runway for each aircraft from a provided set of runway candidates. For each runway, the two aircraft radar hits that are closest to a user-assigned point on the final-approach course are determined. The logic then uses a process of elimination to identify the most likely landing runway. If all candidate runways are eliminated, the aircraft is identified as not having landed. The logic also identifies a time of threshold crossing for each landing aircraft. The radar track data are filtered using a fourth-order Butterworth-characteristic filter before application of the logic.

A.1 Input Parameters

Parameter	Units	Value	Definition
No-reassign distance before threshold	nm	0.5	Position of a reference point on the final-approach course, defined in terms of a distance before the threshold. For each aircraft, radar data closest to this point are used to identify the landing runway.
Radar error	nm	0.1	Approximation of expected terminal radar range error.
Zero point	nm	0.5	Distance on runway past each runway threshold. Used as a runway touchdown point in range- and bearing-to-runway computations.
Climb rate limit	ft/min	2000	Aircraft climb rate elimination parameter. If aircraft computed climb rate exceeds the value of this parameter at the no-reassign point, runway is eliminated as a landing candidate.
Approach gamma limit	deg	6	Aircraft approach flightpath angle elimination parameter. Used to compute altitude AGL maximum limit. If the maximum limit is exceeded at the no-reassign point, runway is eliminated as a landing candidate.
Approach altitude above gamma	ft	500	Aircraft altitude above the maximum approach path elimination parameter. Used to compute altitude AGL maximum limit. If the maximum limit is exceeded at the no-reassign point, runway is eliminated as a landing candidate.
Heading difference limit	deg	15	Aircraft heading difference elimination parameter. If the difference between the aircraft heading and the runway heading exceeds the value of this parameter at the no-reassign point, runway is eliminated as a landing candidate.
Distance limit	nm	2	Aircraft distance elimination parameter. If the distance between the no-reassign point and the closest radar hit exceeds the value of this parameter, runway is eliminated as a landing candidate.

A.2 Selection Logic

1. For each runway, the radar hit closest to the runway no-reassign point is identified.

2. The previous radar hit is identified. If there is no previous radar hit or if the data record is too short for aircraft speed data to be reliable, the aircraft is identified as not having landed.

3. The aircraft true heading and bearing to the runway zero point, the aircraft climb rate, and its rate of distance closure to the runway zero point are determined based on the x and y positions of the two radar hits.

4. The runway candidate tests are performed for each runway. All the following tests must be passed:

   a. The aircraft distance to the no-reassign point must be less than the distance limit.

   b. The distance closure to the runway must be positive.

   c. The difference between the aircraft heading and the runway heading must be less than the heading difference limit.

   d. The aircraft climb rate must be less than the climb rate limit.

   e. The aircraft must be below the altitude maximum limit.

5. Of the remaining runway candidates, the most likely runway is selected. The closest runway is identified, and all runways with a distance greater than the bounds defined by the radar error are eliminated. If two or more runways remain as viable candidates, the candidate having the lowest difference between runway true bearing and aircraft true heading is selected.

6. The threshold crossing time is estimated by computing the distance between the aircraft and the identified runway. The aircraft ground speed, computed by CTAS from radar hits using a Kalman filter, is used to extrapolate to the threshold.

Appendix B – Required Separations Model

B.1 Trajectories Used by the Required Separations Model

Figure B-1. Heavy aircraft IMC final-approach profiles.

Figure B-2. Large-jet aircraft IMC final-approach profiles.
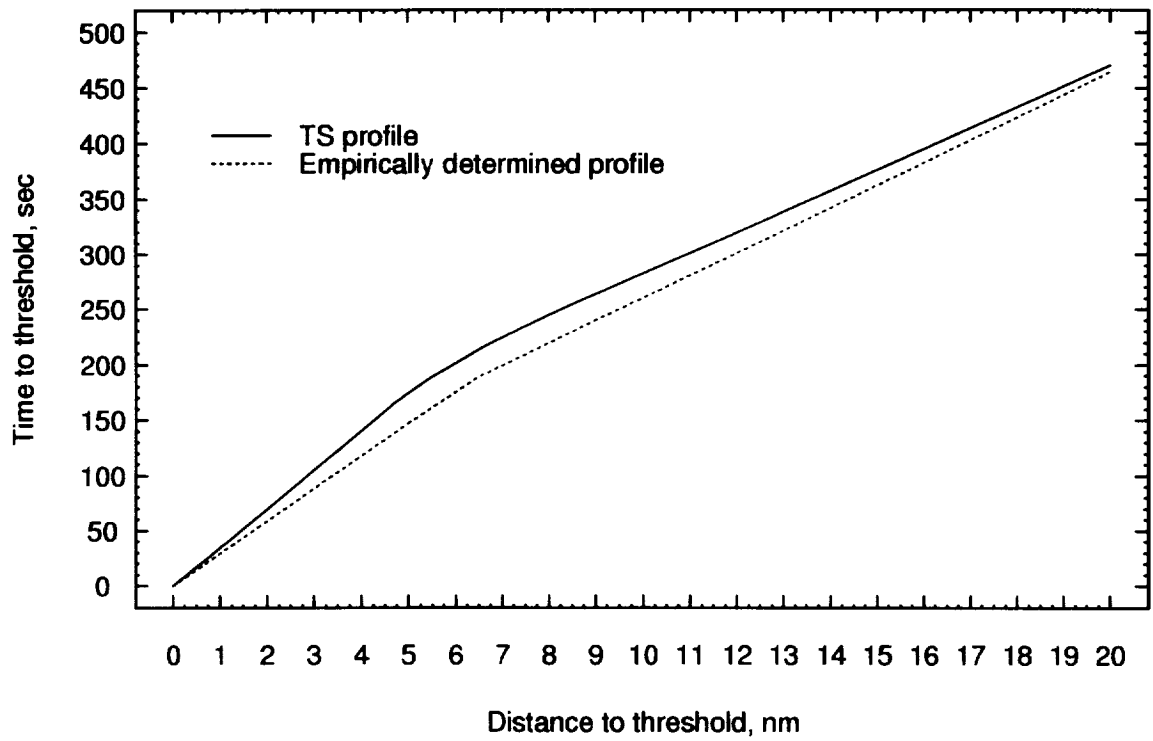
Figure B-3. Large-turboprop aircraft IMC final-approach profiles.

54
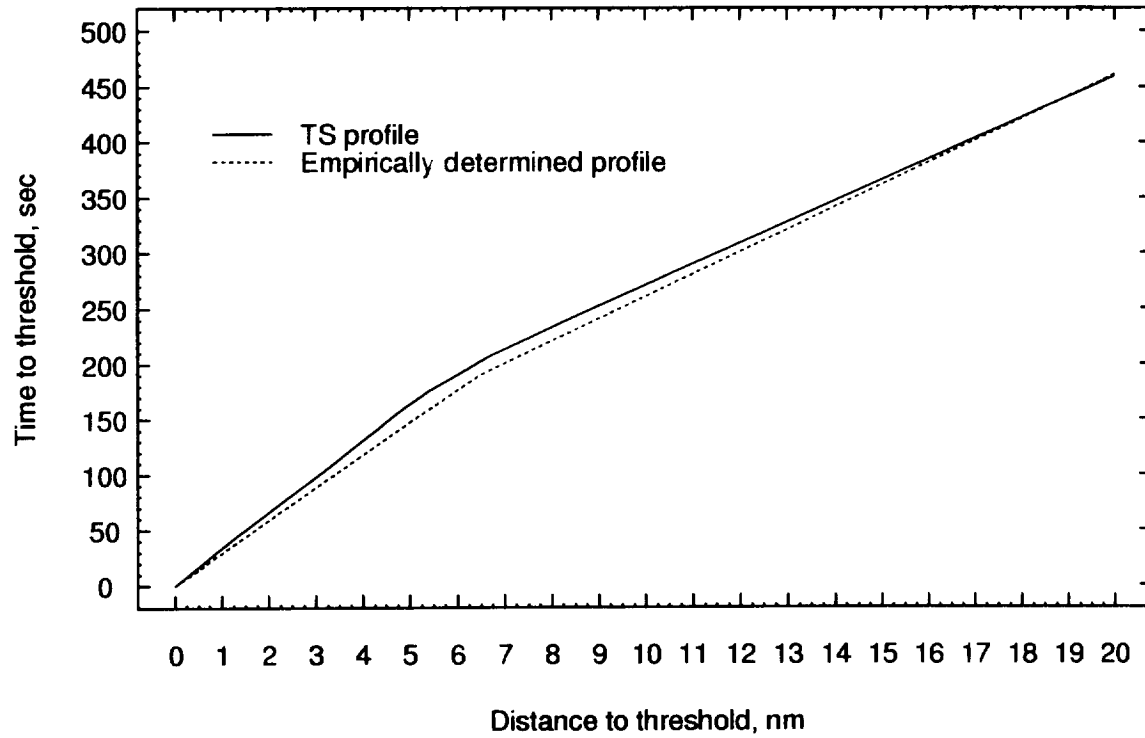
Figure B-4. Small-turboprop aircraft IMC final-approach profiles.
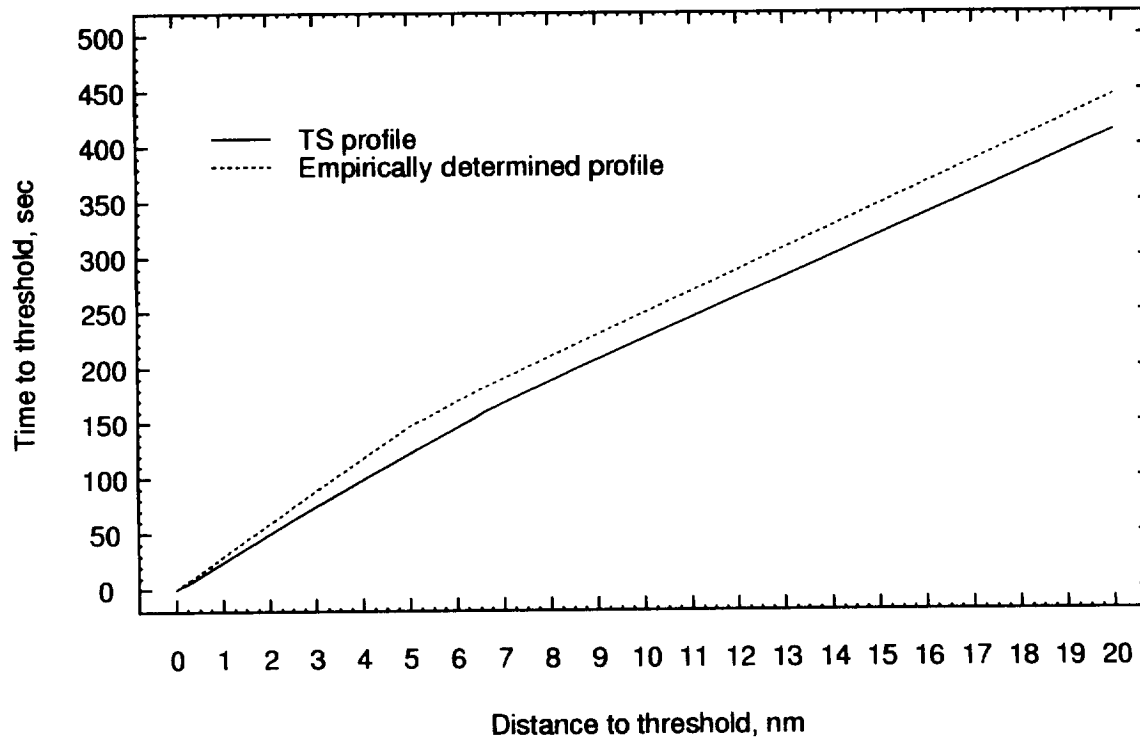
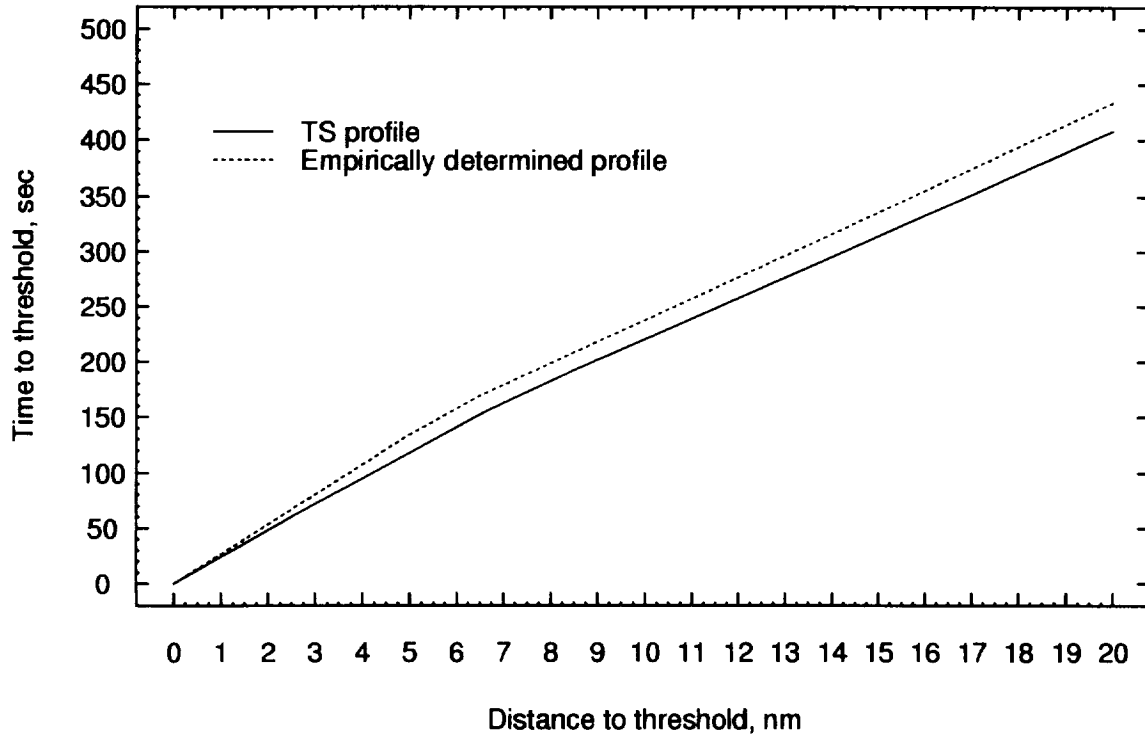Figure B-5. B757 aircraft IMC final-approach profiles.

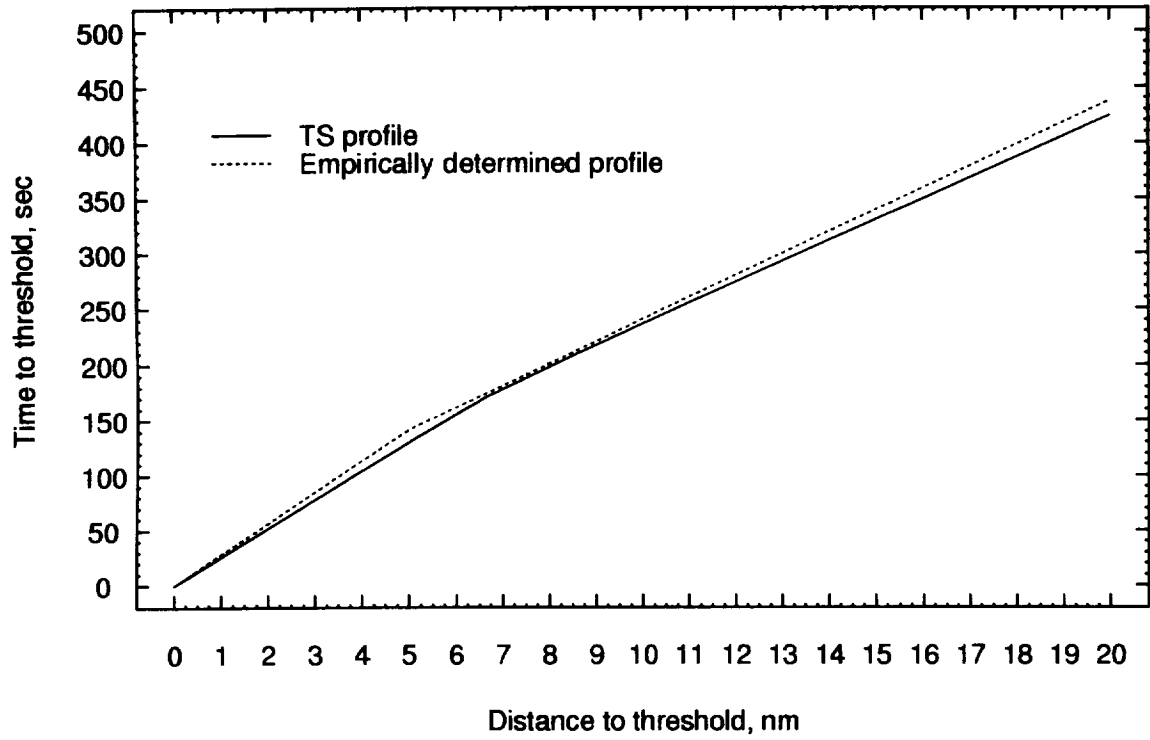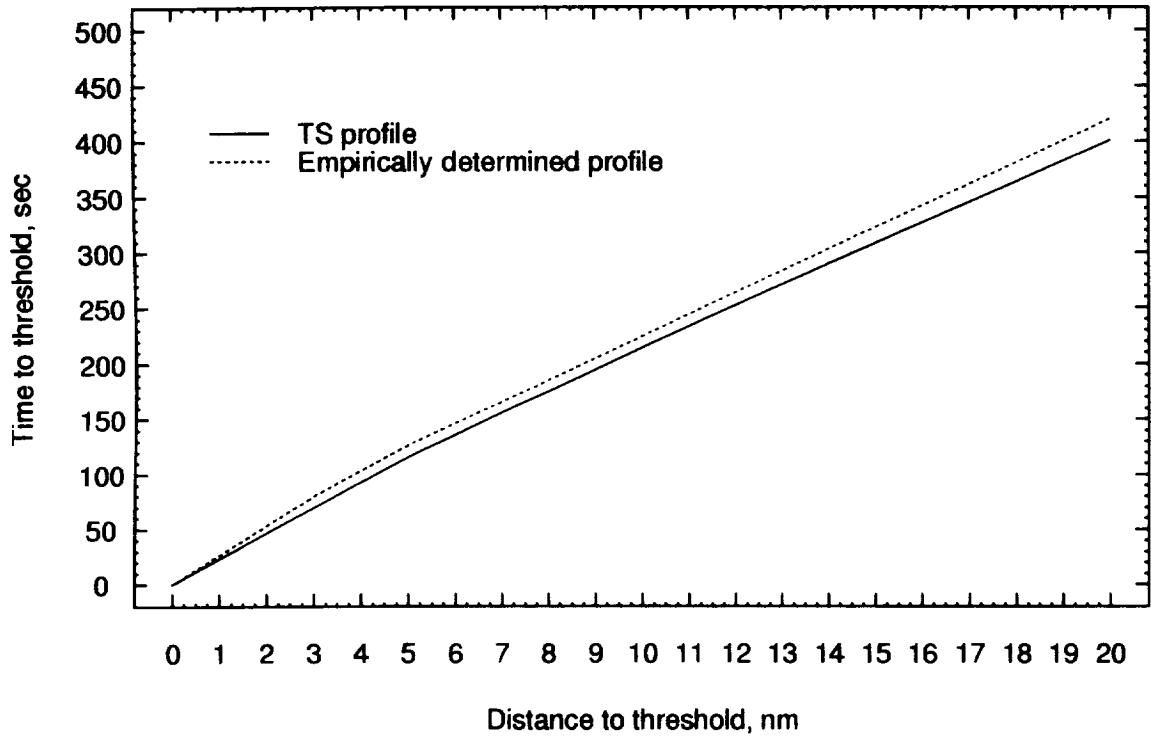*Figure B-6. Heavy aircraft VMC final-approach profiles.*
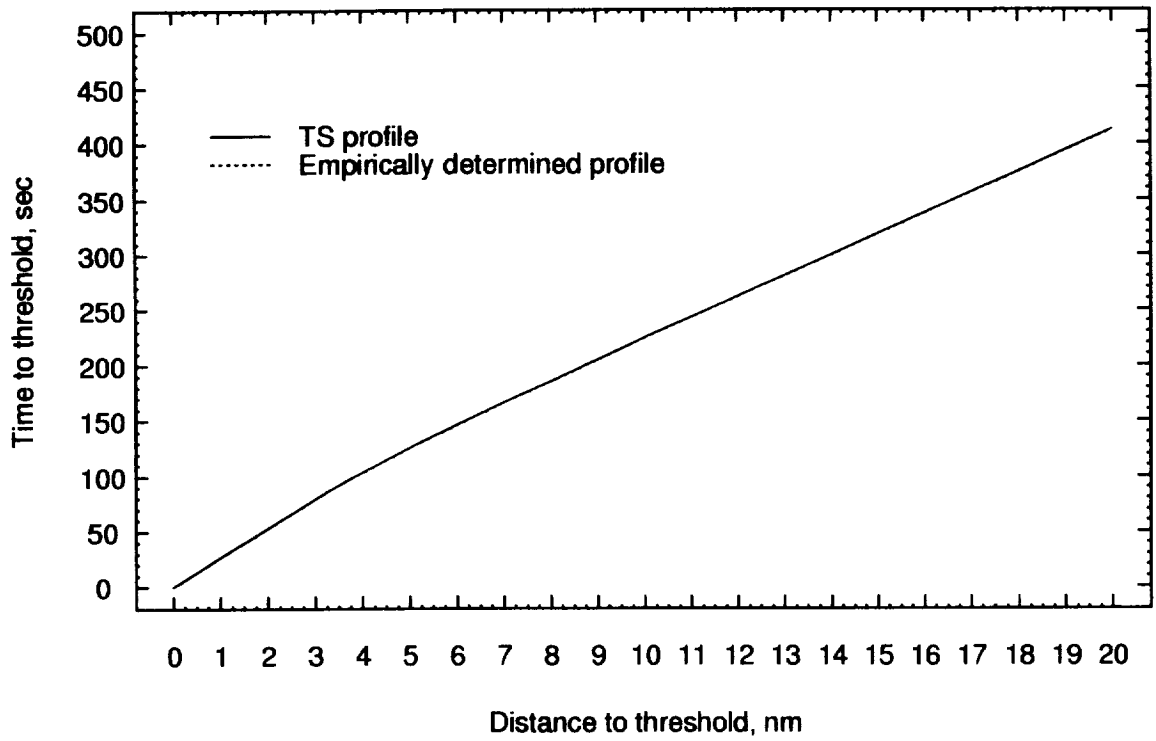
Figure B-7. Large-jet aircraft VMC final-approach profiles.
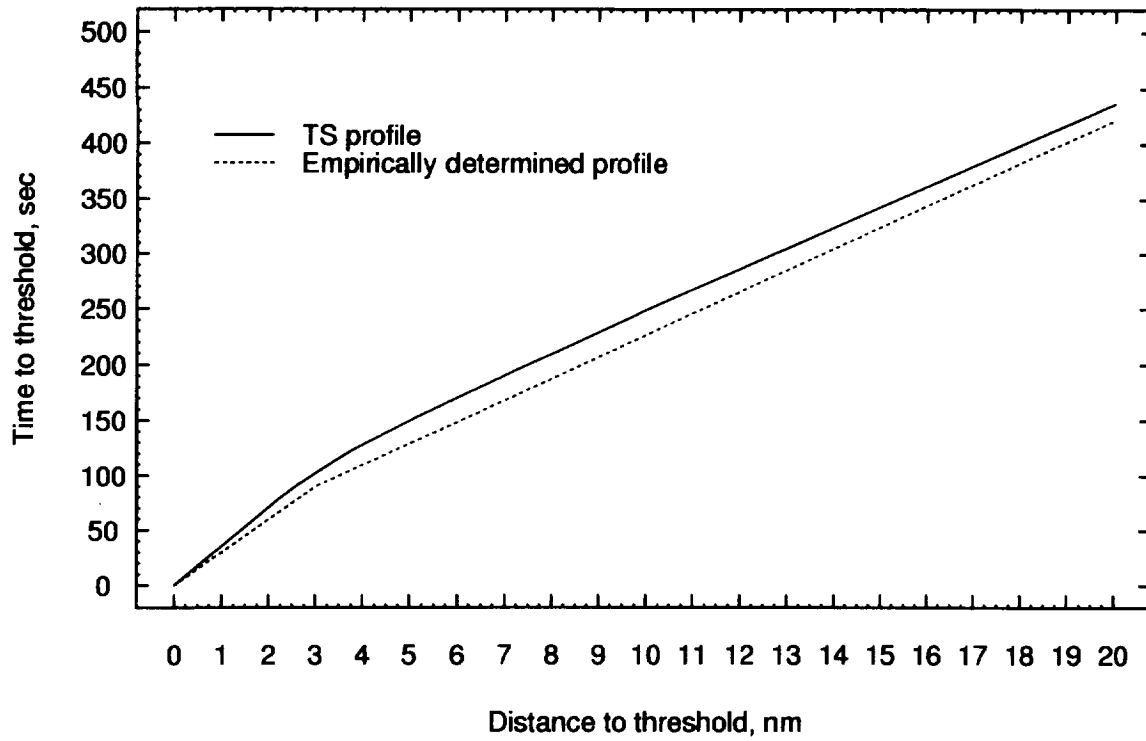
Figure B-8. Large-turboprop aircraft VMC final-approach profiles.
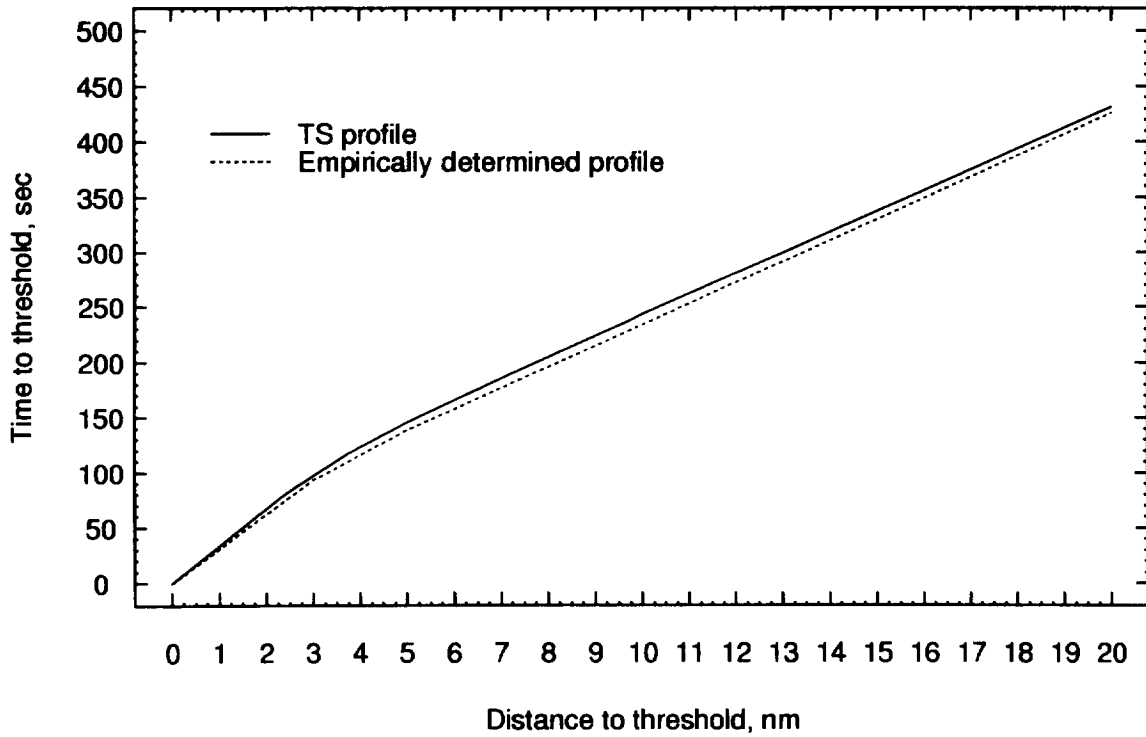
Figure B-9. Small-turboprop aircraft VMC final-approach profiles.
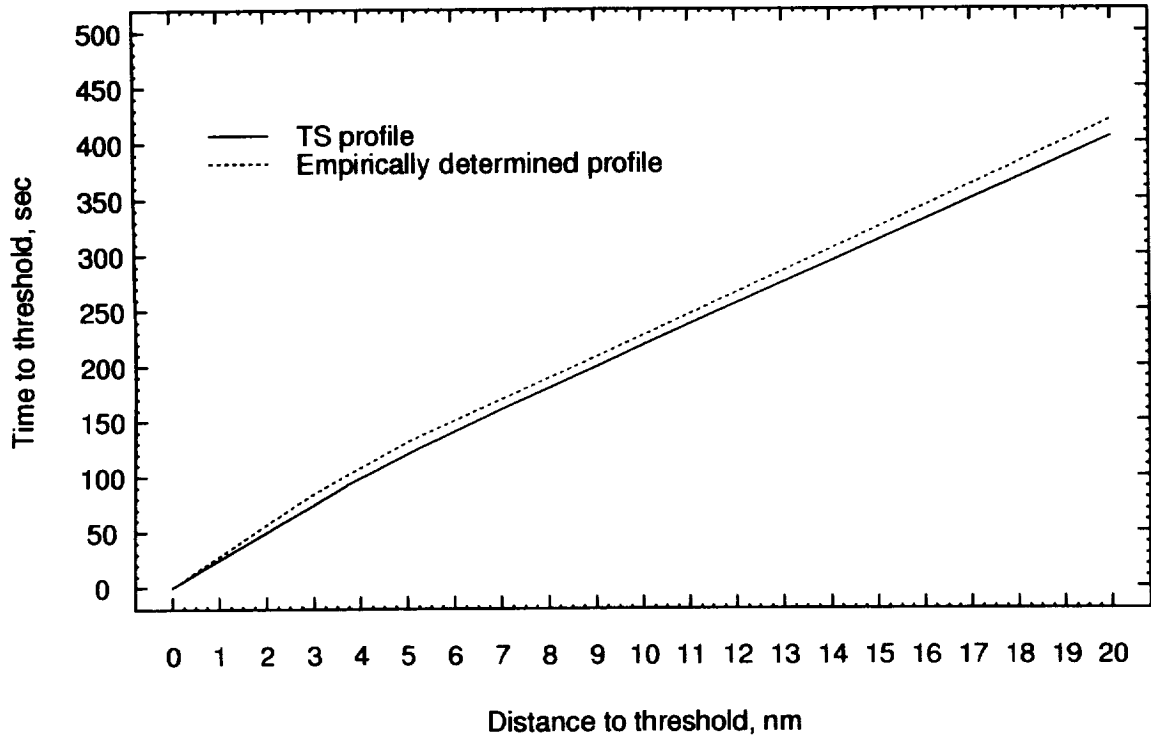
Figure B-10. B757 aircraft VMC final-approach profiles.

B.2 Model Results

Abbreviations used in tables

Req'd min sep	Required minimum separation
Com path sep	Separation at start of common path
Thresh sep	Separation at threshold
Lead a/c min sep pos	Position of leading aircraft that corresponds to the minimum separation
Trail a/c thresh time	Time for trailing aircraft to cross threshold from the start of the common path

Table B-1. TS-derived separations for IMC

Common path length: 9.0 nm
No extra separation buffers

Leading aircraft down, trailing aircraft across		Heavy	Large jet	Large turbo-prop	Small turbo-prop	Small prop	B757
Heavy	Req'd min sep, nm	4.0	5.0	5.0	6.0	6.0	5.0
	Com path sep, sec	94.8	122.9	136.3	167.5	234.9	118.8
	Thresh sep, sec	94.8	131.4	176.9	190.3	301.6	121.6
	Com path sep, nm	4.5	5.4	5.4	6.4	6.0	5.4
	Thresh sep, nm	4.0	5.0	5.1	6.0	6.7	5.0
	Lead a/c min sep pos, nm	0	1.6	1.6	0.6	3.0	0
Large jet	Req'd min sep, nm	2.5	2.5	2.5	4.0	4.0	2.5
	Com path sep, sec	73.9	65.4	64.7	108.9	147.0	71.9
	Thresh sep, sec	60.2	65.4	110.1	138.3	243.0	61.8
	Com path sep, nm	3.6	3.1	3.1	4.6	4.0	3.4
	Thresh sep, nm	2.5	2.5	3.1	4.2	5.4	2.5
	Lead a/c min sep pos, nm	0	2.5	2.9	1.4	5.0	0
Large turbo-prop	Req'd min sep, nm	2.5	2.5	2.5	4.0	4.0	2.5
	Com path sep, sec	106.1	104.4	88.5	138.9	157.0	105.6
	Thresh sep, sec	60.2	65.3	88.5	130.7	206.7	61.9
	Com path sep, nm	5.0	4.7	4.0	5.5	4.2	4.9
	Thresh sep, nm	2.5	2.5	2.5	4.0	4.5	2.5
	Lead a/c min sep pos, nm	0	0	1.8	0	2.8	0
Small turbo-prop	Req'd min sep, nm	2.5	2.5	2.5	2.5	2.5	2.5
	Com path sep, sec	99.7	96.6	82.0	82.3	81.5	98.8
	Thresh sep, sec	60.2	65.3	92.6	82.3	171.0	61.8
	Com path sep, nm	4.7	4.4	3.8	3.8	2.5	4.6
	Thresh sep, nm	2.5	2.5	2.6	2.5	3.7	2.5
	Lead a/c min sep pos, nm	0	0	2.2	2.4	6.5	0
Small prop	Req'd min sep, nm	2.5	2.5	2.5	2.5	2.5	2.5
	Com path sep, sec	128.5	131.5	129.6	132.0	115.2	129.5
	Thresh sep, sec	60.2	65.3	87.7	82.3	115.2	61.3
	Com path sep, nm	5.9	5.7	5.2	5.3	3.3	5.9
	Thresh sep, nm	2.5	2.5	2.5	2.5	2.5	2.5
	Lead a/c min sep pos, nm	0	0	0	0	0	0
B757	Req'd min sep, nm	4.0	4.0	4.0	5.0	5.0	4.0
	Com path sep, sec	98.7	98.4	102.6	136.6	189.7	98.6
	Thresh sep, sec	95.4	106.3	151.5	165.3	275.1	98.6
	Com path sep, nm	4.6	4.4	4.4	5.5	5.0	4.6
	Thresh sep, nm	4.0	4.1	4.3	5.1	6.1	4.0
	Lead a/c min sep pos, nm	0.2	1.1	2.6	1.6	4.0	0.2
All	Trail a/c thresh time, sec	201.4	217.4	263.4	252.4	374.0	206.4

Table B-2. TS-derived separations for VMC

Common path length: 6.0 nm
No extra separation buffers

Leading aircraft down, trailing aircraft across		Heavy	Large jet	Large turbo-prop	Small turbo-prop	Small prop	B757
Heavy	Req'd min sep, nm	4.0	5.0	5.0	6.0	6.0	5.0
	Com path sep, sec	93.2	122.7	139.1	164.7	255.7	118.8
	Thresh sep, sec	93.2	125.6	149.4	164.7	255.7	119.7
	Com path sep, nm	4.2	5.1	5.1	6.0	6.0	5.1
	Thresh sep, nm	4.0	5.0	5.0	6.0	6.0	5.0
	Lead a/c min sep pos, nm	0	0	0	0	0	0
Large jet	Req'd min sep, nm	2.5	2.5	2.5	4.0	4.0	2.5
	Com path sep, sec	67.5	66.3	66.2	111.6	164.5	66.8
	Thresh sep, sec	58.5	66.3	88.7	122.1	202.6	62.3
	Com path sep, nm	3.1	3.0	2.9	4.4	4.0	3.1
	Thresh sep, nm	2.5	2.5	2.5	4.0	4.4	2.5
	Lead a/c min sep pos, nm	0	0	1.2	0	2.0	0
Large turbo-prop	Req'd min sep, nm	2.5	2.5	2.5	4.0	4.0	2.5
	Com path sep, sec	84.8	86.2	87.9	124.8	167.9	85.5
	Thresh sep, sec	58.6	66.3	87.9	122.2	187.4	62.0
	Com path sep, nm	3.8	3.7	3.7	4.8	4.1	3.8
	Thresh sep, nm	2.5	2.5	2.5	4.0	4.1	2.5
	Lead a/c min sep pos, nm	0	0	0	0	1.1	0
Small turbo-prop	Req'd min sep, nm	2.5	2.5	2.5	2.5	2.5	2.5
	Com path sep, sec	81.6	82.6	83.3	83.2	95.2	82.0
	Thresh sep, sec	58.6	66.3	88.0	83.2	145.1	62.0
	Com path sep, nm	3.7	3.6	3.5	3.5	2.5	3.7
	Thresh sep, nm	2.5	2.5	2.5	2.5	3.2	2.5
	Lead a/c min sep pos, nm	0	0	0	0	3.5	0
Small prop	Req'd min sep, nm	2.5	2.5	2.5	2.5	2.5	2.5
	Com path sep, sec	95.9	99.2	106.1	105.0	115.0	97.7
	Thresh sep, sec	58.6	65.9	88.0	83.0	115.0	62.0
	Com path sep, nm	4.3	4.2	4.2	4.2	2.9	4.3
	Thresh sep, nm	2.5	2.5	2.5	2.5	2.5	2.5
	Lead a/c min sep pos, nm	0	0	0	0	1.8	0
B757	Req'd min sep, nm	4.0	4.0	4.0	5.0	5.0	4.0
	Com path sep, sec	95.2	100.1	108.9	137.4	210.5	98.5
	Thresh sep, sec	93.1	103.3	127.2	144.5	230.5	98.5
	Com path sep, nm	4.3	4.3	4.3	5.2	5.0	4.3
	Thresh sep, nm	4.0	4.0	4.0	5.0	5.2	4.0
	Lead a/c min sep pos, nm	0	0	0	0	1.0	0
All	Trail a/c thresh time, sec	136.0	146.0	170.0	165.0	256.0	140.0

Table B-3. Empirically derived separations for IMC

Common path length: 9.0 nm
No extra separation buffers

Leading aircraft down, trailing aircraft across		Heavy	Large jet	Large turbo-prop	Small turbo-prop	Small prop	B757
Heavy	Req'd min sep, nm	4.0	5.0	5.0	6.0	6.0	5.0
	Com path sep, sec	107.0	137.0	139.8	171.3	235.1	138.4
	Thresh sep, sec	107.0	141.7	148.6	177.4	293.1	145.8
	Com path sep, nm	4.9	6.0	5.6	6.6	6.0	5.9
	Thresh sep, nm	4.0	5.0	5.1	6.0	6.5	5.0
	Lead a/c min sep pos, nm	0.9	0	1.5	0.5	2.1	0
Large jet	Req'd min sep, nm	2.5	2.5	2.5	4.0	4.0	2.5
	Com path sep, sec	73.6	71.2	62.1	115.5	149.3	69.5
	Thresh sep, sec	67.2	71.2	76.2	119.7	232.9	75.2
	Com path sep, nm	3.6	3.6	2.9	4.7	4.0	3.4
	Thresh sep, nm	2.5	2.5	2.6	4.1	5.1	2.6
	Lead a/c min sep pos, nm	0	2.5	2.5	2.5	4.1	2.5
Large turbo-prop	Req'd min sep, nm	2.5	2.5	2.5	4.0	4.0	2.5
	Com path sep, sec	80.8	77.0	73.8	117.3	150.6	75.9
	Thresh sep, sec	67.2	71.3	73.8	117.3	228.8	73.3
	Com path sep, nm	3.9	3.9	3.3	4.8	4.1	3.7
	Thresh sep, nm	2.5	2.5	2.5	4.0	5.1	2.5
	Lead a/c min sep pos, nm	0	0	1.6	0.8	4.1	0
Small turbo-prop	Req'd min sep, nm	2.5	2.5	2.5	2.5	2.5	2.5
	Com path sep, sec	80.9	77.1	74.6	73.8	85.0	76.3
	Thresh sep, sec	67.2	71.3	73.8	73.8	184.6	73.3
	Com path sep, nm	3.9	3.9	3.3	3.3	2.6	3.7
	Thresh sep, nm	2.5	2.5	2.5	2.5	4.0	2.5
	Lead a/c min sep pos, nm	0	0	1.6	1.6	5.6	0
Small prop	Req'd min sep, nm	2.5	2.5	2.5	2.5	2.5	2.5
	Com path sep, sec	130.4	128.8	134.1	134.5	115.2	130.4
	Thresh sep, sec	66.9	70.9	73.7	73.7	115.2	72.9
	Com path sep, nm	5.7	5.8	5.4	5.4	3.3	5.6
	Thresh sep, nm	2.5	2.5	2.5	2.5	2.5	2.5
	Lead a/c min sep pos, nm	0	0	0	0	0	0
B757	Req'd min sep, nm	4.0	4.0	4.0	5.0	5.0	4.0
	Com path sep, sec	116.1	116.3	116.7	146.4	193.2	116.5
	Thresh sep, sec	107.1	113.3	117.5	147.0	258.8	116.5
	Com path sep, nm	5.2	5.3	4.8	5.8	5.1	5.1
	Thresh sep, nm	4.0	4.0	4.0	5.0	5.7	4.0
	Lead a/c min sep pos, nm	0	0	1.0	1.5	3.1	0.8
All	Trail a/c thresh time, sec	218.0	221.0	240.0	241.0	374.0	229.0

Table B-4. Empirically derived separations for VMC

Common path length: 6.0 nm
No extra separation buffers

Leading aircraft down, trailing aircraft across.		Heavy	Large jet	Large turbo-prop	Small turbo-prop	Small prop	B757
Heavy	Req'd min sep, nm	4.0	5.0	5.0	6.0	6.0	5.0
	Com path sep, sec	103.2	125.2	126.3	157.0	255.7	129.5
	Thresh sep, sec	103.2	125.5	128.7	157.0	255.7	130.7
	Com path sep, nm	4.4	5.2	5.3	6.0	6.0	5.3
	Thresh sep, nm	4.0	5.0	5.0	6.0	6.0	5.0
	Lead a/c min sep pos, nm	0	0	0	0	0	0
Large jet	Req'd min sep, nm	2.5	2.5	2.5	4.0	4.0	2.5
	Com path sep, sec	66.1	66.3	66.9	108.5	164.5	66.0
	Thresh sep, sec	66.8	66.3	76.6	115.2	202.6	71.7
	Com path sep, nm	3.0	3.0	3.3	4.4	4.0	3.0
	Thresh sep, nm	2.5	2.5	2.6	4.0	4.4	2.5
	Lead a/c min sep pos, nm	0	0	0.5	0	2.0	0.5
Large turbo-prop	Req'd min sep, nm	2.5	2.5	2.5	4.0	4.0	2.5
	Com path sep, sec	75.6	75.7	75.3	113.9	164.5	75.4
	Thresh sep, sec	66.9	66.3	75.3	115.3	195.7	71.0
	Com path sep, nm	3.3	3.3	3.6	4.6	4.0	3.4
	Thresh sep, nm	2.5	2.5	2.5	4.0	4.3	2.5
	Lead a/c min sep pos, nm	0	0	0.5	0	2.0	0
Small turbo-prop	Req'd min sep, nm	2.5	2.5	2.5	2.5	2.5	2.5
	Com path sep, sec	77.9	77.9	77.6	77.8	95.3	77.8
	Thresh sep, sec	66.9	66.3	75.2	77.8	151.5	71.0
	Com path sep, nm	3.4	3.4	3.6	3.4	2.5	3.4
	Thresh sep, nm	2.5	2.5	2.5	2.5	3.3	2.5
	Lead a/c min sep pos, nm	0	0	0	0.5	3.5	0
Small prop	Req'd min sep, nm	2.5	2.5	2.5	2.5	2.5	2.5
	Com path sep, sec	99.7	99.2	100.1	103.0	115.0	100.9
	Thresh sep, sec	66.9	65.9	75.2	77.7	115.0	71.1
	Com path sep, nm	4.2	4.2	4.4	4.2	2.9	4.3
	Thresh sep, nm	2.5	2.5	2.5	2.5	2.5	2.5
	Lead a/c min sep pos, nm	0	0	0	0	1.8	0
B757	Req'd min sep, nm	4.0	4.0	4.0	5.0	5.0	4.0
	Com path sep, sec	105.9	105.7	106.9	135.8	210.6	107.7
	Thresh sep, sec	103.3	103.3	109.2	137.6	227.1	107.7
	Com path sep, nm	4.5	4.5	4.6	5.3	5.0	4.5
	Thresh sep, nm	4.0	4.0	4.0	5.0	5.1	4.0
	Lead a/c min sep pos, nm	0	0	0	0	1.0	0
All	Trail a/c thresh time, sec	146.5	146.0	148.5	157.2	256.0	150.2

Table B-5. Empirically derived separations for IMC

Common path length: 9.0 nm
Extra separation buffers included

Leading aircraft down, trailing aircraft across		Heavy	Large jet	Large turbo-prop	Small turbo-prop	Small prop	B757
Heavy	Req'd min sep, nm	4.2	5.2	5.6	6.2	6.2	5.2
	Com path sep, sec	112.4	141.2	157.3	177.1	244.3	143.1
	Thresh sep, sec	112.4	145.7	164.6	182.7	298.7	150.1
	Com path sep, nm	5.1	6.2	6.2	6.8	6.2	6.1
	Thresh sep, nm	4.2	5.2	5.6	6.2	6.7	5.2
	Lead a/c min sep pos, nm	0.8	0	0.9	0.3	1.9	0
Large jet	Req'd min sep, nm	3.2	3.2	3.6	4.2	4.2	3.1
	Com path sep, sec	93.4	91.2	102.3	121.4	157.9	88.4
	Thresh sep, sec	85.9	91.2	107.0	125.4	238.4	92.3
	Com path sep, nm	4.3	4.4	4.3	4.9	4.2	4.2
	Thresh sep, nm	3.2	3.2	3.6	4.3	5.3	3.2
	Lead a/c min sep pos, nm	0	1.8	1.4	2.3	3.9	1.9
Large turbo-prop	Req'd min sep, nm	3.1	3.1	3.2	4.2	4.2	3.1
	Com path sep, sec	95.1	92.8	94.3	123.2	159.1	91.7
	Thresh sep, sec	83.3	88.3	94.3	123.2	234.6	90.7
	Com path sep, nm	4.4	4.5	4.0	5.0	4.3	4.3
	Thresh sep, nm	3.1	3.1	3.2	4.2	5.2	3.1
	Lead a/c min sep pos, nm	0	0	1.1	0.8	3.9	0
Small turbo-prop	Req'd min sep, nm	3.1	3.1	3.1	3.1	3.1	3.1
	Com path sep, sec	95.1	92.8	91.4	91.4	110.8	91.7
	Thresh sep, sec	83.3	88.3	91.4	91.4	202.7	90.7
	Com path sep, nm	4.4	4.5	3.9	3.9	3.2	4.3
	Thresh sep, nm	3.1	3.1	3.1	3.1	4.4	3.1
	Lead a/c min sep pos, nm	0	0	1.9	1.9	5.0	0
Small prop	Req'd min sep, nm	3.1	3.1	3.1	3.1	3.1	3.1
	Com path sep, sec	139.7	139.3	145.3	145.6	142.9	141.6
	Thresh sep, sec	83.0	88.0	91.4	91.4	142.9	90.8
	Com path sep, nm	6.1	6.1	5.8	5.8	3.9	6.0
	Thresh sep, nm	3.1	3.1	3.1	3.1	3.1	3.1
	Lead a/c min sep pos, nm	0	0	0	0	0	0
B757	Req'd min sep, nm	4.2	4.2	4.2	5.2	5.2	4.2
	Com path sep, sec	121.0	121.8	122.6	152.2	201.7	122.4
	Thresh sep, sec	112.4	119.0	123.4	152.8	264.6	122.4
	Com path sep, nm	5.4	5.5	5.0	6.0	5.3	5.3
	Thresh sep, nm	4.2	4.2	4.2	5.2	5.9	4.2
	Lead a/c min sep pos, nm	0	0	0.8	1.3	2.9	0.8
All	Trail a/c thresh time, sec	218.0	221.0	240.0	241.0	374.0	229.0

Table B-6. Empirically derived separations for VMC

Common path length: 6.0 nm
Extra separation buffers included

Leading aircraft down, trailing aircraft across		Heavy	Large jet	Large turbo-prop	Small turbo-prop	Small prop	B757
Heavy	Req'd min sep, nm	4.2	5.2	5.6	6.2	6.2	5.2
	Com path sep, sec	108.0	129.6	139.5	160.9	262.2	133.5
	Thresh sep, sec	108.0	129.8	140.4	160.9	262.2	134.5
	Com path sep, nm	4.6	5.4	5.7	6.2	6.2	5.4
	Thresh sep, nm	4.2	5.2	5.6	6.2	6.2	5.2
	Lead a/c min sep pos, nm	0	0	0	0	0	0
Large jet	Req'd min sep, nm	3.2	3.2	3.6	4.2	4.2	3.1
	Com path sep, sec	84.4	84.6	95.5	113.7	173.7	82.9
	Thresh sep, sec	84.8	84.6	101.4	119.6	208.0	87.3
	Com path sep, nm	3.7	3.7	4.2	4.6	4.2	3.6
	Thresh sep, nm	3.2	3.2	3.6	4.2	4.6	3.1
	Lead a/c min sep pos, nm	0	0	0	0	1.8	0
Large turbo-prop	Req'd min sep, nm	3.1	3.1	3.2	4.2	4.2	3.1
	Com path sep, sec	89.5	89.4	93.8	118.4	173.6	90.8
	Thresh sep, sec	82.4	81.9	93.8	119.6	201.7	87.3
	Com path sep, nm	3.9	3.9	4.2	4.7	4.2	3.9
	Thresh sep, nm	3.1	3.1	3.2	4.2	4.4	3.1
	Lead a/c min sep pos, nm	0	0	0	0	1.8	0
Small turbo-prop	Req'd min sep, nm	3.1	3.1	3.1	3.1	3.1	3.1
	Com path sep, sec	91.4	91.1	93.7	95.2	122.9	92.7
	Thresh sep, sec	82.4	81.9	91.9	95.2	165.8	87.2
	Com path sep, nm	3.9	3.9	4.2	4.0	3.1	4.0
	Thresh sep, nm	3.1	3.1	3.1	3.1	3.6	3.1
	Lead a/c min sep pos, nm	0	0	0	0	2.9	0
Small prop	Req'd min sep, nm	3.1	3.1	3.1	3.1	3.1	3.1
	Com path sep, sec	108.9	108.2	110.9	114.9	142.7	110.9
	Thresh sep, sec	82.5	81.9	91.9	95.2	142.7	87.2
	Com path sep, nm	4.6	4.6	4.7	4.6	3.5	4.6
	Thresh sep, nm	3.1	3.1	3.1	3.1	3.1	3.1
	Lead a/c min sep pos, nm	0	0	0	0	1.2	0
B757	Req'd min sep, nm	4.2	4.2	4.2	5.2	5.2	4.2
	Com path sep, sec	110.2	110.0	111.0	140.0	219.8	112.3
	Thresh sep, sec	108.0	107.9	113.1	141.4	232.6	112.3
	Com path sep, nm	4.6	4.7	4.7	5.4	5.2	4.7
	Thresh sep, nm	4.2	4.2	4.2	5.2	5.3	4.2
	Lead a/c min sep pos, nm	0	0	0	0	0.8	0
All	Trail a/c thresh time, sec	146.5	146.0	148.5	157.2	256.0	150.2

1. AGENCY USE ONLY *(Leave blank)*	2. REPORT DATE July 1996	3. REPORT TYPE AND DATES COVERED Technical Memorandum

4. TITLE AND SUBTITLE	5. FUNDING NUMBERS
An Analysis of Landing Rates and Separations at the Dallas/Fort Worth International Airport	505-64-13

6. AUTHOR(S)

Mark G. Ballin and Heinz Erzberger

7. PERFORMING ORGANIZATION NAME(S) AND ADDRESS(ES)	8. PERFORMING ORGANIZATION REPORT NUMBER
Ames Research Center Moffett Field, CA 94035-1000	A-961649

9. SPONSORING/MONITORING AGENCY NAME(S) AND ADDRESS(ES)	10. SPONSORING/MONITORING AGENCY REPORT NUMBER
National Aeronautics and Space Administration Washington, DC 20546-0001	NASA TM-110397

11. SUPPLEMENTARY NOTES

Point of Contact: Mark G. Ballin, Ames Research Center, MS 210-9, Moffett Field, CA 94035-1000; (415) 604-5771

12a. DISTRIBUTION/AVAILABILITY STATEMENT	12b. DISTRIBUTION CODE
Unclassified — Unlimited Subject Category 03	

13. ABSTRACT *(Maximum 200 words)*

Advanced air traffic management systems such as the Center/TRACON Automation System (CTAS) should yield a wide range of benefits, including reduced aircraft delays and controller workload. To determine the traffic-flow benefits achievable from future terminal airspace automation, live radar information was used to perform an analysis of current aircraft landing rates and separations at the Dallas/Fort Worth International Airport. Separation statistics that result when controllers balance complex control procedural constraints in order to maintain high landing rates are presented. In addition, the analysis estimates the potential for airport capacity improvements by determining the unused landing opportunities that occur during rush traffic periods. Results suggest a large potential for improving the accuracy and consistency of spacing between arrivals on final approach, and they support earlier simulation findings that improved air traffic management would increase capacity and reduce delays.

14. SUBJECT TERMS Air traffic automation, Air traffic control, Center/TRACON Automation System, CTAS	15. NUMBER OF PAGES 70
	16. PRICE CODE A04

17. SECURITY CLASSIFICATION OF REPORT Unclassified	18. SECURITY CLASSIFICATION OF THIS PAGE Unclassified	19. SECURITY CLASSIFICATION OF ABSTRACT	20. LIMITATION OF ABSTRACT